A

Dissertation Report

On

Nonlinear Vibration Analysis of Unbalanced Flexible Rotor Supported on Ball Bearings with Internal Radial Clearance and Surface Waviness

For partial fulfillment of the requirements for the award of degree of

Master of Technology in **Mechanical Engineering**

By

KAPIL AGRAWAL

2014PDE5032

Under the Guidance of

Dr. T. C. Gupta

Associate Professor

Department of Mechanical Engineering

Malaviya National Institute of Technology, Jaipur

DEPARTMENT OF MECHANICAL ENGINEERING

MALAVIYA NATIONAL INSTITUTE OF TECHNOLOGY, JAIPUR

JUNE-2016

DEPARTMENT OF MECHANICAL ENGINEERING

MALAVIYA NATIONAL INSTITUTE OF TECHNOLOGY, JAIPUR

CERTIFICATE

This is certified that the dissertation entitled **Nonlinear Vibration Analysis of Unbalanced Flexible Rotor Supported on Ball Bearings with Internal Radial Clearance and Surface Waviness** prepared by **Kapil Agrawal** in partial fulfillment of the requirement for the award of the degree of **Master of Technology** in **Mechanical Engineering** of **Malaviya National Institute of Technology, Jaipur**, is found to be satisfactory and hereby approved for the submission. The work embodied in this Dissertation in full or in parts has not been submitted in any other Institutes or University for the award of any other degree or Diploma.

Kapil Agrawal

2014PDE5032

This Dissertation work is hereby approved for the submission.

Date:

Dr. T. C. Gupta

Associate Professor

Department of Mechanical Engineering

Place:

Malaviya National Institute of Technology, Jaipur

ACKNOWLEDGEMENT

I would like to take this opportunity to extend my gratitude towards my mentor **Dr. T. C. Gupta** for his constant encouragement and insightful guidance for completion of this dissertation work. His vast expense of knowledge in the area of Rotor Dynamics and Mechanical Vibrations has helped me understand my own efforts and implement them with great precision.

I am extremely grateful to respected **Dr. Himanshu Chaudhary**, **Dr. Amit Kumar Singh**, and **Dr. Dinesh Kumar** for always being a source of encouragement.

I would also like to thank **Mr. Manoj Gupta** and **Mr. Ajit Singh** for helping me throughout my dissertation work.

In the end, I would like to pay high regards to my parents and friends for their sincere inspiration and motivation to support me throughout my dissertation work.

Kapil Agrawal

Design Engineering

(2014PDE5032)

Abstract

A nonlinear model of an unbalanced flexible rotor using finite element method is developed. The rotor is supported on deep groove ball bearings. The bearings are affected by geometric imperfection such as surface waviness on inner and outer race both. The finite element model of rotor is prepared by considering Euler Bernoulli beam element, and the ball bearing model is developed using Gupta's bearing model. The surface waviness of bearing's races causes the variation between inner and outer race during rotation, and there by continuous changes the Hertzian contact force, that acts at the contact of balls and races. The internal clearance, surface waviness, time-varying rotating imbalance force, nonlinear nature of Hertzian contact force of bearing and makes the system complex and nonlinear. The governing differential equation of the system is solved by using numerical integration technique Newmark β with Newton Raphson iteration in MATLAB. The nonlinear dynamic response is studied using displacement plots, dynamic orbits and frequency spectra. The frequency spectra of the system are analyzed along with and without bearing's surface waviness at certain rotational speed. These frequency spectra are plotted using Fast Fourier Transformation (FFT) in MATLAB and the impact of surface waviness on it is identified by varying the surface waviness order of both inner race's and outer race's waviness. The dynamic response has been validated using frequency spectra with surface waviness with the results available in the literature for certain waviness-order.

Contents

List of Figures

List of Tables

Nomenclature

Roman Symbols

B	Small angle rotation about X-axis
D	Ball Diameter of ball bearing
E	Young's Modulus of rotor
I_s	Diametric Area Moment of Inertia of rotor shaft.
I	Mass moment of inertia
K	Load-Deflection factor
K_i	Elastic Stiffness between inner race and ball of the ball bearing
K_o	Elastic Stiffness between outer race and ball of the ball bearing
L	Arc length of race
N_b	Number of balls in the ball bearing
N_w	Number of waves (Waviness order)
Q	Contact Force in the bearing
T	Small angle rotation about Y-axis
V	Small translational displacement in X-axis
W	Small translational displacement in Y-axis
a, n	Arbitrary positive constants
f_r	Rotational frequency in Hz.
f_{vc}	Varying Compliance frequency in Hz.
f_c	Cage rotational frequency in Hz.
g	Gravitational acceleration
l	Length of rotor shaft element

l_s	Length of shaft
m_d	Mass of rigid disk
p	Curvature
r	Radius
r_i	Inner race groove radius
r_o	Outer race groove radius
t	Time
v	Tangential velocity

Greek Symbols

$\mathcal{P}$	Elastic Bending Energy
$\mathcal{T}$	Translational Kinetic Energy
μ	Mass of rotor element per unit length
Φ	Spin angle of rotor
$\mathcal{I}$	Mass moment of inertia of rotor element per unit length
$\psi_1, \psi_2, \psi_3, \psi_4$	Spatial shape functions
Υ_{ij}	Amplitude of inner race waviness
Υ_{oj}	Amplitude of outer race waviness
Υ_{pi}	Maximum amplitude of inner race waviness
Υ_{po}	Maximum amplitude of outer race waviness
λ	Wavelength
θ_j	Angular position of j^{th} ball
ω	Angular velocity

ω_{vc}	Varying Compliance Frequency
δ	Deformation
δ^*	Dimensionless contact parameter
ς, β	Newmark β Parameters
ν	Angular Separation between balls of ball bearing

Matrices

Ψ	Spatial Constraint Matrix
Φ	Rotation Shape Matrix
q	Displacement vector
$\mathrm{M_T}$	Translational Mass Matrix
$\mathrm{M_R}$	Rotational Mass Matrix
G	Gyroscopic Matrix
K	Stiffness Matrix
Q	Globalized Force Vector
Q_g	Gravity Force Vector
Q_{un}	Unbalance Force Vector
Q_b	Bearing Force Vector

Subscripts

in	Inner race
out	Outer race
d	Diametric

p	Polar
pt	Pitch
eff	Effective
r	Rotor
c	Cage
j	Ball number of ball bearing

Superscripts

e	Shaft finite element
d	Rigid disk
T	Transpose of a Matrix
′	Differentiate with respect to space
.	Differentiate with respect to time

1 Introduction

In the industries, rotating machineries are widely used for power generation and transmission where the primary concern is high efficiency and reliability. These machineries experience significant vibrations during their running period. There are many reasons of generation of these vibrations, for example, the time varying unbalance force of rotor, gravity load and nonlinear bearing force etc. The dynamic behavior of the rotor-bearing systems is highly complex because of the bearing's nonlinear character. The bearing to be discussed here is rolling element bearing viz. ball bearing. These rolling bearings are using in several rotating machineries including small hand-held device to large heavy duty machineries. Sometimes these bearings become a key cause of breakdown of the rotating machines. Therefore, to predict the vibration response of the system together with the ball bearing dynamic behavior is very vital to analyze.

Depending on shaft's elasticity, the rotor is characterized as rigid rotor and flexible rotor. The rigid rotor is assumed not to deform elastically and the vibrations produced by it are less complex. With the rigid rotor, bearing stiffness is the chief factor in deciding the vibration amplitude and its pattern. Flexible rotors have non negligible elastic deformation and produce high and complex vibrations. To model such rotors, finite element method is endorsed. The finite element model can be developed by using Euler Bernoulli beam element or the Timoshenko beam element. Both elements include the effect of elastic bending energy, translational kinetic energy, gyroscopic moment, axial load, and axial torque to determine mass matrix, stiffness matrix, damping matrix and gyroscopic matrix of the flexible rotor. However, the Timoshenko beam element has an advantage over Euler Bernoulli beam element, as it also takes account of shear deformation and rotary inertia effect in the finite element matrices.

The Rolling element bearings subjected to vibrations generally because of its inherent nonlinearity, which arises due to Hertzian force-deformation relationship, varying compliance, internal radial clearance and the bearing defects, like localized defects and continuous surface waviness. Hertzian force is the nonlinear contact force which is generated between races and balls of the ball bearing by the elastic deformation at contacts of balls and races. Incorporating the bearing defects and the internal clearance in the bearing model, the elastic deformation is altered and this in turn changes the effective bearing stiffness and Hertzian contact force. This

creates a periodic change in bearing stiffness and the system experiences nonlinear vibration under dynamic conditions.

The defects of ball bearing are either localized defects or continuous defects. The localized defects are the pits, cracks, and spalls etc., which are generated preliminary due to fatigue of mating surface, like balls and races contacts. These defects remain unnoticed in the initial stage and yields progressive noises and vibrations, which leads the rotor bearing system towards failure. The continuous defects like surface waviness, are the geometric imperfections produced by the irregularities of manufacturing process, like uneven wear of the grinding wheel in the grinding operations, fluctuating interactions between the work and tool, vibrations of machine element itself and work's movement in the fixture, etc. The amplitude of surface waviness is generally too small, but it enhances the vibration of the system significantly. These surface waviness imperfections are assumed of sinusoidal shaped and present on the surface of balls, inner race and outer race. The waviness can be both axial and radial as well. The wavelength of the surface waviness is much longer than the Hertzian contact width. In the running state of bearing, the surface waviness changes the elastic contact deformation acting between balls and races, which in turn modify the Hertzian contact force. Because of such contact load variation, vibrations get generated in the bearing. Surface waviness of different amplitudes and/or different wave number, excites different vibrational frequencies. These vibrations due to surface waviness enhance the whole system's vibrations.

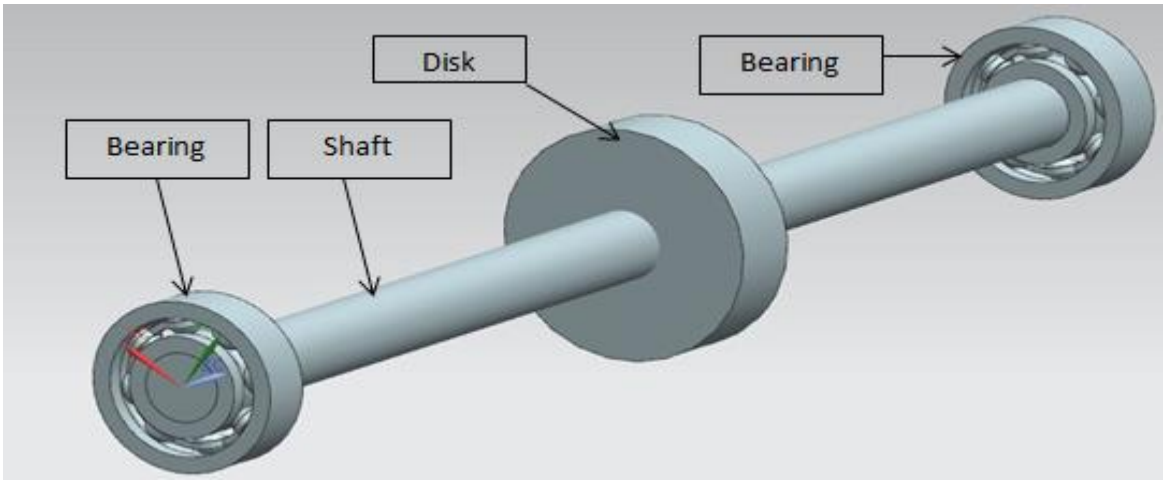

Fig. 1.1 Rotor-Bearing system

2 Literature Review

Babu, C. et al. [1] did the Vibration modeling of a rigid rotor having six degrees of freedom, supported on angular contact bearing. Radial waviness was taken on the balls; both radial and axial sinusoidal surface waviness was taken on the inner race's outer face as well as on the outer race's inner face of the angular contact bearing. The waviness order and waviness amplitude was varied in the modeling. The angular contact bearing exerted Hertzian force and moments with frictional moments (load dependent and load independent) to the rotor. Numerical analysis was done using Runge Kutta Method for numerical integration. The load dependent frictional moments enhanced the vibration, as compared to the load independent frictional moment. The vibrations were found to increase as the waviness order and the amplitude were increased. The inner race surface waviness produced more vibrations than the outer race surface waviness.

Babu, C. et al. [2] performed the nonlinear dynamic modeling of a flexible rotor held by angular contact bearing, by integrating surface waviness on balls, and inner and outer race of the angular contact bearing. To model the rotor, two noded Timoshenko beam element was taken with 6 degrees of freedom per node. Angular bearing exerted Hertzian contact force as a bearing force and frictional moment (both Load dependent and load independent) on the rotor. Waviness amplitude and waviness order both were varied in the analysis. With higher waviness amplitude and waviness order, the vibration amplitude was found to escalate. The outer race waviness had higher influence on the system's vibration than the inner race waviness bearing. This conclusion was opposite to the rigid rotor system. In case of rigid rotor, inner race waviness enhanced the system's vibration significantly, as compared to the outer race waviness.

Bai, C. et al. [3] performed both numerical and experimental analysis on the dynamic behavior of flexible rotor system, supported on ball bearings. The author focused on sub harmonic resonance characteristics of the system. The offset-disk rotor system was analyzed by finite element method with the ball bearing model of 2 degrees of freedom. Numerical analysis was done by numerical integration method with Newton Raphson Iteration. The Numerical analysis data were also compared with the experimental data and were found to be in very good agreement with the results. The sub harmonic resonance occurred at twice that of sychroresonance frequency due to nonlinearity of ball bearing. This sub harmonic resonance

caused high vibrations and noise of the system. This made the rotor unstable and caused damage to it.

Datta, J. et al. [4] created a mathematical model of a rigid rotor- rolling element bearing system to study its vibrations responses. The mathematical model was made using Lagrange principle. The formulation was carried out by considering individual masses of race, rolling elements and shaft. This comprises the role of tangential and radial motion of rolling element, inner and outer race. The nonlinear governing differential equation was then solved using Runge Kutta Numerical integration scheme.

Datta, J. et al. [5] used the mathematical formulation of rigid rotor-roller bearing system to study the effects of different operating conditions on bearing structural vibrations. These different operating conditions included size of roller, size of inner and outer race, and magnitude and nature of loads (linear or rotational) acting on the bearing. Numerical analysis was done using sixth order Runge Kutta integration method. Vibration amplitude enhanced with the increase in roller size. Comparing the roller bearing and ball bearing of comparable size, roller bearing was found to have higher oscillating frequencies than ball bearing.

El-Sayed, H. [6] derived the expression for calculation of bearing stiffness of the ball bearing for given bearing dimension. Earlier to this work, the bearing stiffness was obtained using bearing catalogue or Handbook. In the derivation, the bearing internal clearance was neglected, which may produce some error in the calculation of bearing stiffness. The analytical expression was validated with the experimental work.

Gupta, T. et al. [7] considered a flexible rotor with unbalanced disk, supported on deep groove ball bearings on either ends of rotor for Nonlinear Vibration analysis. The ball bearing with internal radial clearance exerted a Hertzian contact force to the rotor which is nonlinear in nature. The Numerical analysis was done using time integration technique Newmark β with Newton Raphson iteration. In the analysis, the dynamic behavior of rotor was studied by varying rotor speed. Dynamic response at disk location was higher at lower rotor speed. Effect of varying compliance of ball bearing faded out for the excitations at disk location at higher rotation speed.

Harsha, S. and Kankar, P [8] performed stability analysis of rigid rotor system supported on ball bearing. Author considered surface waviness on inner and outer race both of the ball bearing. The governing differential equation was solved using integration technique Newmark β

along Newton Raphson iteration. Author discussed the impact of surface waviness and number of balls on the vibration characteristics of the system. The Nonlinear dynamic responses were more allied to the ball passage frequency. The axial vibration were achieved at an integer multiple of ball passage frequency. The numerical results were validated by the experimental data of previous researches.

Harsha, S. et al. [9] prepared a critical model to analyze nonlinear dynamics of the system of a rigid rotor, supported on ball bearings. The ball bearing had surface waviness on its inner and outer races. The mass of shaft with disk, inner race and outer race were taken individually. The governing differential equation was derived using Energy Principle. By using Lagrange principle, equation of motion was evaluated. Newmark β Numerical integration approach was used along Newton Raphson iteration scheme to estimate the solution of governing differential equation. In the analysis, the numbers of waves on both inner and outer race were varied. Considering outer race waviness only, the serve vibration occurs when number of balls and number of waves becomes equal and the vibrating frequency would be an integer multiple of varying compliance frequency. Considering inner race waviness only, the vibrations occurs at the integer multiple of wave passage frequency and/or sum of integer multiple of wave passage frequency and rotational frequency.

Kankar, P et al. [10] considered a rigid rotor system supported on ball bearing. Ball bearing has race defect as surface waviness on inner race and outer race both. To derive governing differential equation, inertia principle was used, by calculating inertia force, damping force, stiffness force and the force of excitation of the system. Bearing exerted Hertzian force as the bearing force to the rotor. To solve the differential equation, a numerical integration approach was used, with the iteration scheme as Newmark β with Newton Raphson method. The number of waves on inner race and outer race were varied in the analysis of obtaining vibrations characteristics. The waviness amplitude was varied along the surface of races to get the real time situation of surface roughness on the bearing races. With the outer race waviness, the high vibration takes place at an integer multiple of varying compliance frequency. Bearing with inner race waviness produced higher complex spectrum than outer race waviness. Vibration occurred at integer multiple of ball passage frequency and/or sum with rotational frequency.

Li, Y. et al. [11] proposed a general dynamic modeling method of ball bearing-rotor system. In this work, lubrication traction and bearing clearance, three dimensional motions of outer race, inner race, and balls of the angular contact ball bearing were considered. The finite element method was used to model shaft elastic deformation and combined it to rigid motion of bearing, to obtain a real time state of the flexible rotor-bearing system. The governing differential equation of the system was solved by Runge-Kutta-Fehlberg Integration method. The analytical results were then verified by an experimental work, and it showed a good agreement of results. With the increase in bearing's clearance, the vibration became higher, and the complication of frequency spectrum arose, which includes rotational frequency, varying compliance frequency, its harmonics and other frequencies too.

Meyer, L. et al. [12] prepared an analytical technique to get the vibration frequency response of the rotor bearing system. In the analysis, major defects that comes to the rolling element bearings in its service were considered. These major defects were race misalignment, off-sized rolling elements and distributed defects like surface waviness on the races and/or on balls. Analytical model was prepared for ideal bearing with no defects and then several defects were introduced to the model and the effects of these defects were predicted on the spectral vibrations of the system.

Nelson, H. and McVaugh, J. [13] proposed a dynamic model of flexible rotor bearing system in both fixed and rotating reference frames. The fixed frame taken was the global frame and rotating frame was defined by whirling motion of the rotor. The components taken in the modeling were rigid disk, rotor as distributed mass and elasticity, and the linear bearing. The finite element method was used, considering this system of 4 degrees of freedom to formulate the governing equation of the system. The Elastic Bending energy, Kinetic Energy, gyroscopic effect, rotary inertia, and axial load was included in the formulation. An overhung system was taken and its natural whirl speed and responses were calculated for an undamped isotropic and undamped orthotropic bearing system.

Nelson, H., [14] modeled a flexible rotor system using Timoshenko beam theory to add the effect of shear deformation and inertia torque. In the previous studies, author had included the gyroscopic effect, rotary inertia and axial load effect for the formulation of flexible rotor analysis.

Niu, L. et al. [15] proposed a dynamic model of a rigid rotor supported on high speed rolling ball bearings, having localized surface defects like material absence on its races. Governing differential equations were solved using fourth order Runge Kutta Fehlberg method. Defects width and inner race rotation both were varied to see its effect on vibration responses

N. Aktürk, [16] considered a 3 degree of freedom rigid rotor system supported on the pair of angular contact ball bearing. Author performed axial as well as radial vibrations of the system. Surface waviness on the races and balls of the bearing were also included in the formulation. Numerical analysis was done by Runge Kutta integration approach. Author analyzed for the variation of net force and phase angle (angle between total net force and vertical axis) with the variation of waviness number of outer race only. Vibration becomes intense at ball passage frequency and when its harmonics coincided with natural frequencies. The peak vibrations occurred when the number of balls and wave number became equal.

Patel, V. et al. [17] executed a dynamic Vibration Analysis of Deep-groove Ball Bearing having defects on the surface of races. The author considered masses of the shaft, races, balls and housing individually to develop the Governing Differential Equation of the system. Solution of the equation of motion is governed by using Runge Kutta numerical integration method. Numerical results were validated by experimental results by selecting healthy bearing and defective bearing. In case of healthy bearing, vibration peaks came at shaft rotation frequency and cage rotation frequency with their harmonics. With defective bearing, peaks came at ball passage frequency of inner race and ball passage frequency of outer race.

Wardle, F. [18] derived an analytical expression to consider the effect of surface waviness of the thrust bearing on the rotor vibrating forces and the frequencies. The waviness is considered on all the three components of the bearing, that is, balls inner race and outer race.

Yhland, E., [19] considered a 3 d.o.f. rigid and flexible rotor supported on double row self-aligned ball bearing. In the analysis, external load is applied in three perpendicular directions, with considering internal clearance in the bearing and surface waviness on the bearing races and balls. The Runge Kutta method of fourth order was used to solve the nonlinear governing differential equation iteratively. A relation between waviness order and excited frequencies is proposed for both rigid and flexible rotor. Vibration became intense in axial direction when

radial load equaled the unbalanced force. Vibrations decreased if the applied radial load increased beyond the unbalanced force.

Armentrount, R. and Gunter, E. [20] considered a flexible rotor supported on nonlinear squeeze filler damper, to run the transient analysis, based on modal technique to predict the nonlinear unbalance response. The formulation was then applied to the aircraft turbofan engine to get the unbalanced response, so that the characteristics of squeeze filler damper and bearing supports could be optimized.

2.1 Research Gap

From above literature survey, it was concluded that most of the studies on dynamic analysis of rotor bearing system have been performed, assuming the rotor as rigid rotors. The bearing models were mainly for angular contact bearing and deep groove ball bearing with internal radial clearance. There are a few publications which consider the rotor as flexible and incorporate surface waviness and radial clearance. In the proposed work, nonlinear vibration analysis is performed for a flexible rotor supported on deep groove ball bearing considering internal radial clearance and surface waviness of inner and outer races, as geometric imperfection.

2.2 Problem Statement

Nonlinear Vibration Analysis is conducted for an unbalanced flexible rotor ball-bearing system. The rotor is assumed as an elastic axis-symmetric body with continuous mass distribution. The unbalanced rigid disk is positioned at mid span of the shaft. The rotor is supported by deep groove ball bearings at either ends. The bearings are considered having an internal radial clearance between balls and races and surface waviness on the outer periphery of their inner race and on the inner periphery of its outer race. The spectral vibration analysis is performed on the system, to determine its vibration characteristics and to predict the impact of surface waviness present on the races of bearing to the frequency spectra of the system. The displacement plots, dynamic orbits and frequency spectra are used to describe the dynamic behavior of the system. The frequency spectra are further used to determine the impact of surface waviness of different orders on the vibration characteristics of the system

3 Mathematical Modeling

In the mathematical modeling of Flexible Rotor-Bearing system, the rotor and the ball bearing are modeled as separate systems. The interaction between ball bearing and rotor is by the mode of bearing forces only. The mathematical model of the flexible rotor is developed by employing finite element method [17] and the ball bearing is modeled as 2-degrees of freedom system [9]. The surface waviness is incorporated on the inner race and outer race of the bearing model [12]. The Rotor is discretized into six finite elements, where each element has 2 nodes and each node has 4 degree of freedom. A typical rotor-bearing system in motion is shown in Fig. 3.1

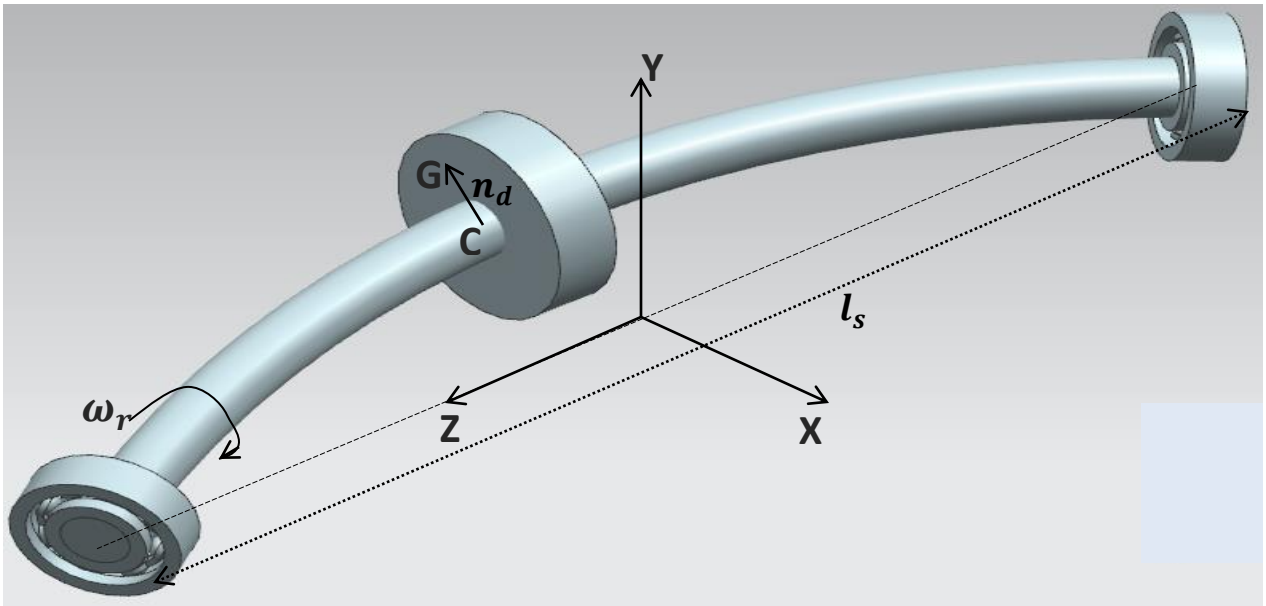

Fig. 3.1: Rotor-Bearing system

3.1 Finite Element Model

The Finite element modeling of the flexible rotor is performed by considering Euler-Bernoulli beam element. It involves the elastic bending energy and translational kinetic energy. The rotary inertia effect and the gyroscopic moment have also been included to the rotor model. The rotor is comprised of a rigid disk, which is positioned at the center of the rotor, and a flexible shaft,

which is supported by the bearings. The equation of motion for rigid disk is derived by calculating its kinetic energy and importing it to Lagrangian formulation. The finite element of flexible rotor is modeled as an integration of infinite set of differential disks whose equations of motion are derived by considering spatial shape functions. The rotor is divided into six finite elements. These are 2 node elements where each node is having 4-dof. The two degree of freedom are translational and two are rotational in nature. As a result, the system would have total 7 nodes and 28 degrees of freedom.

3.1.1 Finite Element Model of Shaft

The Flexible rotor shaft is discretized into 6 circular Euler-Bernoulli beam elements. Each element has 2 nodes and each node is having 4 degree of freedoms.

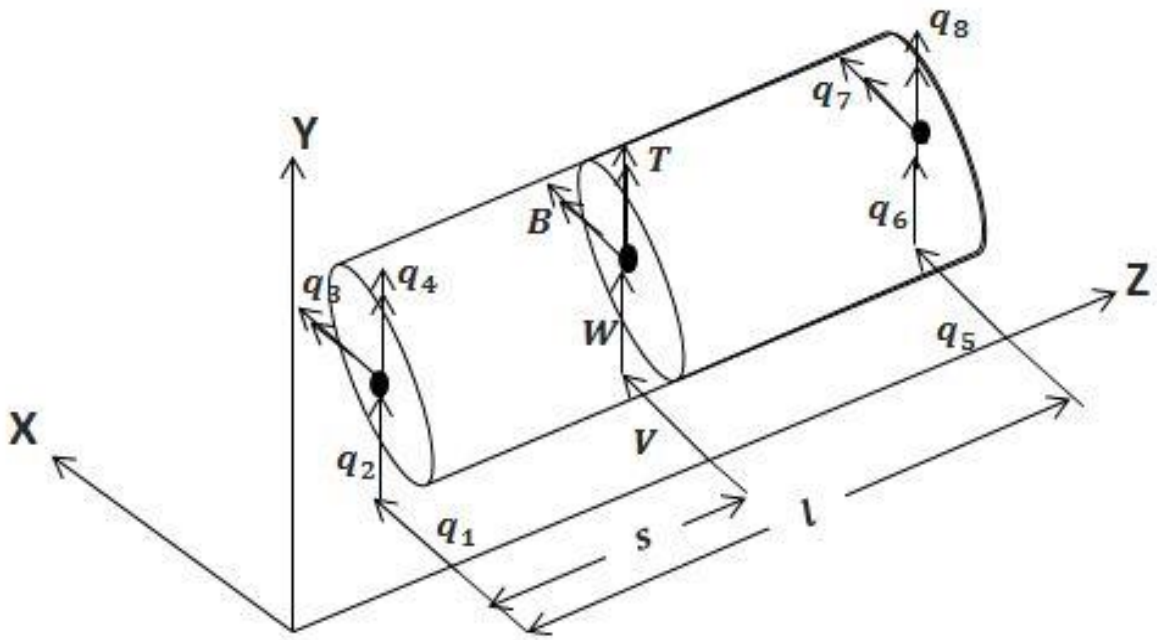

Fig. 3.2: Finite element of shaft

From the Fig. 3.2 it is observed that, the first node has two translational dof,('q_1' in positive x-direction, 'q_2' in positive y-direction) and two rotational dof, (q_3 in positive x-direction, q_4 in positive y-direction). Similarly two translational dof 'q_5' and 'q_6', and two rotational dof q_7 and q_8 are associated with the second node. In this way, each finite element of shaft has 2-nodes and 8 degrees of freedoms.

V, W, B and T are time (t) and position (s) dependent cross-section displacement of a typical internal point of an element as shown in the Fig. 3.2, where V and W are translational displacement and B and T are angular displacement. B and T are related to V and W respectively by the relation shown in Equation 3.1:

$$B = -\frac{dW}{ds}$$
$$T = \frac{dV}{ds} \tag{3.1}$$

The translation of internal point of an element obeys the following relation:

$$\begin{Bmatrix} V(s,t) \\ W(s,t) \end{Bmatrix} = [\Psi(s)]\{q(t)\} \tag{3.2}$$

$\{q_e\}$ is the displacement vector of the element $\{q_1, q_2, q_3, q_4, q_5 q_6, q_7, q_8\}$

$\Psi(s)$ is a spatial constraint matrix and can be expressed as:

$$[\Psi] = \begin{bmatrix} \psi_1 & 0 & 0 & \psi_2 & \psi_3 & 0 & 0 & \psi_4 \\ 0 & \psi_1 & -\psi_2 & 0 & 0 & \psi_3 & -\psi_4 & 0 \end{bmatrix} \tag{3.3}$$

$\psi_1, \psi_2, \psi_3, \psi_4$ are spatial shape functions

$$\psi_1 = 1 - 3\left(\frac{s}{l}\right)^2 + 2\left(\frac{s}{l}\right)^3$$
$$\psi_2 = s\left[1 - 2\left(\frac{s}{l}\right) + \left(\frac{s}{l}\right)^2\right]$$
$$\psi_3 = 3\left(\frac{s}{l}\right)^2 - 2\left(\frac{s}{l}\right)^3 \tag{3.4}$$
$$\psi_4 = l\left[-\left(\frac{s}{l}\right)^2 + \left(\frac{s}{l}\right)^3\right]$$

The angular displacements B and T are expressed as:

$$\begin{Bmatrix} B(s,t) \\ T(s,t) \end{Bmatrix} = [\Phi(s)]\{q(t)\} \tag{3.5}$$

Matrix of Rotation shape function is:

$$[\Phi] = \begin{bmatrix} \Phi_B \\ \Phi_T \end{bmatrix} = \begin{bmatrix} 0 & -\psi_1' & \psi_2' & 0 & 0 & -\psi_3' & \psi_4' & 0 \\ \psi_1' & 0 & 0 & \psi_2' & \psi_3' & 0 & 0 & \psi_4' \end{bmatrix} \tag{3.6}$$

The elastic bending energy and translational kinetic energy of the differential disk located at 's' in the finite element as shown in the Fig. 3.2,

$$\begin{aligned} d(\mathcal{P}^e) &= \frac{1}{2}\begin{Bmatrix} V'' \\ W'' \end{Bmatrix}^T \begin{bmatrix} E\,I_s & 0 \\ 0 & E\,I_s \end{bmatrix} \begin{Bmatrix} V'' \\ W'' \end{Bmatrix} ds \\ d(\mathcal{T}^e) &= \frac{1}{2}\begin{Bmatrix} \dot{V} \\ \dot{W} \end{Bmatrix}^T \begin{bmatrix} \mu & 0 \\ 0 & \mu \end{bmatrix} \begin{Bmatrix} \dot{V} \\ \dot{W} \end{Bmatrix} ds + \frac{1}{2}\varphi^2 \mathcal{I}_p ds + \frac{1}{2}\begin{Bmatrix} \dot{B} \\ \dot{T} \end{Bmatrix}^T \begin{bmatrix} \mathcal{I}_d & 0 \\ 0 & \mathcal{I}_d \end{bmatrix} \begin{Bmatrix} \dot{B} \\ \dot{T} \end{Bmatrix} ds - \dot{\varphi}\dot{T}B\,\mathcal{I}_p ds \end{aligned} \tag{3.7}$$

where, $\mathcal{P}^e$ is elastic bending energy of element; and $\mathcal{T}^e$ is translational kinetic energy of element.

Using the relation given in equations 3.2, 3.5 and 3.7; and then integrating equation 3.7 for the whole element length, the above relation is deduced to:

Total Energy:

$$\mathcal{P}^e + \mathcal{T}^e = \frac{1}{2}\{q_e\}^T[K]^e\{q_e\} + \frac{1}{2}\{q_e\}^T([M_T^e + M_R^e])\{q_e\} + \frac{1}{2}\,\mathcal{I}_p\dot{\varphi}^2 + \dot{\varphi}\,\{q_e\}^T[N]\{q_e\} \tag{3.8}$$

where,

$$\begin{aligned} [M_T^e] &= \int_0^l \mu[\Psi]^T[\Psi]\,ds \\ [M_R^e] &= \int_0^l \mathcal{I}_d[\varphi]^T[\varphi]\,ds \\ [N^e] &= \int_0^l \mathcal{I}_p[\varphi_T]^T[\varphi_B]\,ds \\ [K^e] &= \int_0^l E\,I_s[\Psi'']^T[\Psi'']\,ds \\ [G^e] &= ([N] - [N]^T)^e \end{aligned} \tag{3.9}$$

Using Lagrangian method, the total energy in equation 3.8 is used in equation 3.10; and the final elemental equation of motion of shaft element derived is given in equation 3.11:

$$\frac{\mathrm{d}}{\mathrm{dt}}\frac{\partial \mathcal{T}}{\partial\{\dot{\mathrm{q}}\}} - \frac{\partial \mathcal{T}}{\partial\{\mathrm{q}\}} + \frac{\partial \mathcal{P}}{\partial\{\mathrm{q}\}} = \{\mathrm{Q}\} \tag{3.10}$$

$$([\mathrm{M}_{\mathrm{T}}^{\mathrm{e}} + \mathrm{M}_{\mathrm{R}}^{\mathrm{e}}])\{\ddot{\mathrm{q}}_{\mathrm{e}}\} - \omega_r[\mathrm{G}]^{\mathrm{e}}\{\dot{\mathrm{q}}_{\mathrm{e}}\} + [\mathrm{K}]^{\mathrm{e}}\{\mathrm{q}_{\mathrm{e}}\} = \{\mathrm{Q}_{\mathrm{g}}^{\mathrm{e}}\} \tag{3.11}$$

$$\{\mathrm{Q}_{\mathrm{g}}^{\mathrm{e}}\} = \int_0^{\mathrm{l}} \mu\mathrm{g}\,(\psi_{\mathrm{i}})\,\mathrm{ds}; \quad i=1, 2, 3, 4$$

$\dot{\varphi}$ is rotor angular velocity, so it can also be written as ω_r.

μg is the finite element weight per unit length.

3.1.2 Rigid Disk Modeling

Rigid disk is positioned at the mid span of the rotor, such that the centroid of disk is considered to be at the center node of the rotor (node 4) in the finite element formulation. All nodes in the finite element model have 4 degrees of freedoms, so the disk node will also has the same 4 degrees of freedoms. The generalized displacement vector corresponding to the center node of rotor at disk location is given by equation 3.12

$$\{\mathrm{q}^{\mathrm{d}}\} = \begin{Bmatrix} \mathrm{q}_1 \\ \mathrm{q}_2 \\ \mathrm{q}_3 \\ \mathrm{q}_4 \end{Bmatrix} ; \tag{3.12}$$

Where, q_1 and q_2 are translational DOF, and q_3 and q_4 are rotational DOF in the same manner as taken of shaft displacement vector of shaft element nodes.

The translational kinetic energy is calculated for the rigid disk, and then this energy is used to calculate equation of motion of the disk, through Lagrangian method.

$$\mathcal{T}^{d} = \frac{1}{2}\begin{Bmatrix} \dot{\mathrm{q}}_1 \\ \dot{\mathrm{q}}_2 \end{Bmatrix}^{\mathrm{T}} \begin{bmatrix} \mathrm{m_d} & 0 \\ 0 & \mathrm{m_d} \end{bmatrix} \begin{Bmatrix} \dot{\mathrm{q}}_1 \\ \dot{\mathrm{q}}_2 \end{Bmatrix} + \frac{1}{2}\begin{Bmatrix} \dot{\mathrm{q}}_3 \\ \dot{\mathrm{q}}_4 \end{Bmatrix}^{\mathrm{T}} \begin{bmatrix} \mathrm{I_d^d} & 0 \\ 0 & \mathrm{I_d^d} \end{bmatrix} \begin{Bmatrix} \dot{\mathrm{q}}_3 \\ \dot{\mathrm{q}}_4 \end{Bmatrix} - \dot{\varphi}\dot{\mathrm{T}}\mathrm{B}\,\mathrm{I_p^d} \tag{3.13}$$

Equation of Motion derived for rigid disk, using Lagrangian Method:

$$\left(\left[\mathrm{M}_{\mathrm{T}}^{\mathrm{d}} + \mathrm{M}_{\mathrm{R}}^{\mathrm{e}}\right]\right)\{\ddot{\mathrm{q}}_{\mathrm{d}}\} - \omega_r\left[\mathrm{G}^{\mathrm{d}}\right]\{\dot{\mathrm{q}}_{\mathrm{d}}\} = \left\{\mathrm{Q}_{\mathrm{un}}^{\mathrm{d}}\right\} \tag{3.14}$$

$\{Q_{un}^{d}\}$ shown in the Equation 3.14 is the generalized force vector, comprising of the rotating imbalanced force due to eccentricity of disk center of mass from its Geometric center. Let n_d be the eccentricity of disk's center of mass, then the generalized force vector would be:

$$\{Q_{un}^{d}\} = \begin{Bmatrix} n_d \\ 0 \\ 0 \\ 0 \end{Bmatrix} Cos\omega_r t + \begin{Bmatrix} 0 \\ n_d \\ 0 \\ 0 \end{Bmatrix} Sin\omega_r t \quad (3.15)$$

3.2 Ball Bearing Modeling

The ball bearing is supposed as a mass-spring system of 2-degrees of freedom as shown in Fig. 3.3, where the contacts between balls and races act as a nonlinear spring because of the existence of Hertzian force at the mating points of balls and races. The Hertzian force can be produced only by elastic contact deformation at the mating points of ball and races, such that, the assumed spring at the contact point must be in compression state to yield Hertzian Contact Force. It implies that the length of spring should always be less than its original length in order to produce a Hertzian Force. If the length of spring becomes equal to or more than its original length, then the spring will not be in compression state anymore and no Hertzian force will be produced. Therefore, the bearing force produced by that spring is considered as zero.

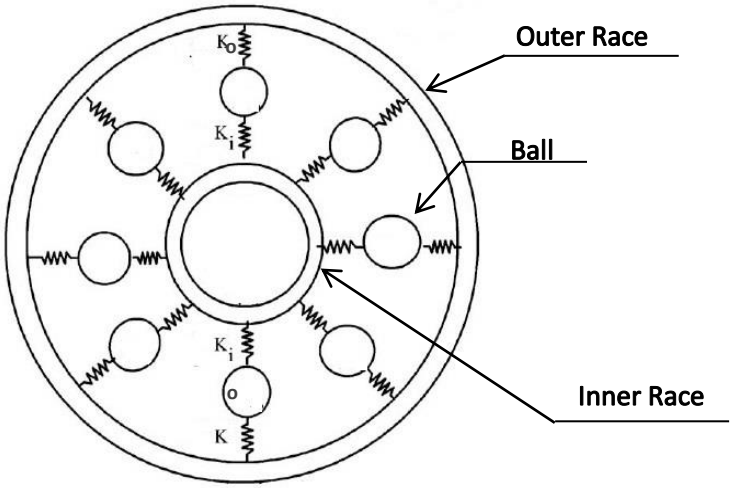

Fig. 3.3: Ball Bearing as Spring-Mass System [20]

3.2.1 Race Surface Waviness

In the vibration of rotor bearing system, surface waviness on the ball bearing's races has a significant role [13]. This assumed global sinusoidal shaped imperfection consists of peaks and valleys of varying width and height. In Fig. 3.4, the surface waviness on inner race and outer race is shown. Due to this, in the running condition of bearing, the amplitude of waviness imperfection varies continuously at the contact point of balls and races. The imperfection of different wave number excites distinct frequencies of vibration. In this way, the surface waviness cause additional vibrations [12]. The waviness wavelength is assumed to be greater than ball to race foot print so that due to contact deformation, the wave geometry can be considered as unaffected.

3.2.1.1 Inner Race Waviness

The balls of the Ball Bearing track the surface of races continuously. Assuming no-slip condition between the balls and races, the balls will always be in the contact of inner race and outer race. The waviness present on the inner race is radial and of the form of sinusoidal wave. The amplitude of inner surface waviness can be calculated as [12]:

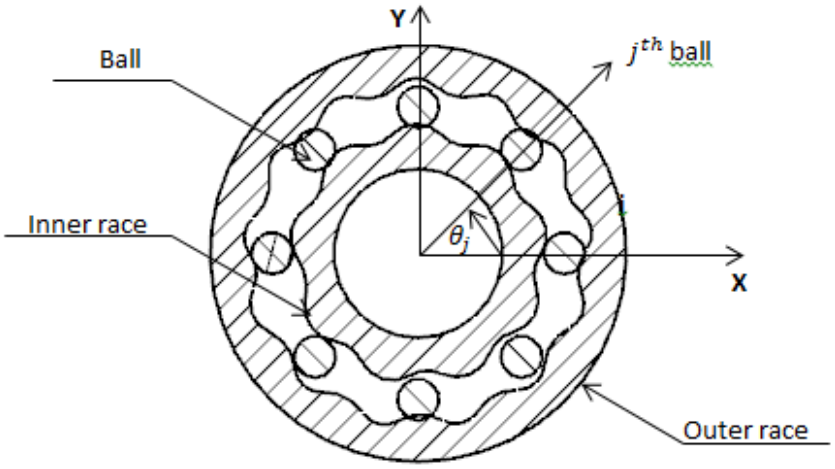

Fig. 3.4: Surface Waviness at inner race and outer race

$$\Upsilon_{ij} = \Upsilon_{pi} \sin\left(2\pi\frac{L}{\lambda}\right) \tag{3.16}$$

where, ' Υ_{pi}' is maximum amplitude of inner race surface waviness

Waviness wavelength can be expressed as:

$$\lambda = \frac{2\pi r_{in}}{N_w} \tag{3.17}$$

where, 'N_w' is the wave number or waviness order and r_{in} is inner race radius

The angular position for j^{th} ball of ball bearing is:

$$\theta_j = \frac{2\pi}{N_b}(j-1) + \omega_c t\,; \quad j = 1, 2, 3, \ldots\ldots N_b \tag{3.18}$$

where, 'ω_c' is the cage angular velocity

- Expression for 'ω_c' [10]

Tangential velocity of inner race:

$$v_{in} = r_{in}\,\omega_r \tag{3.19}$$

Tangential velocity of outer race:

$$v_{out} = r_{out}\,\omega_{out} \tag{3.20}$$

where, r_{out} is outer race radius and ω_{out} is the angular velocity of outer race

Tangential velocity of cage:

$$v_c = r_{pt}\,\omega_c \tag{3.20}$$

where pitch radius is $$r_{pt} = \frac{r_{in} + r_{out}}{2} \tag{3.22}$$

Considering pure rolling motion between balls and races:

$$v_c = {(v_{in} + v_{out})}/{2} \tag{3.23}$$

$$\omega_{out} = 0\,;\; v_{out} = 0$$

From equation 3.21 and 3.23

$$r_{pt}\,\omega_c = \left(\frac{r_{in}\,\omega_{in}}{2}\right) \tag{3.24}$$

From Equation 3.22 and 3.24

$$\omega_c = \omega_r \left(\frac{r_{in}}{r_{in}+r_{out}}\right) \tag{3.25}$$

Varying Compliance Frequency

$$\omega_{vc} = \omega_c\, N_b, \tag{3.26}$$

The rotor-bearing system vibrates at varying compliance frequency because of the ball bearings. The ball bearing caries load on the balls, whose angular position θ_j changes continuously with time with respect to line of action of the load. Such a change of angular position of balls causes the inner and outer race to undergo the periodic motion [10]. As a result, the system undergoes vibration at varying compliance frequency.

The balls of the ball-bearing are retained in a cage, because of it; the balls rotate at the same angular velocity as that of cage. Thus the angular displacement of balls is '$\omega_c t$' at time 't'. The inner race is secured to the rotor's shaft and rotates at shaft's angular velocity. This gives the angular displacement to inner race as '$\omega_r t$' at time 't'. Angular displacements of both inner race and ball are in the same direction; this mere makes the angular displacement of inner race and ball contact point after time 't' as '$(\omega_c - \omega_r)t$'.

The inner race waviness's amplitude at angular position of inner race and j^{th} ball contact is derived as:

$$\Upsilon_{ij} = \Upsilon_{pi} \sin\left(N_w(\theta_j - \omega_r t)\right) \tag{3.27}$$

Considering the inner race surface waviness, the inner race profile modified as [13]:

$$r_{in} + \Upsilon_{pi} \sin\left(N_w(\theta_j - \omega_r t)\right) \tag{3.28}$$

3.2.1.2 Outer Race Waviness

The outer race circumferential unevenness is taken as of same order of magnitude as that of inner race waviness. Outer race is fixed to the housing and the balls are rotating at the cage's speed. The mating point of outer race and balls is believed to move through an angular distance of '$\omega_c t$' in time t. For j^{th} ball of the bearing this angular distance can be expressed as:

$$\theta_j = \frac{2\pi}{N_b}(j-1) + \omega_c\, t \tag{3.29}$$

The outer race waviness at θ_j angular position is given by [12]:

$$\Upsilon_{oj} = = \Upsilon_{po} \sin(N_w \theta_j) \tag{3.30}$$

where, ' Υ_{po} ' is maximum amplitude of outer race surface waviness

Outer race profile including the outer race waviness is given by [13]:

$$r_{out} + \Upsilon_{po} \sin(N_w \theta_j) \tag{3.31}$$

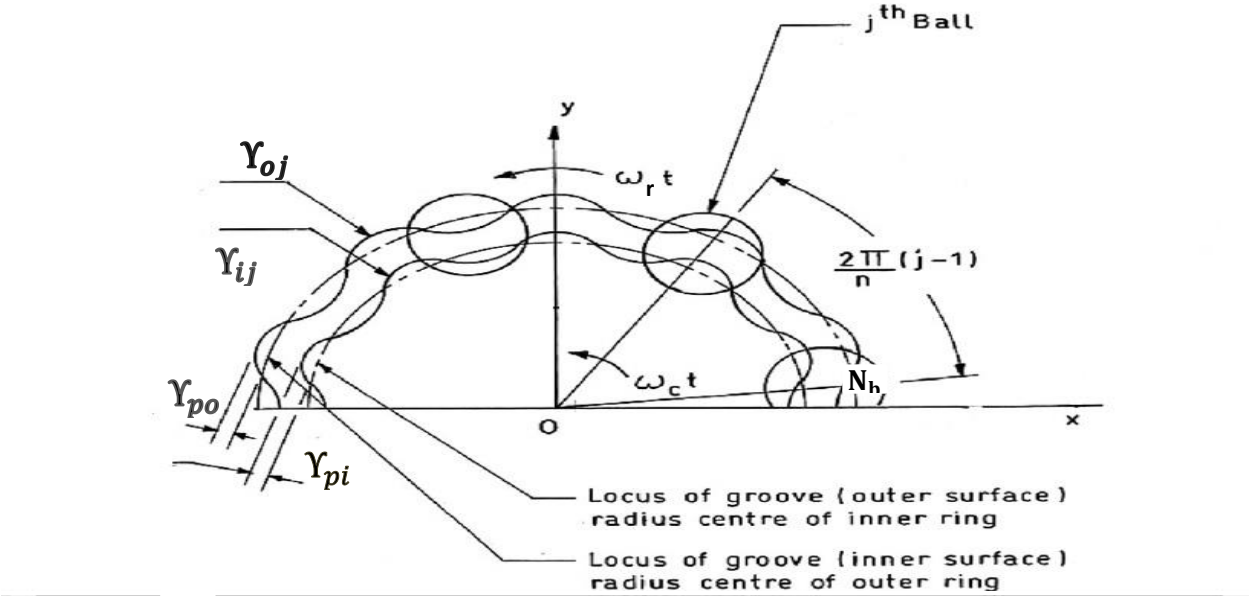

Fig. 3.5: Schematic Diagram of Waviness [2]

3.2.2 Contact Stiffness

Hertz point out that the stress at the mating point of balls and races in the ball bearing are distributed over an ellipsoidal contact area, it avoids the situation of infinite stress [10]. To evaluate contact stiffness between balls and races, the curvature sum and curvature difference is needed to calculate first [12].

Curvature Sum:

$$\sum \rho = \rho_{I1} + \rho_{I2} + \rho_{II1} + \rho_{II2} = \frac{1}{r_{I1}} + \frac{1}{r_{II1}} + \frac{1}{r_{I2}} + \frac{1}{r_{II2}} \tag{3.32}$$

Curvature Difference:

$$F(\rho) = \frac{(\rho_{I1} - \rho_{I2}) + (\rho_{II1} - \rho_{II2})}{\sum \rho} \tag{3.33}$$

where, ρ is the curvature

The curvature is considered negative for concave surface and positive for convex surface.

- The curvature at the contact point of inner race and ball using Fig. 3.6:

Body I denotes the contacting Ball and Body II denotes Inner race

$$r_{I1} = \frac{D}{2},\ r_{I2} = \frac{D}{2},\ r_{II1} = r_{in},\ r_{II2} = r_i$$
$$\rho_{I1} = \frac{2}{D},\ \rho_{I2} = \frac{2}{D};\ \rho_{II1} = \frac{1}{r_{in}},\ \rho_{II2} = -\frac{1}{r_i} \tag{3.34}$$

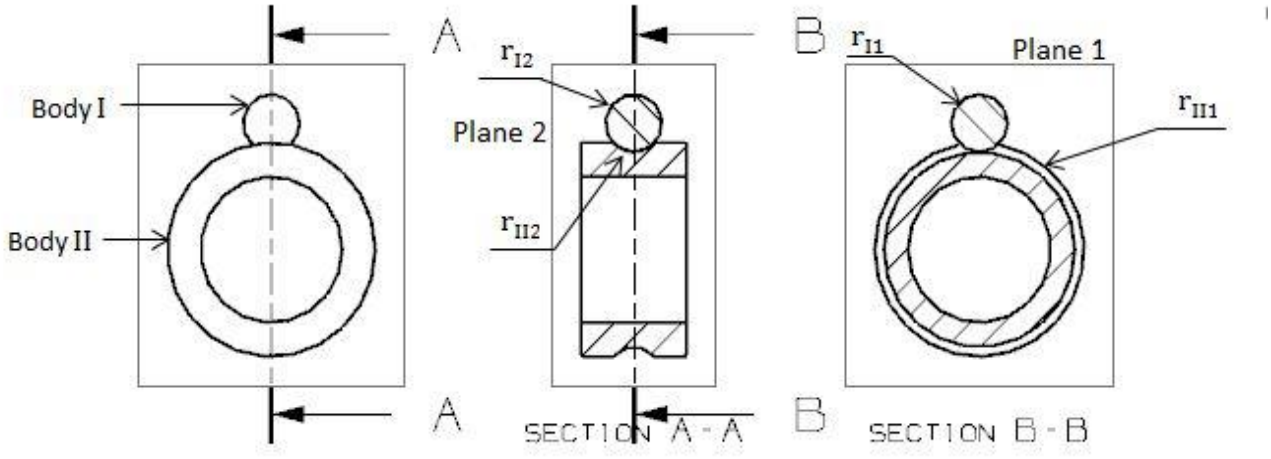

Fig. 3.6: Cut section of inner race-ball contact

➢ The curvature at the contact point of outer race and ball using Fig. 3.7 :

Body I denotes the contacting Ball and Body II denotes Outer Race

$$r_{I1} = \frac{D}{2},\ r_{I2} = \frac{D}{2},\ r_{II1} = r_{out},\ r_{II2} = r_o$$
$$\rho_{I1} = \frac{2}{D},\ \rho_{I2} = \frac{2}{D};\ \rho_{II1} = -\frac{1}{r_{out}},\ \rho_{II2} = -\frac{1}{r_o} \tag{3.35}$$

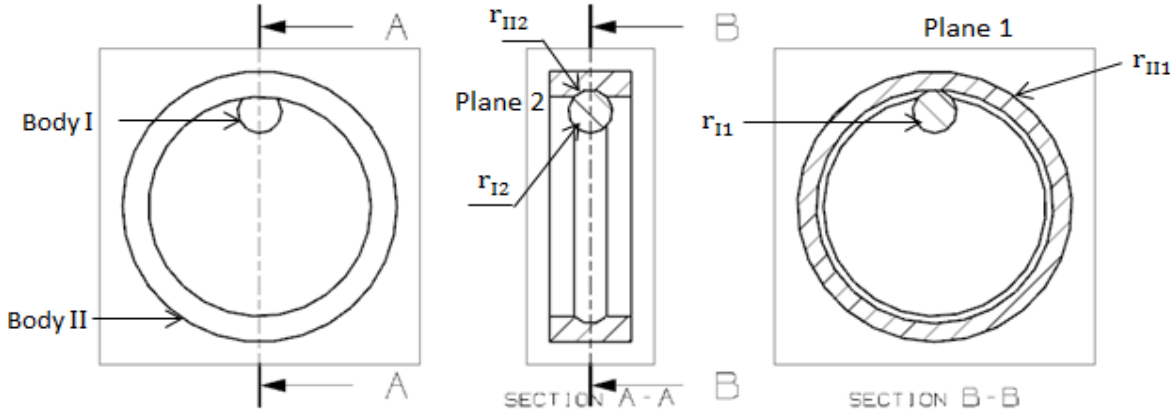

Fig. 3.7: Cut-Section of outer race and ball contact

➢ The relative approach between the mating balls and races is

$$\delta = 2.787 \times 10^{-8}\, Q^{\frac{2}{3}} \left(\sum \rho\right)^{\frac{1}{3}} \delta^{*}\ (\text{mm}) \tag{3.36}$$

where, δ^{*} is the dimensionless contact parameter.

➢ The Contact force Q at the mating point of balls and races:

$$Q = \left\{3.587 \times 10^{7} \left(\sum \rho\right)^{-\frac{1}{2}} \delta^{*-\frac{3}{2}}\right\} \delta^{\frac{3}{2}}\ \ (\text{N}). \tag{3.37}$$

➢ The Elastic Stiffness at the contact of balls and inner race of Ball Bearing

$$K_i = \left\{3.587 \times 10^{7} \left(\sum \rho_i\right)^{-\frac{1}{2}} \delta_i^{*-\frac{3}{2}}\right\} \quad \left(\frac{N}{mm^{-\frac{3}{2}}}\right) \tag{3.38}$$

- The Elastic Stiffness at the contact of balls and outer race of Ball Bearing

$$K_o = \left\{3.587 \times 10^7 \left(\sum \rho_o\right)^{-\frac{1}{2}} \delta_o^{*\,-\frac{3}{2}}\right\} \left(\frac{N}{mm^{-\frac{3}{2}}}\right) \tag{3.39}$$

- Effective Contact Stiffness

Ball bearing is assumed as a spring mass system, as shown in Fig. 3.3

$$Q_{in} = K_i \delta_{in}^{\frac{3}{2}}$$

$$Q_{out} = K_o \delta_{out}^{\frac{3}{2}} \tag{3.40}$$

$$Q_{eff} = K_{eff} \delta_{eff}^{\frac{3}{2}}$$

Based on the configuration of assumed spring mass system,

$$Q_{eff} = Q_{out} = Q_{in} \text{ and } \delta_{eff} = \delta_{out} + \delta_{in}$$

$$\frac{Q_{eff.}^{2/3}}{K_{eff.}} = \frac{Q_{in}^{2/3}}{K_i} + \frac{Q_{out}^{2/3}}{K_o} \tag{3.41}$$

$$K_{eff.} = \left(\frac{1}{\frac{1}{K_i}^{\frac{2}{3}} + \frac{1}{K_o}^{\frac{2}{3}}}\right)^{3/2} \tag{3.42}$$

To evaluate elastic stiffness at the contact point of both inner race and outer race with the ball, first, curvature sum and curvature difference is calculated for both inner race and outer race using equations 3.32 to 3.35. Then using Table 3.1, the dimensionless contact parameter is calculated. All three values: curvature sum, curvature difference and dimensionless contact parameter are used in 3.38 and 3.39 to calculate elastic stiffness of inner race and outer race respectively. These elastic stiffness values are used in equation 3.42, to calculate effective elastic stiffness of the ball bearing at the contact point of inner race and outer race with ball.

Table 3.1: Dimensionless Contact Parameter [10]

Curvature Difference ($F(\rho)$)	Dimensionless Contact Parameter (δ^*)
0	1
0.1075	0.997
0.3204	0.9761
0.4795	0.9429
0.5916	0.9077
0.6717	0.8733
0.7332	0.8394
0.7948	0.7961
0.83595	0.7602
0.87366	0.7169
0.90999	0.6636
0.93657	0.6112
0.95738	0.5551
0.97290	0.4960
0.983979	0.4352
0.990902	0.3745
0.995112	0.3176
0.995300	0.2705
0.9981847	0.2427
0.9989156	0.2106
0.9994785	0.17167
0.9998527	0.11995
1	0

3.2.3 Restoring Force

The effective contact force between balls and race also called the restoring force is expressed as:

$$Q = K\delta^{\frac{3}{2}} \tag{3.43}$$

δ is the elastic deformation taking place at the mating point of balls and races. When the rotor node at bearing location displace due to rotor deflection, it builds an interaction between the inner race, balls and the outer race of the bearing. It generates an elastic deformation δ at mating of balls and races.

The surface waviness modifies the profile of races by adding varying peaks and valleys along the race circumference as given in the equation 3.28 and 3.31. This mere alters the elastic deformation of contact point of balls and races.

The internal radial clearance is provided between balls and races of the bearing to compensate the thermal expansion that takes place during running state of bearing. The internal clearance changes the distance between the balls and races, therefore modifies the elastic deformation of contact points of races and balls. Hence, the internal clearance and surface waviness has to be included in the calculation of elastic deformation.

$$\delta_j = q_1 \mathrm{Cos}\theta_j + q_2 \mathrm{Sin}\theta_j + \Upsilon_{ij} - \Upsilon_{oj} - \mathrm{clearance} \tag{3.44}$$

where,

$$\theta_j = \frac{2\pi}{N_b}(j-1) + \omega_c t \tag{3.45}$$

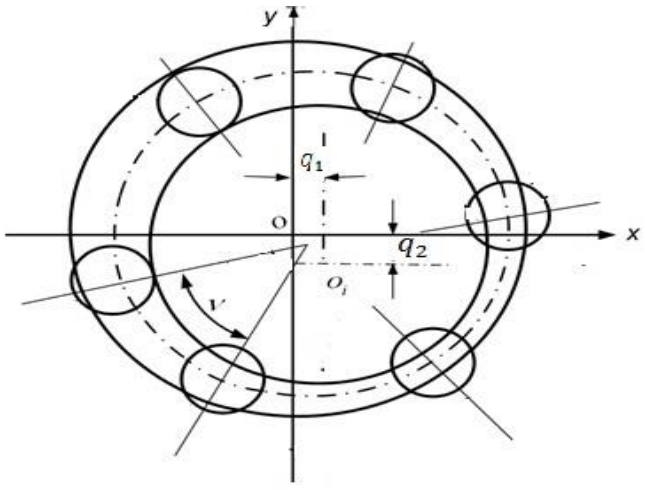

Fig. 3.8: Deformation in balls and races [26]

The balls of the ball bearing are retained to the cage with the precise angular separation of 'ν':

$$\nu = \frac{2\pi}{N_b}$$

where, N_b is the number of balls in the bearing.

Fig. 3.8 shows a typical ball bearing in the deformed state at contact of balls and races. When the bearing center node is displaced from its center position O to the displaced position O_i, the balls in the region of node's displaced direction gets deformed. The deformation also depends on the values of internal clearance and surface waviness amplitude at the interaction point. The deformation at the ball-race contact is considered only if the value of equation 3.44 comes out to be greater than zero. Such contact deformation generates a restoring force between balls and races with nonlinear characteristics.

Contact force:

$$Q_j = K\delta_j^{\frac{3}{2}} \tag{3.46}$$

$$Q_j = K_{eff}(q_1 Cos\theta_j + q_2 Sin\theta_j + \Upsilon_{ij} - \Upsilon_{oj} - clearance)^{3/2} \tag{3.47}$$

The Restoring force in equation 3.47 is calculated at an angular position θ_j of the j^{th} ball. If δ_j of j^{th} ball location appears greater than zero, it contributes to raise the restoring force Q_j at that location. However, if δ_j at the j^{th} ball location approaches to zero or less than zero, the j^{th} balls would not remain in the deformed state and the restoring contact force becomes zero. The net restoring force generated by ball bearing is the sum of restoring force generated at each ball-races contact. Net restoring force in horizontal x-direction and in Vertical y-direction is given by equation 3.48:

$$\begin{aligned} Q_X &= \sum_{j=1}^{Nb} K_{eff}(q_1 Cos\theta_j + q_2 Sin\theta_j + \Upsilon_{ij} - \Upsilon_{oj} - clearance)^{3/2} Cos\theta_j \\ Q_Y &= \sum_{j=1}^{Nb} K_{eff}(q_1 Cos\theta_j + q_2 Sin\theta_j + \Upsilon_{ij} - \Upsilon_{oj} - clearance)^{3/2} Sin\theta_j \end{aligned} \tag{3.48}$$

These restoring force components are shown in Fig. 3.9. They impact the rotor in opposite direction of deformation taking place between balls and races. The components of Restoring forces shown in equation 3.48 are added algebraically to the global load vector of rotor at the

respective global degree of freedom in such a manner that, these restoring forces would influence the rotor in opposite direction of ball deformation.

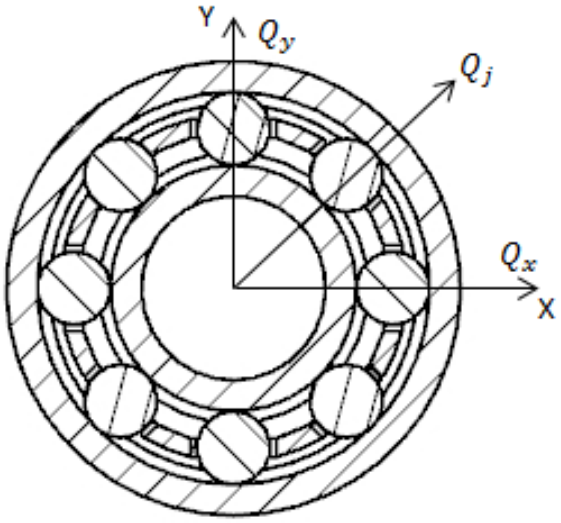

Fig. 3.9: Restoring force components

3.3 The Complete Rotor-Ball Bearing System

The rotor ball bearing system is demonstrated by modeling the rotor and ball bearing separately. The rotor shaft is modeled through finite element technique and ball bearing is modeled by considering 2-degree of freedom bearing model. The bearing is attached to rotor by the means of restoring force only, which is generated between balls and races, as discussed in section 3.2.3. A typical finite element model is shown in Fig. 3.10.

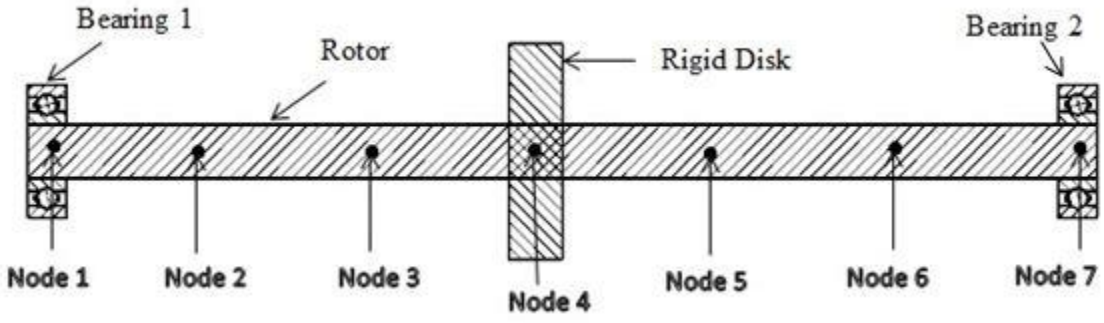

Fig. 3.10: Finite Element Model of Rotor

3.3.1 Rotor Shaft Model

In the finite element method applied to rotor, the rotor is discretized into six elements, as described in section 3.1.1. The elemental equation of the rotor derived earlier is reproduced here as:

$$([M_T^e + M_R^e])\{\ddot{q}_e\} - \omega_r[G]^e\{\dot{q}_e\} + [K]^e\{q_e\} = \{Q_g^e\} \tag{3.49}$$

Each element has its own mass matrix, gyroscopic matrix, stiffness matrix and generalized force vector. These matrices are assembled node wise to form corresponding global matrices of system.

3.3.2 Rigid Disk Model

Equation derived for the rigid disk in section 3.2.1 is reproduced here as:

$$\left([M_T^d + M_R^e]\right)\{\ddot{q}_d\} - \omega_r\,[G^d]\{\dot{q}_d\} = \{Q_{un}^d\} \tag{3.50}$$

The mass matrix, gyroscopic matrix and the force vector of the rigid disk are added to the global system matrices by combining the disk matrices to the corresponding global matrices at the disk node position (Node 4).

3.3.3 Ball Bearing Model

The Bearing produces restoring force by the elastic deformation at the contact point of balls and races. These restoring force components derived in section 3.2.3 are reproduced here as:

$$Q_X = \sum_{j=1}^{N_b} K_{eff}(q_1 Cos\theta_j + q_2 Sin\theta_j + \Upsilon_{ij} - \Upsilon_{oj} - clearance)^{3/2}\ Cos\theta_j$$

$$Q_Y = \sum_{j=1}^{N_b} K_{eff}(q_1 Cos\theta_j + q_2 Sin\theta_j + \Upsilon_{ij} - \Upsilon_{oj} - clearance)^{3/2}\ Sin\theta_j$$

The restoring force generated at each ball-race contact of the bearing got exerted to the rotor in opposite direction of deformation took place at that ball location. All these restoring force components are summed algebraically and are added to the global force vector of the system at the corresponding node location of bearing.

3.3.4 Globalized Equation of Motion

The globalized equation of motion including the matrices corresponding to rotor, disk and bearing are:

$$([\mathrm{M_T} + \mathrm{M_R}])\{\ddot{\mathrm{q}}\} - \omega_r[\mathrm{G}]\{\dot{\mathrm{q}}\} + [\mathrm{K}]\{\mathrm{q}\} = \{\mathrm{Q}\} \tag{3.51}$$

$\{q\}$ is the displacement vector of the system $\{q_1, q_2, q_3, q_4, q_5 \dots \dots q_{26}, q_{27}, q_{28}\}$

Global Force vector {Q} includes Gravity load of shaft and disk, Unbalance time varying force from disk eccentric mass, and Nonlinear Bearing Force (Restoring Force):

$$\{\mathrm{Q}\} = \{\mathrm{Q}_g\} + \{\mathrm{Q}_{un}\} + \{\mathrm{Q}_b\} \tag{3.52}$$

3.4 Numerical Integration

The Governing differential equation 3.51 is solved by time integration technique Newmark β with Newton Raphson iteration method [4], [5]. For such systems, several solutions exist for the same rotor speed, therefore with this method it is strenuous to ascertain as to which solution system would reach at a particular rotational speed. The benefit of using Newmark β is, this method calculates steady state response without bypassing transient response.

- Newmark β with Newton Raphson:

Governing Differential equation derived in section 3.3:

$$([\mathrm{M_T} + \mathrm{M_R}])\{\ddot{\mathrm{q}}\} - \omega_r[\mathrm{G}]\{\dot{\mathrm{q}}\} + [\mathrm{K}]\{\mathrm{q}\} = \{\mathrm{Q}\}$$

At time t_i,

$$([\mathrm{M_T} + \mathrm{M_R}])\{\ddot{\mathrm{q}}\}_i - \omega_r[\mathrm{G}]\{\dot{\mathrm{q}}\}_i + [\mathrm{K}]\{\mathrm{q}\}_i = \{\mathrm{Q}\}_i \tag{3.53}$$

At time t_{i+1},

$$([\mathrm{M_T} + \mathrm{M_R}])\{\ddot{\mathrm{q}}\}_{i+1} - \omega_r[\mathrm{G}]\{\dot{\mathrm{q}}\}_{i+1} + [\mathrm{K}]\{\mathrm{q}\}_{i+1} = \{\mathrm{Q}\}_{i+1} \tag{3.54}$$

According to Newmark β method

$$\{\dot{\mathrm{q}}\}_{i+1} = \{\dot{\mathrm{q}}\}_i + [(1-\varsigma)\Delta t]\{\ddot{\mathrm{q}}\}_i + (\varsigma\Delta t)\{\ddot{\mathrm{q}}\}_{i+1} \tag{3.55}$$

$$\{q\}_{i+1} = \{q\}_i + \{\dot{q}\}_i \Delta t + \left[\left(\frac{1}{2} - \beta\right)(\Delta t)^2\right] \{\ddot{q}\}_i + (\beta(\Delta t)^2)\{\ddot{q}\}_{i+1} \quad (3.56)$$

where ς *and* β are Newmark Constant

For Average Acceleration: $\varsigma = \frac{1}{2}$; $\beta = \frac{1}{4}$

For Linear Acceleration: $\varsigma = \frac{1}{2}$; $\beta = \frac{1}{6}$

In the formulation, Average Acceleration is chosen to keep the algorithm unconditionally stable.

Let:
$$c_1 = \frac{\varsigma}{\beta \Delta t}; \qquad c_2 = \frac{\varsigma}{\beta}; \qquad c_3 = \Delta t\left(1 - \frac{\varsigma}{2\beta}\right);$$
$$c_4 = \frac{1}{\beta(\Delta t)^2}; \quad c_5 = \frac{1}{\beta \Delta t}; \quad c_6 = \frac{1}{2\beta}; \quad (3.57)$$

Using the equations 3.53 to 3.57

$$\{\dot{q}\}_{i+1} = \{\dot{q}\}_i + c_1\{q\}_{i+1} - c_1\{q\}_i - c_2\{\dot{q}\}_i - c_3\{\ddot{q}\}_i \quad (3.58)$$

$$\{\ddot{q}\}_{i+1} = \{\ddot{q}\}_i + c_4\{q\}_{i+1} - c_4\{q\}_i - c_5\{\dot{q}\}_i - c_6\{\ddot{q}\}_i \quad (3.59)$$

Putting equation 3.58 and 3.59 to equation 3.54

$$([M_T + M_R])(\{\ddot{q}\}_i + c_4\{q\}_{i+1} - c_4\{q\}_i - c_5\{\dot{q}\}_i - c_6\{\ddot{q}\}_i) - (\omega_r[G])(\{\dot{q}\}_i + c_1\{q\}_{i+1} - c_1\{q\}_i - c_2\{\dot{q}\}_i - c_3\{\ddot{q}\}_i) + [K]\{q\}_{i+1} = \{Q\}_{i+1} \quad (3.60)$$

Rearranging the terms of equation 3.60

$$(c_4([M_T + M_R]) - c_1\omega_r[G] + [K])\{q\}_{i+1} = \{Q\}_{i+1} - [([M_T + M_R])(\{\ddot{q}\}_i - c_4\{q\}_i - c_5\{\dot{q}\}_i - c_6\{\ddot{q}\}_i)] + [(\omega_r[G])(\{\dot{q}\}_i - c_1\{q\}_i - c_2\{\dot{q}\}_i - c_3\{\ddot{q}\}_i)] \quad (3.61)$$

Let:
$$[\widehat{K}] = c_4([M_T + M_R]) - c_1\omega_r[G] + [K]; \quad (3.62)$$

$$[\widehat{P}]_{i+1} = [([M_T + M_R])(\{\ddot{q}\}_i - c_4\{q\}_i - c_5\{\dot{q}\}_i - c_6\{\ddot{q}\}_i)] - [(\omega_r[G])(\{\dot{q}\}_i - c_1\{q\}_i - c_2\{\dot{q}\}_i - c_3\{\ddot{q}\}_i)]; \quad (3.63)$$

$$[\widehat{\mathrm{K}}]\{\mathrm{q}\}_{i+1} = \{\mathrm{Q}\}_{i+1} - [\widehat{\mathrm{P}}]_{i+1} \tag{3.64}$$

Using equation 3.64, first predicted displacement vector is calculated. This value would have high errors, so the Newton Raphson iteration is used to iterate the displacement vector to get its precise value.

In equation 3.64, $[\widehat{\mathrm{P}}]_{i+1}$ is in the terms of i^{th} time displacement, velocity and acceleration vectors as shown in equation 3.63. So now, after calculating the displacement vector for time $i+1^{th}$ using equation 3.64, the available displacement, velocity and acceleration vectors for time $i+1^{th}$, are used to calculate $[\widehat{\mathrm{P}}]_{i+1}$ again as:

$$[\widehat{\mathrm{P}}]_{i+1} = ([\mathrm{M_T} + \mathrm{M_R}])\{\ddot{\mathrm{q}}\}_{i+1} - \omega_r[\mathrm{G}]\{\dot{\mathrm{q}}\}_{i+1} + [\mathrm{K}]\{\mathrm{q}\}_{i+1} \tag{3.65}$$

Equation 3.64 is evaluated as

$$f(q^*) = \{\mathrm{Q}\}_{i+1} - [\widehat{\mathrm{P}}]_{i+1} \tag{3.66}$$

Such that at displacement vector q^* the equation approaches to zero.

By applying Taylor series expansion to equation 3.66

$$f(q^*) = (\{\mathrm{Q}\}_{i+1} - [\widehat{\mathrm{P}}]_{i+1})^{n-1} + \left(\frac{df(q^*)}{dq}\right)^{n-1}(q^* - q^{n-1}) \tag{3.67}$$

$f(q^*) = 0$, Hence

$$-\left(\frac{df(q^*)}{dq}\right)^{n-1}(q^* - q^{n-1}) = (\{\mathrm{Q}\}_{i+1} - [\widehat{\mathrm{P}}]_{i+1})^{n-1} \tag{3.68}$$

$$dq = (q^* - q^{n-1})$$

$$-\left(\frac{df(q^*)}{dq}\right)^{n-1} = -\left(\frac{d(\{\mathrm{Q}\}_{i+1} - [\widehat{\mathrm{P}}]_{i+1})}{dq}\right)^{n-1} \tag{3.69}$$

$$-\left(\frac{df(q^*)}{dq}\right)^{n-1} = [\mathrm{K}] - \left(\frac{d(\{\mathrm{Q}\})_{i+1}}{dq}\right)^{n-1} \tag{3.70}$$

The force vector $\{Q\}_{i+1}$ includes unbalance time varying force, constant gravity load and nonlinear bearing force which are dependent on time and on displacement vector as well. Therefore, the derivative of $\{Q\}_{i+1}$ with respect of q displacement vector will give Bearing Stiffness matrix only.

$$dq = \left(\{Q\}_{i+1} - \left[\widehat{P}\right]_{i+1}\right)^{n-1} \Big/ -\left(\frac{df(q^*)}{dq}\right)^{n-1} \tag{3.71}$$

The iterations are performed by repeating equation 3.71, by replacing n-1→ n and so on, to get change in displacement vector dq equals to zero. These iterations are Newton Raphson iterations. In these iterations, initial value of displacement is the calculated by Newmark β method from equation 3.64. The above steps from equation 3.58 to 3.71 are repeated for all successive time steps.

In the numerical analysis, the initial conditions and size of time step are important factors to get a continuous and computationally economic solution. Basically in the nonlinear system, different initial condition means a totally different solution. Larger time step makes computation faster, while smaller time step gives solution more accurate. So, an optimized initial condition and time steps should be chosen to get satisfactory and acceptable results [11]. For the analysis considered here, the time step taken is 1/300th part of the time period corresponding to varying compliance frequency of the balls bearing [9] and the initial value of displacement vector and velocity vector is taken as zero.

$$dt = \frac{1}{300}(t_{vc})$$
$$\{q\}_0 = 0 \ , \ \{\dot{q}\}_0 = 0 \tag{3.72}$$

3.5 Specifications of the Model

The rotor's shaft is considered flexible and the bearing is single row deep groove ball bearing; 6306/JIS, to perform parametric studies [9]. Material of whole system is considered as steel. Specifications of shaft and disk, and bearing are given in Table 3.2, Table 3.3 respectively.

Table 3.2: Specifications and parameters of shaft and disk [9]

Parameter	**Value**
Radius of Shaft (r_s)	7.5 (mm)
Length of Shaft (l_s)	400 (mm)
Young's Modulus of steel (E)	2.08×10^{11} (N/m^2)
Density of steel (ρ)	7.8×10^3 (kg/m^3)
Mass of shaft per unit length (μ)	1.3776 (kg/m)
Mass of Disk (m_d)	15.9586 (kg)
Polar Moment of Inertia of Disk (I_p^d)	1.28×10^{-2} (kgm^2)
Diametric Moment of Inertia of Disk (I_d^d)	0.64×10^{-2} (kgm^2)

Table 3.3: Specification of Ball Bearing 6306/JIS [9]

Parameter	**Value**
Number of Balls (N_b)	8
Inner Race Radius (r_{in})	20.0468 (mm)
Outer Race Radius (r_{out})	31.953 (mm)
Radial Clearance	20 (μm)
Effective Stiffness ($K_{eff.}$)	3.529×10^9 ($N/m^{3/2}$)
Surface Waviness Maximum Amplitude of inner race (Υ_{pi})	2 (μm)
Surface Waviness Maximum Amplitude of outer race (Υ_{po})	2 (μm)

The Waviness order of the surface waviness of both inner race and outer race are varied by 5, 8, 13, and 18 to perform parametric study and to predict the dynamic behavior of rotor system proposed here, by changing waviness orders

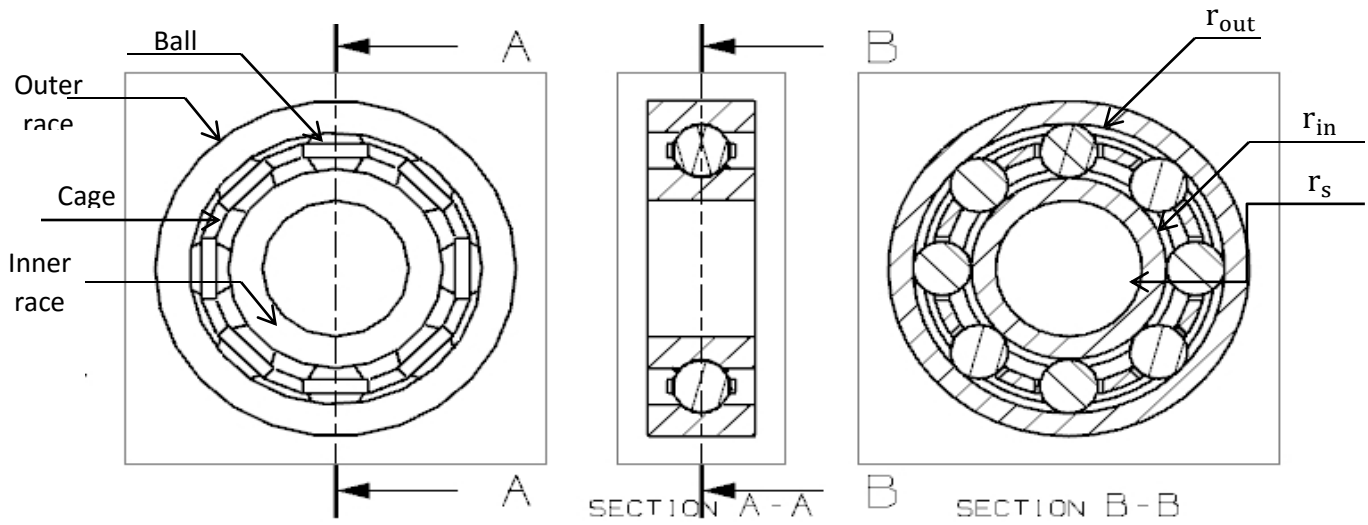

Fig. 3.11: Cut-Section of ball-bearing

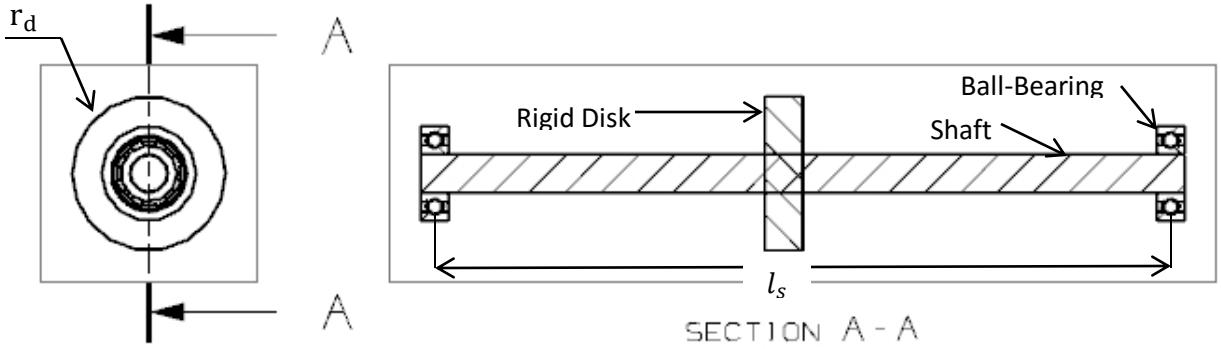

Fig. 3.12: Cut-Section of rotor-bearing system

4 Results and Discussion

The system is highly nonlinear due to the presence of Hertzian contact force in ball bearing and time varying unbalance force of disk, as a result of which, system shows complex dynamic behavior. In order to study nonlinear dynamic behavior of the system, the displacement plots, dynamic orbits and frequency spectra of the system are plotted in MATLAB. The plots are made for rotor node at disc location (node 4) and for rotor node at bearing 1 location (node 1). Both bearings are considered to be identical, so that, the analyses is performed on the bearing 1 only which is located at node 1, as shown in Fig. 3.10. The displacement plots and frequency spectra are plotted along with and without surface waviness on bearing's races. Through frequency spectra, the impact of surface waviness is studied on the dynamic response of the system. The waviness order of the surface waviness is varied by 5, 8, 13 and 16 of both inner race and outer race of the bearing and the corresponding displacement plots and frequency spectra are developed. The obtained frequency spectra having the excited frequencies are validated by Yhland [24].

Rotational speed of rotor is taken as 191 rpm. At this speed, the rotational frequency of inner race or shaft, cage rotational frequency and varying compliance frequency are computed as 3.1817 Hz, 1.2266 Hz and 9.8129 Hz respectively.

4.1 Bearings without Waviness

The displacement plots and dynamic orbits for the bearing without waviness are shown in Fig. 4.1 and Fig. 4.2. The displacement plots are plotted for disk node horizontal and vertical displacement, and bearing node horizontal and vertical displacement. The frequency spectra are formed by transforming the time-domain signal of displacement plots into frequency domains though fast fourier transformation in MATLAB. In this way, the frequency spectra are created for disk node horizontal and vertical displacement, and bearing node horizontal and vertical displacement. These frequency Spectra without considering surface waviness on the races are shown in Fig. 4.3 and Fig. 4.4. The elastic deformation between races will be affected by internal clearance only. In these two figures, the frequencies are present at rotational frequency, varying compliance frequency and at higher harmonics of varying compliance. The frequency spectrum

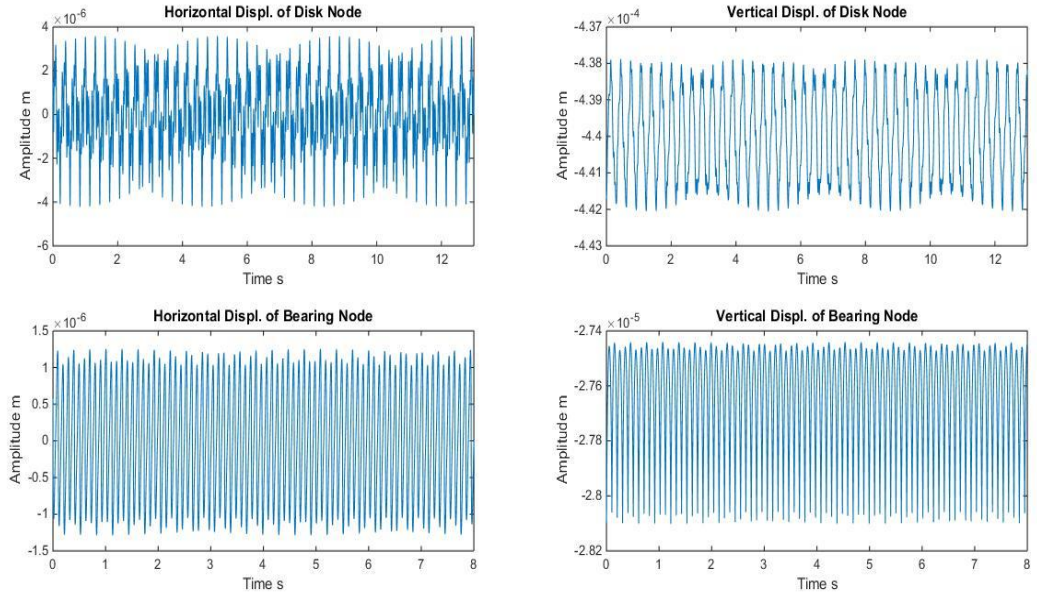

Fig. 4.1: Displacement plots of rotor with bearings without surface waviness on the races

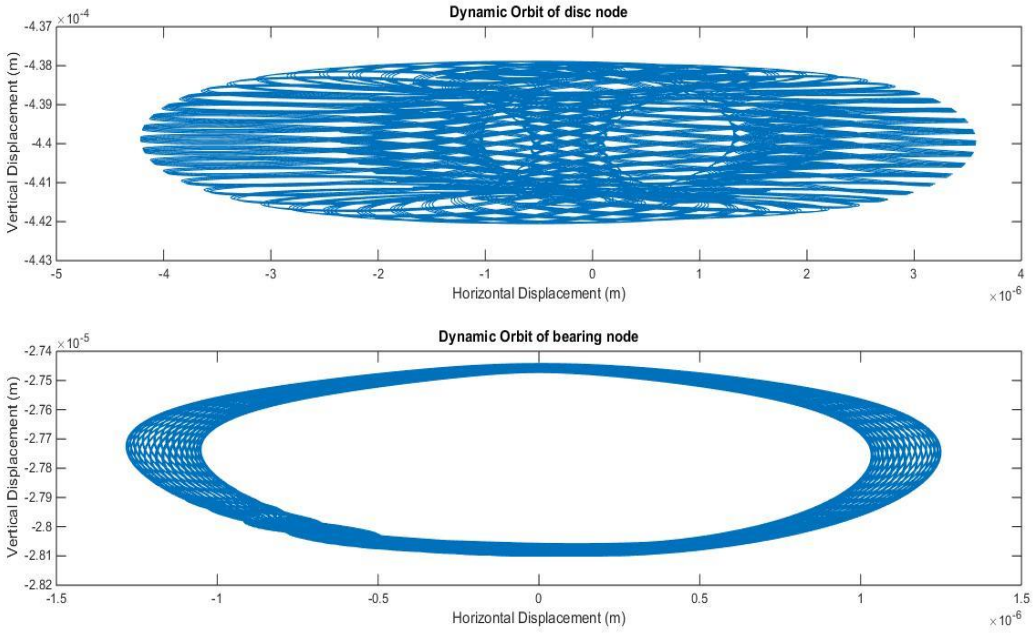

Fig. 4.2: Dynamic orbits of rotor with bearings without surface waviness on the races

shows peaks at varying compliance and its higher harmonics because of nonlinear Hertzian contact force of ball bearing. The varying compliance frequency depends on number of balls in

the bearing and cage rotational frequency. Frequency spectrum shows peak at rotational frequency also, due to the presence rotating imbalance force of the disk. The Fig. 4.3 shows frequency spectra in both horizontal and vertical direction of the rotor node at disk location, in which the rotational frequency f_r dominates by attaining highest peak in FFT plot. It is because; the rotating imbalance force dominates the bearing Hertzian contact force at disk node. The amplitude in FFT plots of horizontal displacement and vertical displacement is coming same at

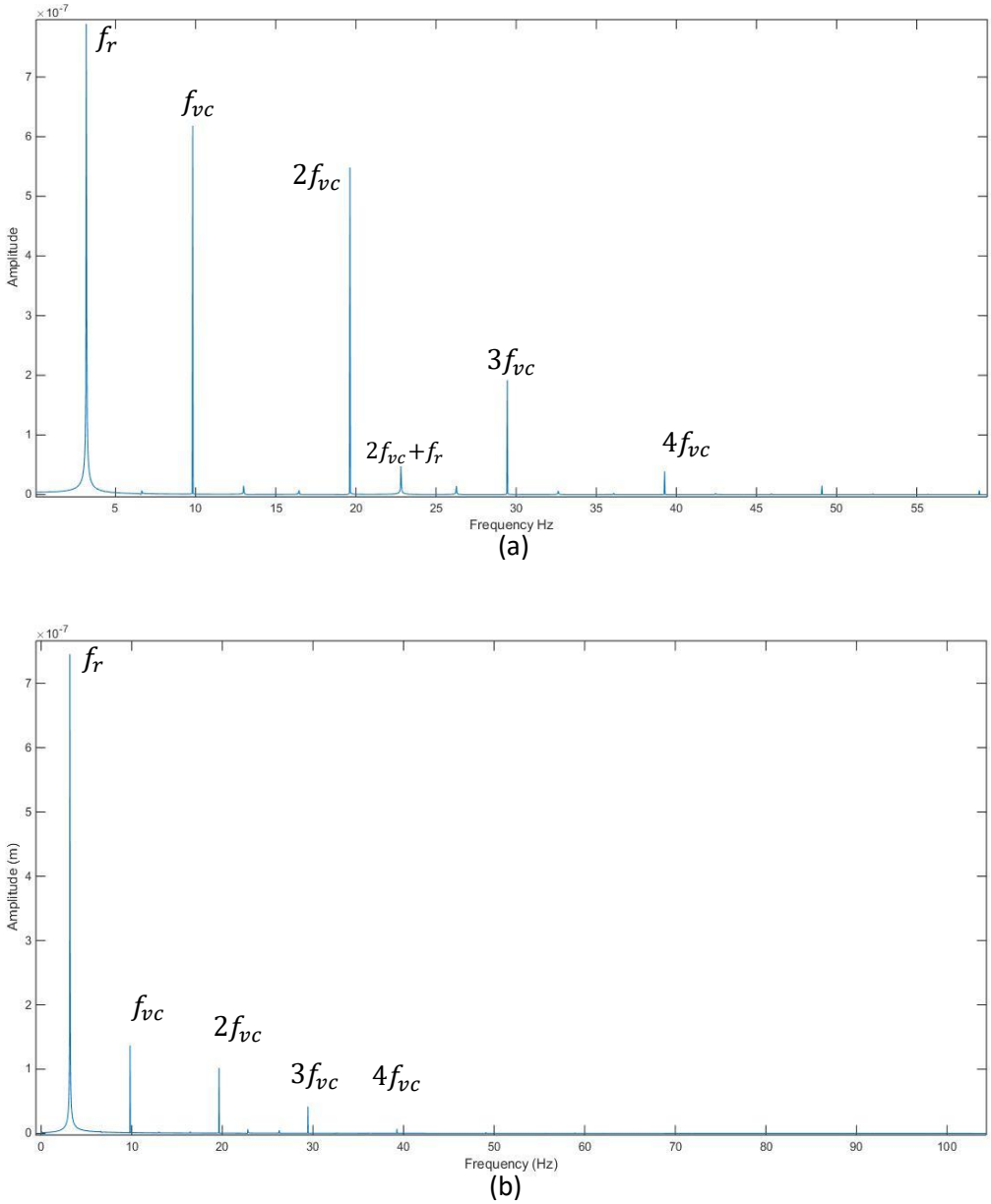

Fig. 4.3: Frequency Spectra of rotor center at disk (a) Horizontal Direction (b) Vertical Direction

rotational frequency f_r. Other amplitude appears at variable compliance frequencies f_{vc} and its higher harmonics. The amplitudes decrease at higher harmonics of varying compliance swiftly in both FFT curves. The highest harmonics of varying compliance appears as $4f_{vc}$ of 0.04 µm amplitude in frequency spectra of horizontal displacement and of 0.01 µm amplitude in the frequency spectra of vertical displacement respectively. The amplitudes at varying compliance frequency and its harmonics in FFT curve of horizontal displacement is higher than the

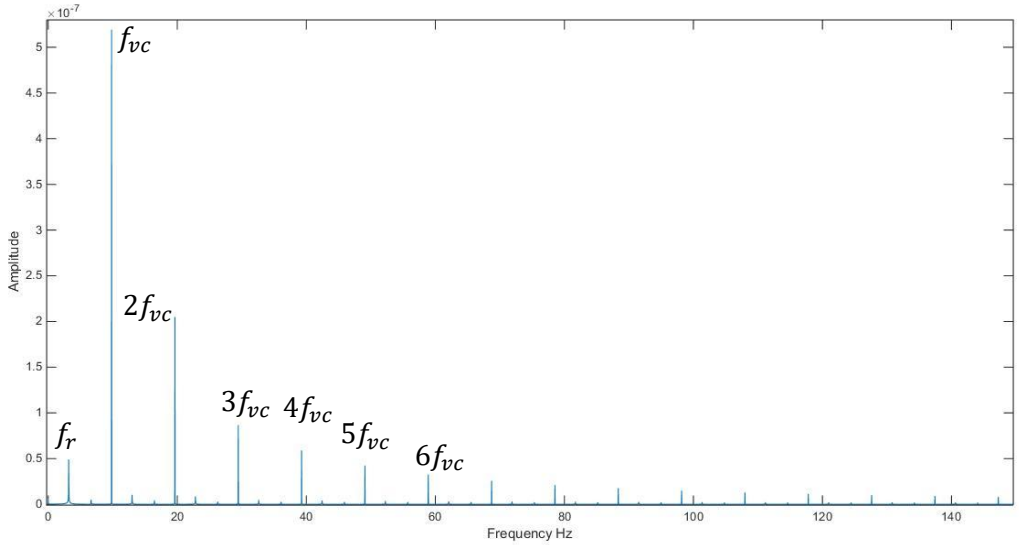

(a)

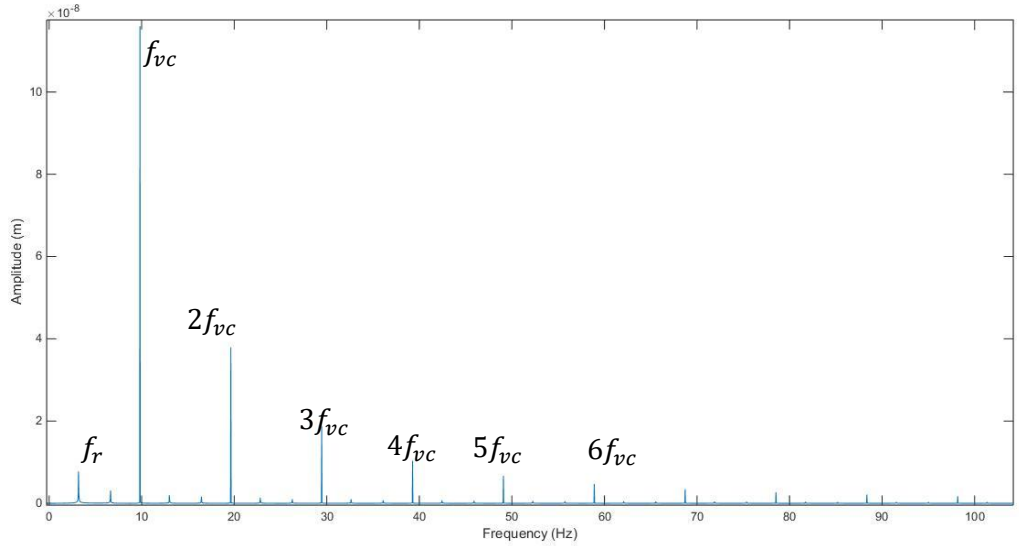

(b)

Fig. 4.4: Frequency Spectra of rotor center at bearings (a) Horizontal direction (b) Vertical direction

amplitudes at varying compliance and its harmonics appearing in FFT curve of vertical displacement. Fig. 4.4 shows FFT plot of horizontal displacement and vertical displacement of rotor node at bearing location. The amplitude at varying compliance frequency dominates in both FFT plots. While, from Fig. 4.3, at disk node, rotational frequency dominates. This shows that, at bearing location Hertzian Contact force dominates the rotational imbalance force. The other frequencies in these FFT plots of Fig. 4.3 and 4.4 are appearing at higher harmonics of varying compliance, with decreasing amplitude as the harmonics increases.

4.2 Inner Race Waviness effect

The inner race waviness is considered at the outer surface of the inner race, as a sinusoidal wave of maximum amplitude of 2 µm. The waviness order is varied by 5, 8, 13 and 16 to predict its effect on dynamic response of the system. The displacement plots and dynamic orbits are plotted for disk node and for the bearing node at different waviness orders. Using these displacement plots obtained for different waviness orders, the frequency spectra are formed. The exciting frequencies appeared in frequency spectra at corresponding waviness orders are validated through Yhland [24]. The relation between inner race waviness order and corresponding exciting vibration frequency are given in Table 4.1.

From Table 4.1, for waviness order 5, the exciting frequencies calculated are 6.09 Hz and 15.908 Hz. The frequency 6.09 Hz is calculated using formula '$aN_b(f_r - f_c) - nf_r$', by keeping value of 'a' as 1 and 'n' as 5. The frequency 15.908 is calculated using formula 'nf_r', by keeping value of 'n' as 5. Similarly, the excited frequencies for waviness order 8 is calculated as 5.82 Hz, 15.64 Hz and 25.45 Hz by using the relations given in Table 4.1. In the same way, frequencies are calculated for remaining inner race waviness order 13 and 16. These calculated frequencies are given in Table 4.2.

Table 4.1: Vibration frequencies excited by inner race waviness [24]

Waviness Order k_i	Vibration Frequency (Hz)
n	nf_r
aN_b	$aN_b(f_r - f_c)$
$aN_b \pm n$	$aN_b(f_r - f_c) \pm nf_r$

Table 4.2: Excited vibration frequencies at given inner race waviness

Waviness Order k_i	Vibration frequency (Hz)			
5	$N_b(f_r - f_c) - 3f_r$ = **6.09**		$5f_r$ = **15.908**	
8	$2N_b(f_r - f_c) - 8f_r = \mathbf{5.82}$	$N_b(f_r - f_c)$ = **15.64**	$8f_r$= **25.45**	
13	$2N_b(f_r - f_c) - 3f_r = \mathbf{21.73}$	$N_b(f_r - f_c) + 5f_r$= **31.54**		$13f_r$=**41.32**
16	$2N_b(f_r - f_c) = \mathbf{31.28}$	$N_b(f_r - f_c) + 8f_r = \mathbf{41.09}$		$16f_r$=**50.9**

The frequency spectra considering inner race waviness as shown in this section shows good agreement to the frequencies calculated in Table 4.2. From Fig. 4.3 and Fig 4.4, it is observed that, these frequencies given by Yhland are absent when ball bearing is considering without surface waviness.

Fig. 4.5 and Fig. 4.6 show the displacement plots and dynamic orbits of the system with inner race surface waviness of order 5. Using displacement plots, the frequency spectra are formed as shown in Fig. 4.7 and Fig. 4.8 of disk node displacement and bearing displacement respectively. It is observed that, the spectrum becomes denser comparing to FFT plots from Fig. 4.3 and

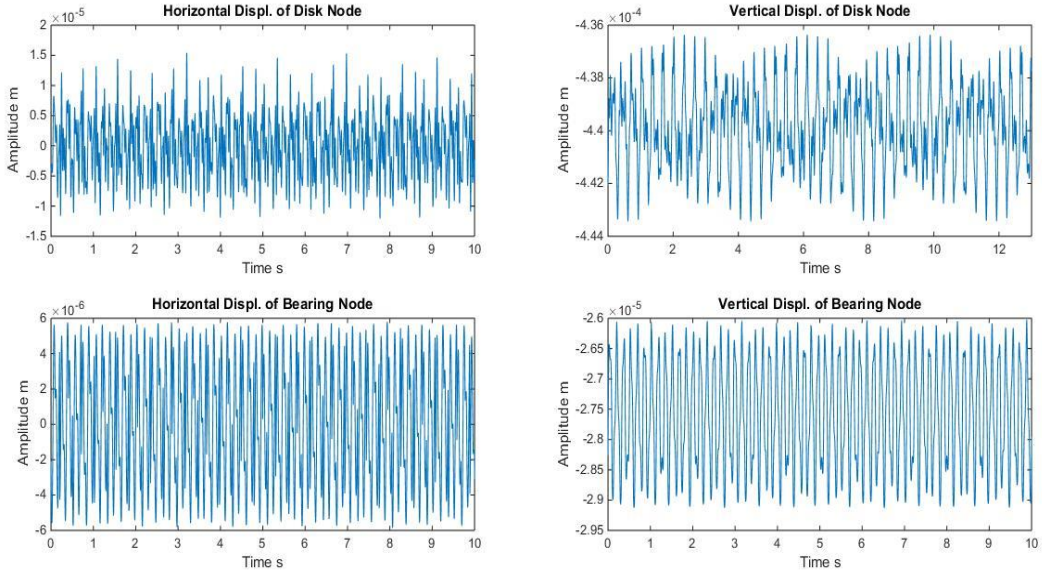

Fig. 4.5: Displacement plots of rotor with bearings having inner race surface waviness of order 5

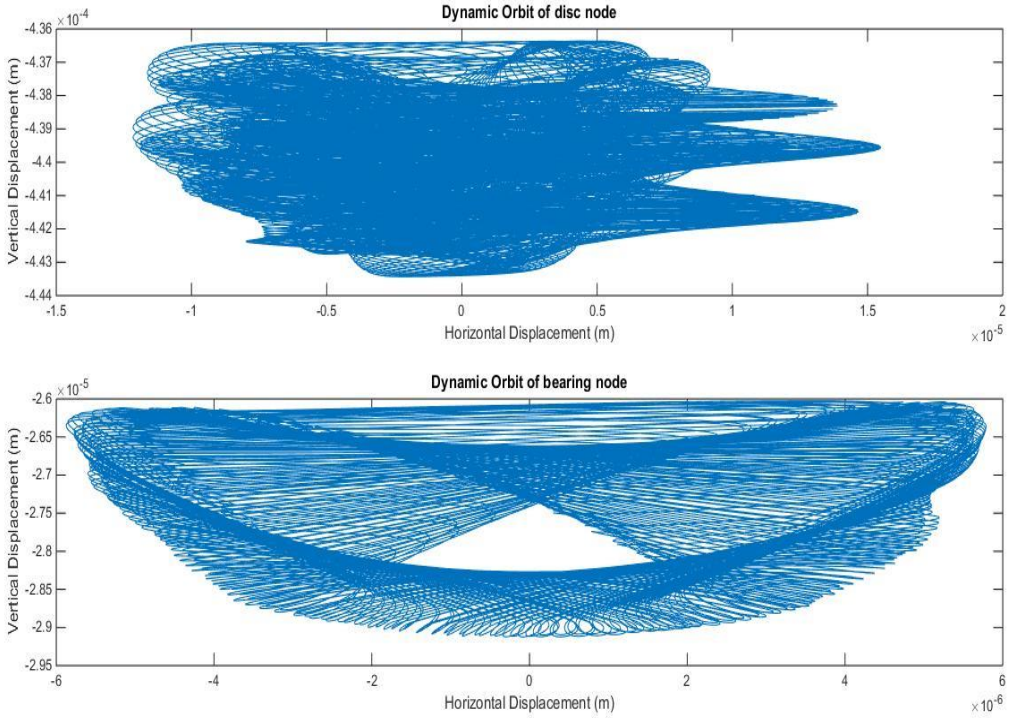

Fig. 4.6: Dynamic orbits of rotor with bearing having inner race surface waviness of order 5

Fig. 4.4 without considering surface waviness. In these plots shown in Fig. 4.7 and Fig. 4.8, the amplitudes appears at rotational frequency, at varying compliance with its higher harmonics and at the sum of integer multiplies of rotational frequency, variable compliance and cage frequency and including the excited frequencies stated by Yhland [24]. In Fig. 4.7 dominating frequency is $N_b(f_r - f_c) - 3f_r$, which is predicted by Yhland. Amplitude at f_r and f_{vc} are nearly same, this indicates that, the role of Hertzian force and rotating imbalance force are same in this case. Whereas from Fig. 4.7(b), the dominating frequency is rotational frequency, it states that in vertical direction at disk node the rotational imbalance force dominates the Bearing Hertzian contact force. At the bearing center, the dominating frequency appears at $N_b(f_r - f_c) - 3f_r$ in both directions, as shown in Fig. 4.8. The amplitudes in FFT plots of horizontal direction are higher than the vertical direction at all rotor node location as shows in Fig 4.7 and Fig. 4.8.

The displacement plots and dynamic orbits for disk node and bearing node with considering inner race waviness order as 8 are shown in Fig 4.9 and Fig 4.10. The Fig. 4.11 shows the FFT plots of disk node displacement. In the FFT plot of horizontal displacement, the rotational

frequency dominates the frequency spectrum. Although, in vertical displacement's FFT plot, the dominating frequency is $N_b(f_r - f_c)$. This frequency is also mentioned by Yhland for '8' waviness order as given in Table 4.2. The horizontal displacement's FFT curve also contains same frequency, but of smaller amplitude. Both FFT plot contain frequencies at varying compliance and sum of integer multiple of varying compliance frequency, rotational imbalance

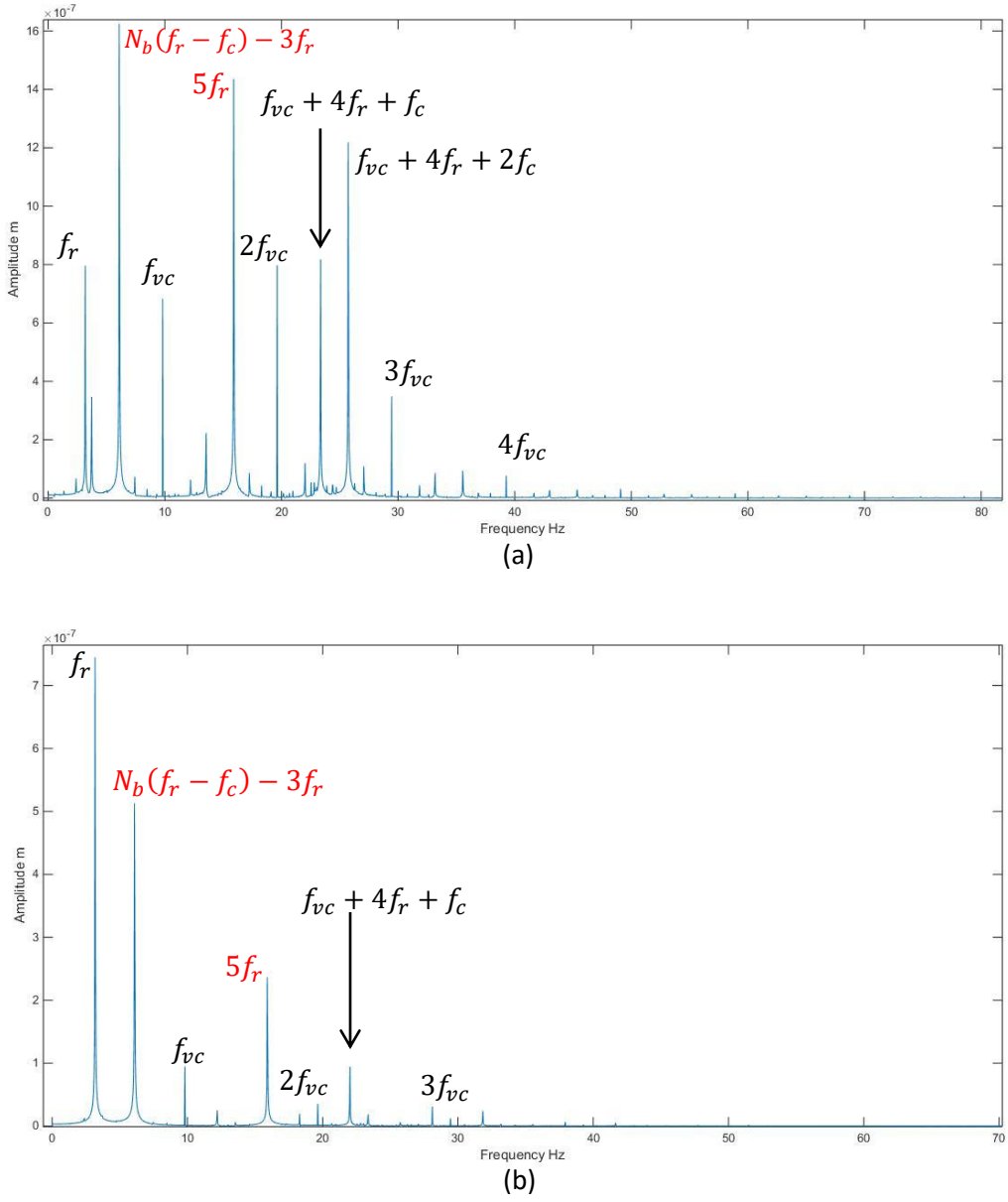

Fig. 4.7: Frequency Spectra of rotor center at disk with inner race waviness of order 5

(a) Horizontal Direction (b) Vertical Direction

frequency and cage rotational frequency. Amplitudes at these frequencies are higher in horizontal displacement's FFT curve then vertical displacement's FFT plot. In the FFT plot of bearing node horizontal displacement shown in Fig. 4.12, the varying compliance frequency dominates. This is because of higher Hertzian contact force than unbalance force at bearing location. Similar to the FFT plot of disk node location, the frequency $N_b(f_r - f_c)$ is dominating in vertical displacement at bearing node location. Other amplitudes are coming at varying

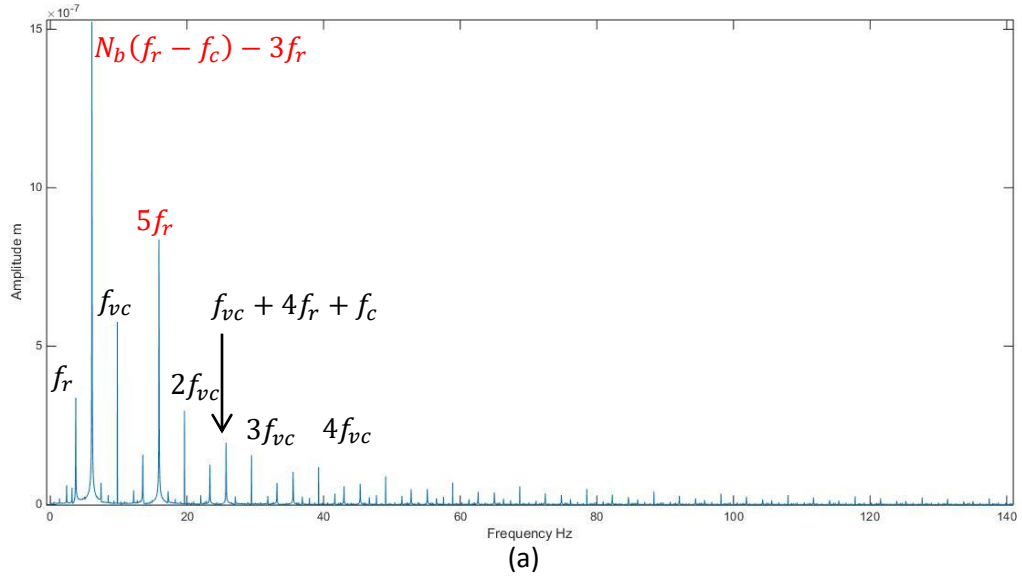

Fig. 4.8: Frequency Spectra of rotor center at bearing with inner race waviness of order 5 (a) Horizontal Direction (b) Vertical Direction

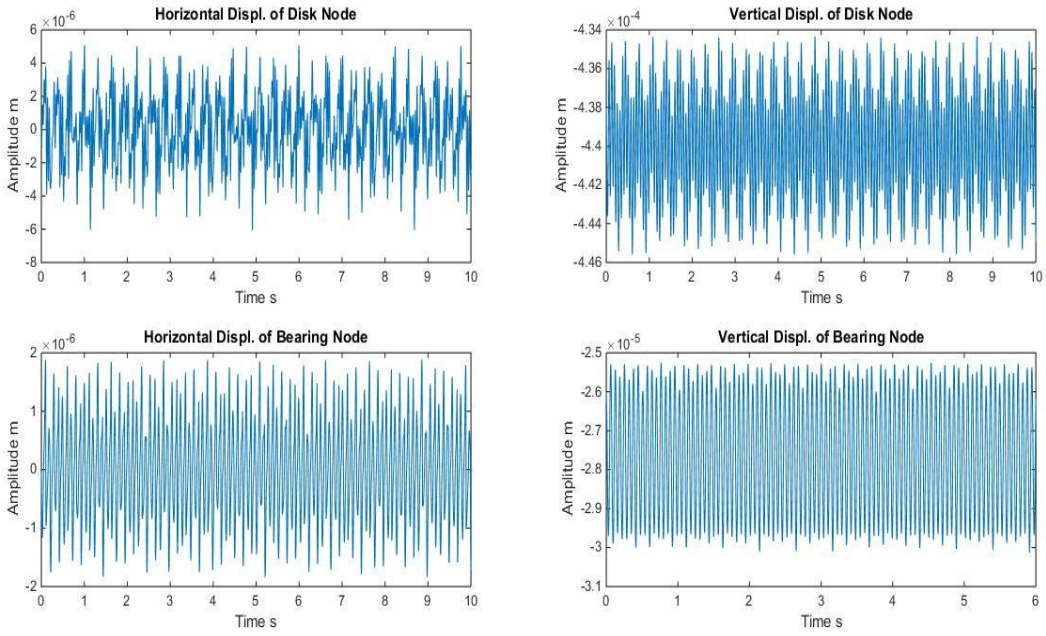

Fig. 4.9: Displacement plots of rotor with bearing having inner race surface waviness of order 8.

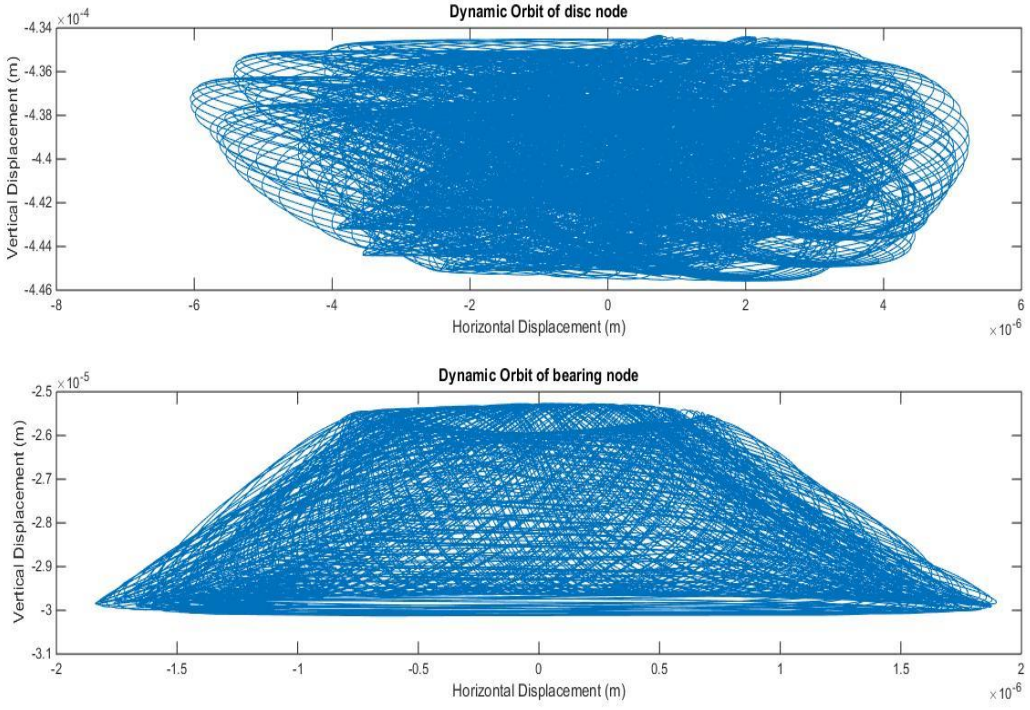

Fig. 4.10: Dynamic orbits of rotor with bearing having inner race surface waviness of order 8.

compliance and sum of the integer multiple of varying compliance frequency, rotational imbalance frequency and cage rotational frequency. The rotational imbalance force has very low impact in the vibrations at bearing node for waviness order as 8. This behavior is shown in Fig. 4.12, which is having very low amplitudes at rotational frequency 'f_r'. The displacement plots, dynamic orbits and frequency spectra of the system with inner race surface waviness of

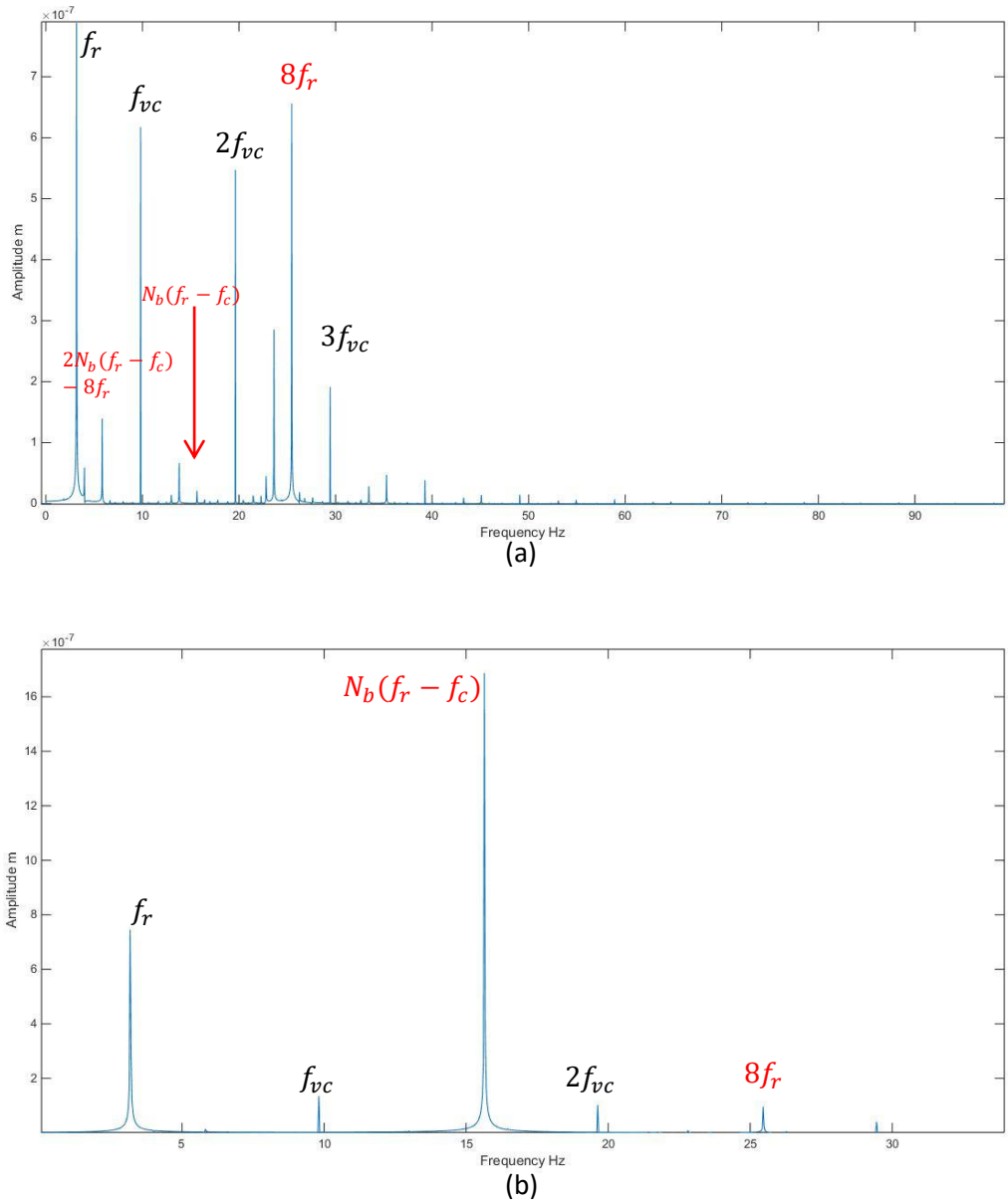

Fig. 4.11: Frequency Spectra of rotor center at disk with inner race waviness of order 8
(a) Horizontal Direction (b) Vertical Direction

order 13 are shown in Fig. 4.13 to Fig. 4.16 respectively. In all 4 FFT plots, the dominating frequency observed '$2N_b(f_r - f_c) - 3f_r$', which is stated by Yhland. In both FFT figures, the frequency $N_b(f_r - f_c) + 5f_r$ is also appearing, which is also predicted by Yhland for the same Waviness order 13. In Fig. 4.15(a), the rotational and varying compliance frequencies are having nearly same magnitude. But in Fig. 4.15(b), Hertzian force is having very low impact on vibration, as only first harmonic is appearing with lower amplitude than rotational frequency.

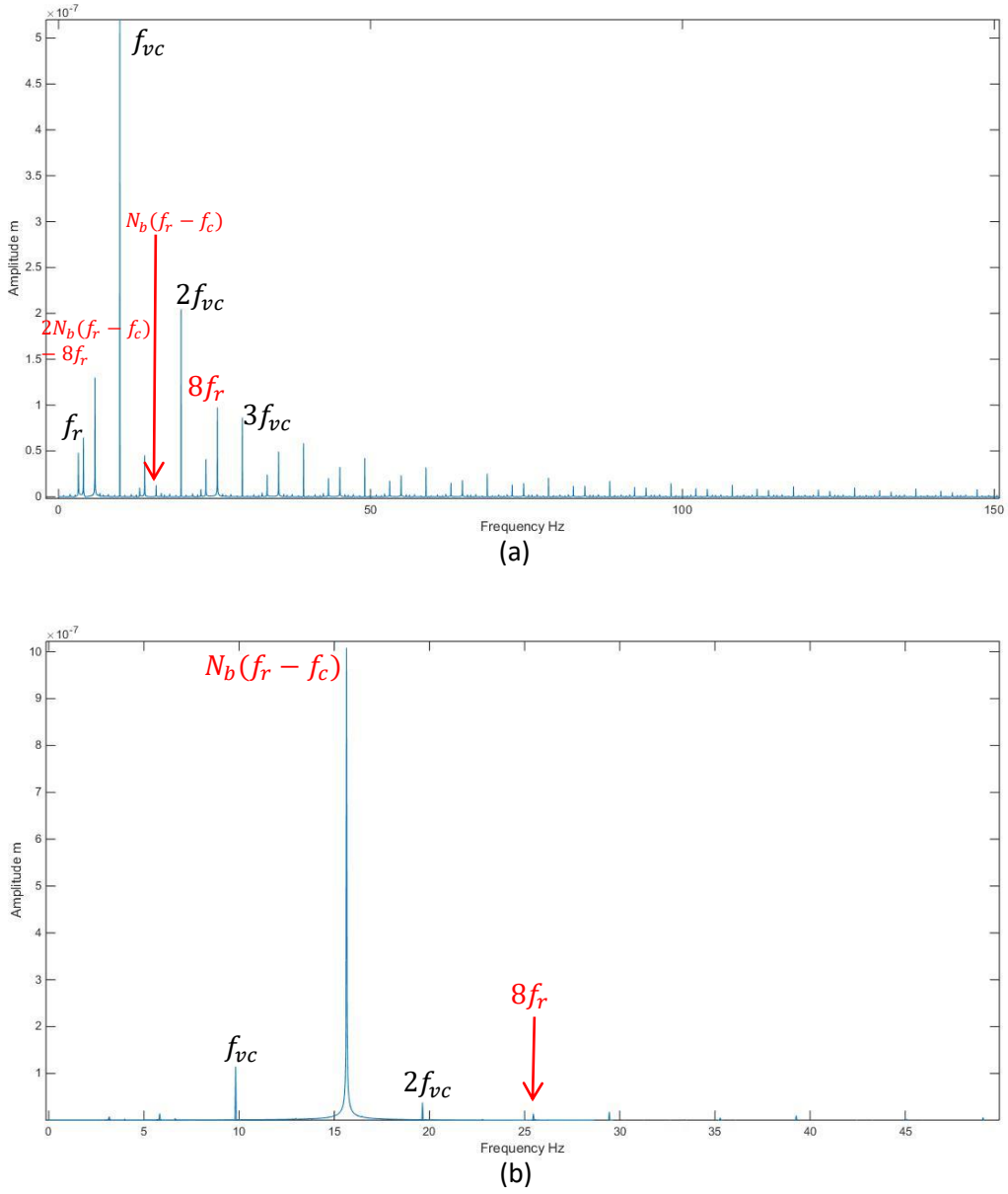

Fig. 4.12: Frequency Spectra of rotor center at bearing with inner race waviness of order 8
(a) Horizontal Direction (b) Vertical Direction

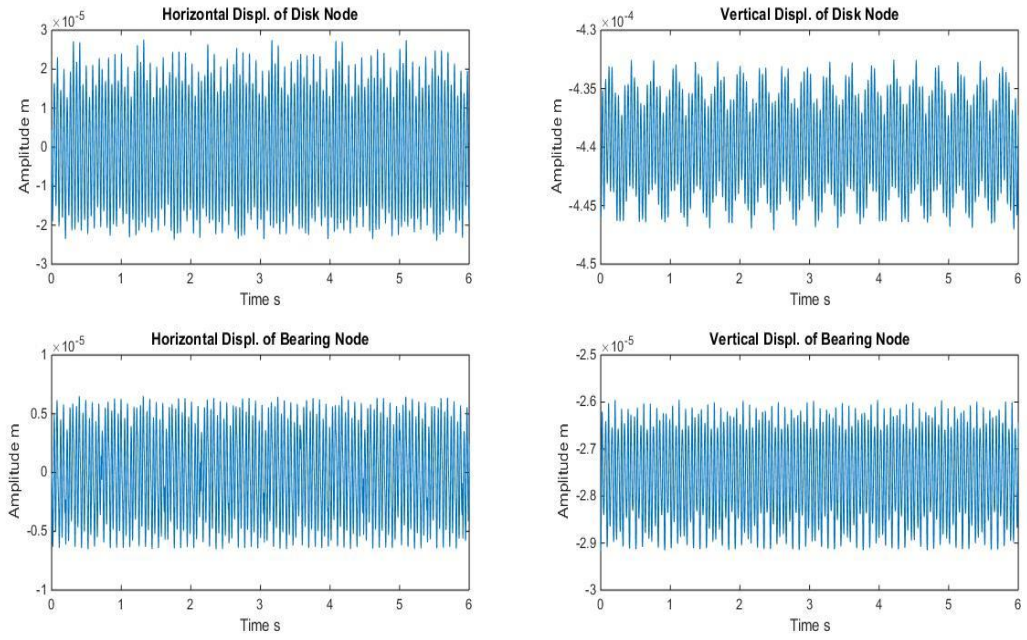

Fig. 4.13: Displacement plots of rotor with bearings having inner race waviness of order 13

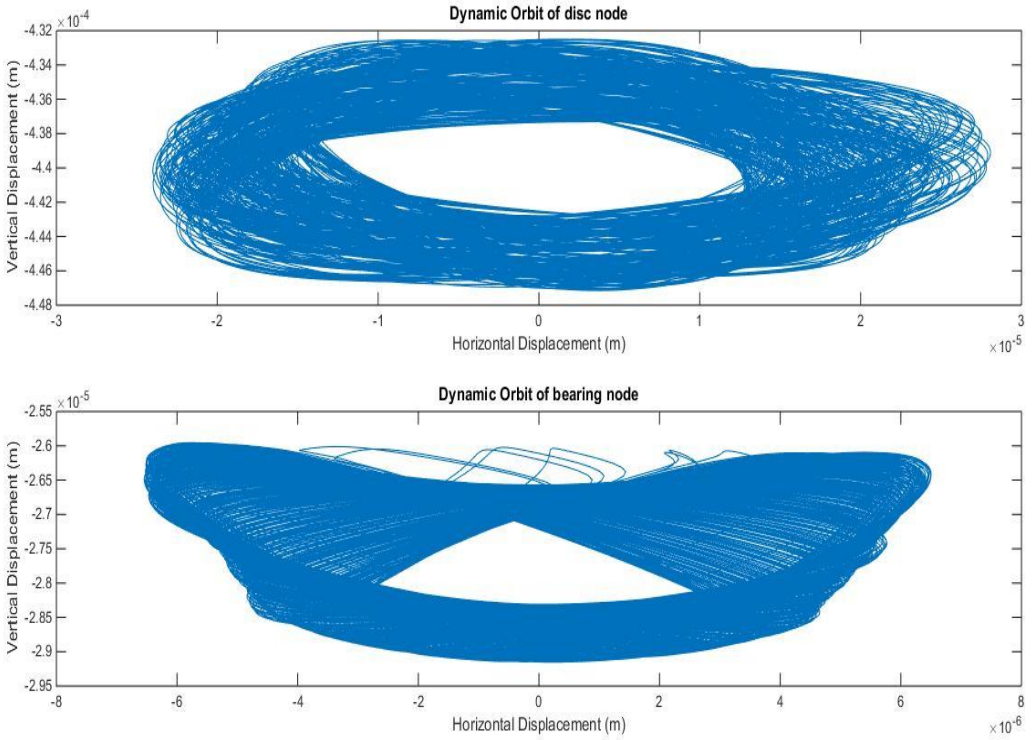

Fig. 4.14: Dynamic orbits of rotor with bearings having inner race waviness of order 13

As previously discussed, the Hertzian force dominates the rotational imbalance force at the bearing location; hence the varying compliance frequency dominates the rotational frequency in the FFT plots as shown in Fig. 4.16. In vertical displacement's FFT plot, the impact of rotational is very low, that can be seen from Fig. 4.16(b), as the amplitude at f_r is nearly negligible compare to the other frequencies. In Fig. 4.15 and 4.16, the other amplitudes are coming at

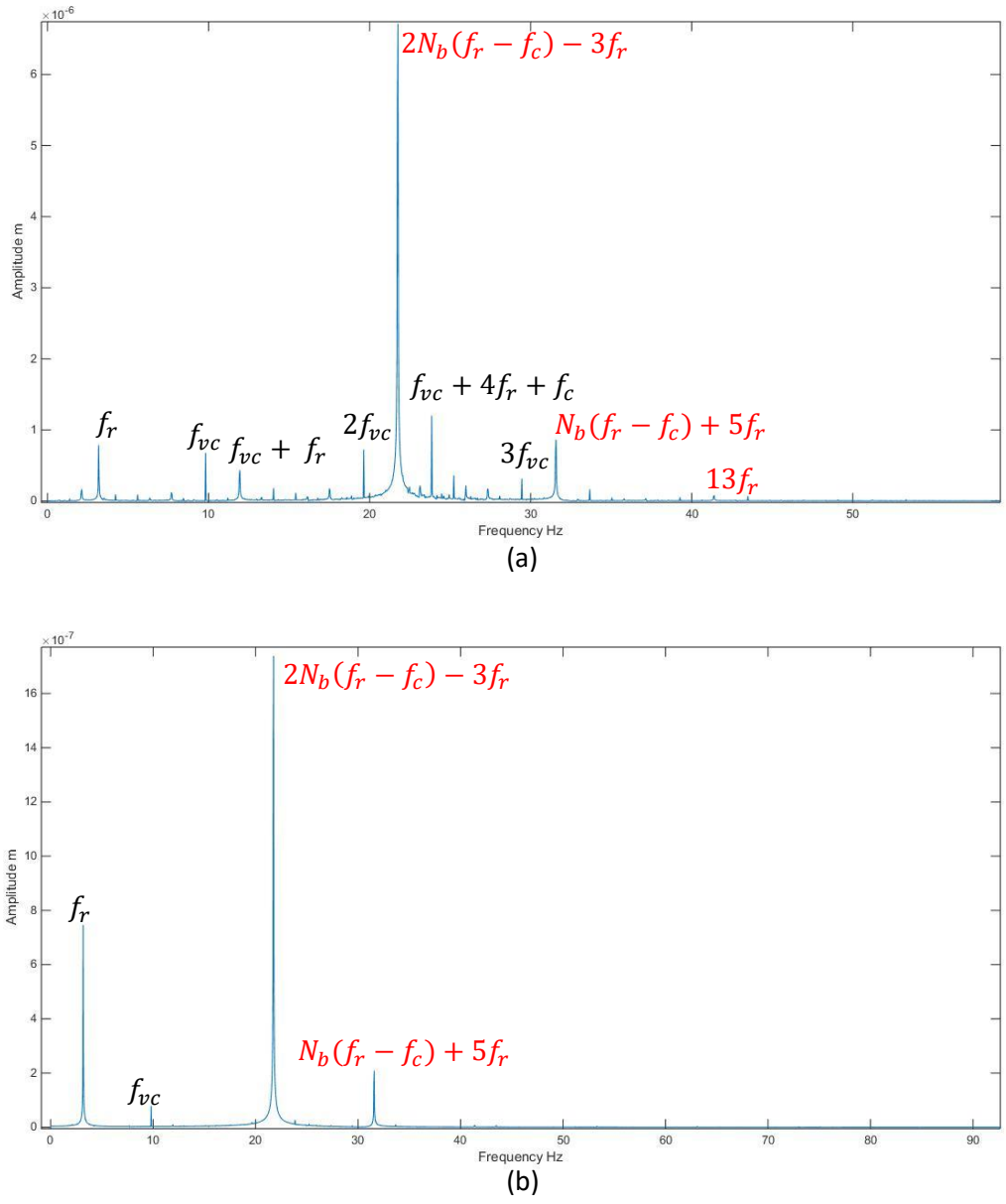

Fig. 4.15: Frequency Spectra of rotor center at disk with inner race waviness of order 13 (a) Horizontal Direction (b) Vertical Direction

varying compliance and sum of the integer multiple of varying compliance frequency, rotational imbalance frequency and cage rotational frequency. The displacement plots, dynamic orbits and frequency spectra of the system with inner race waviness of order 16 are shown in Fig. 4.17 to Fig. 4.18. In horizontal FFT plot rotational frequency dominates as shown in Fig. 4.19.

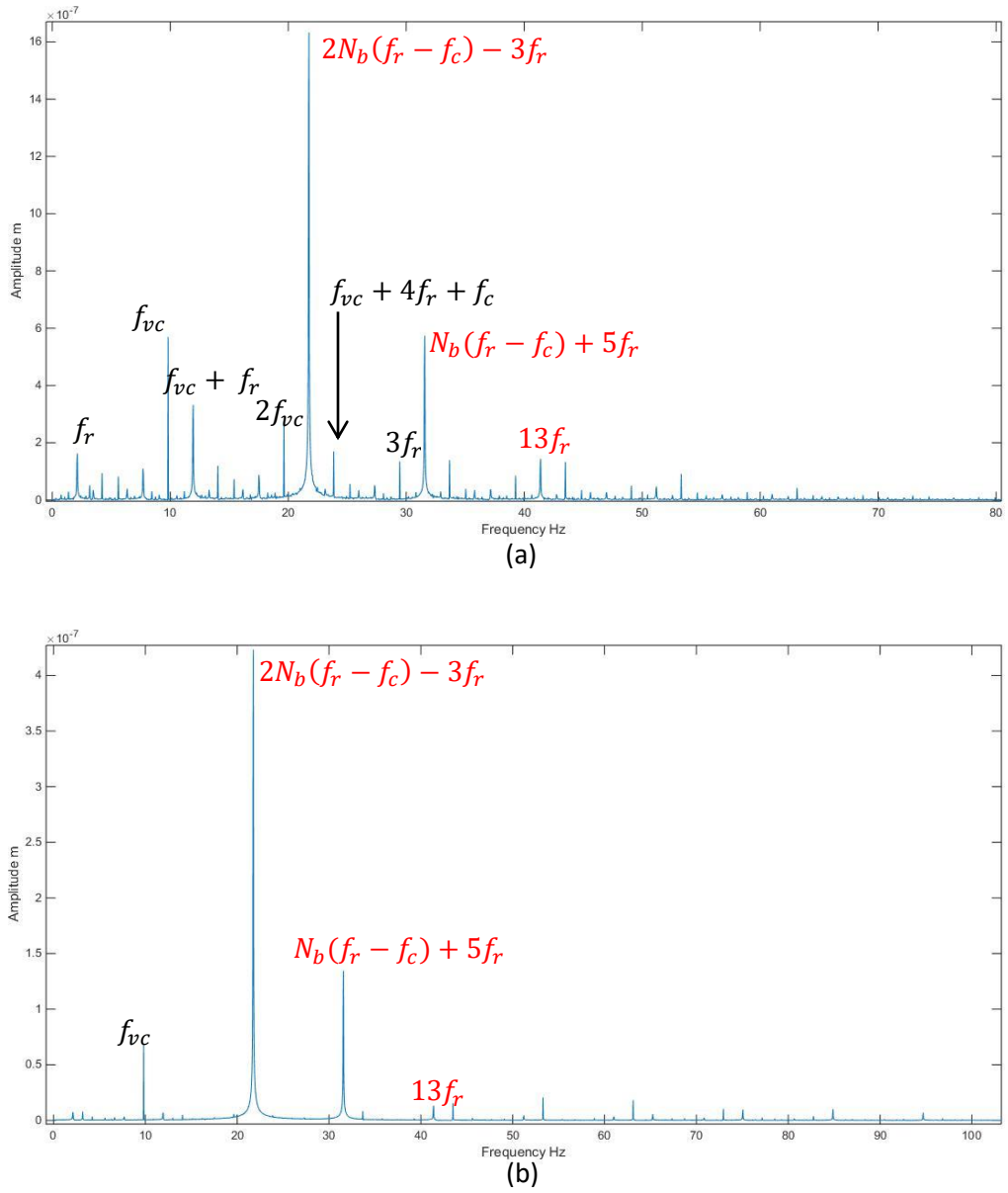

Fig. 4.16: Frequency Spectra of rotor center at bearing with inner race waviness of order 13 (a) Horizontal Direction (b) Vertical Direction

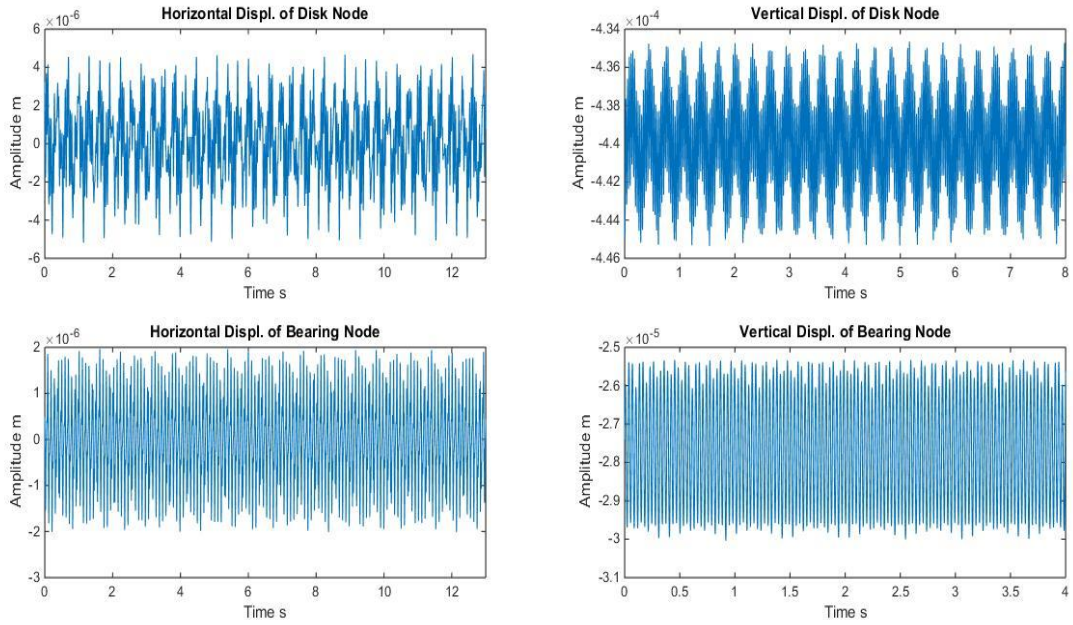

Fig. 4.17: Displacement plots of rotor with bearings having inner race surface waviness of order 16

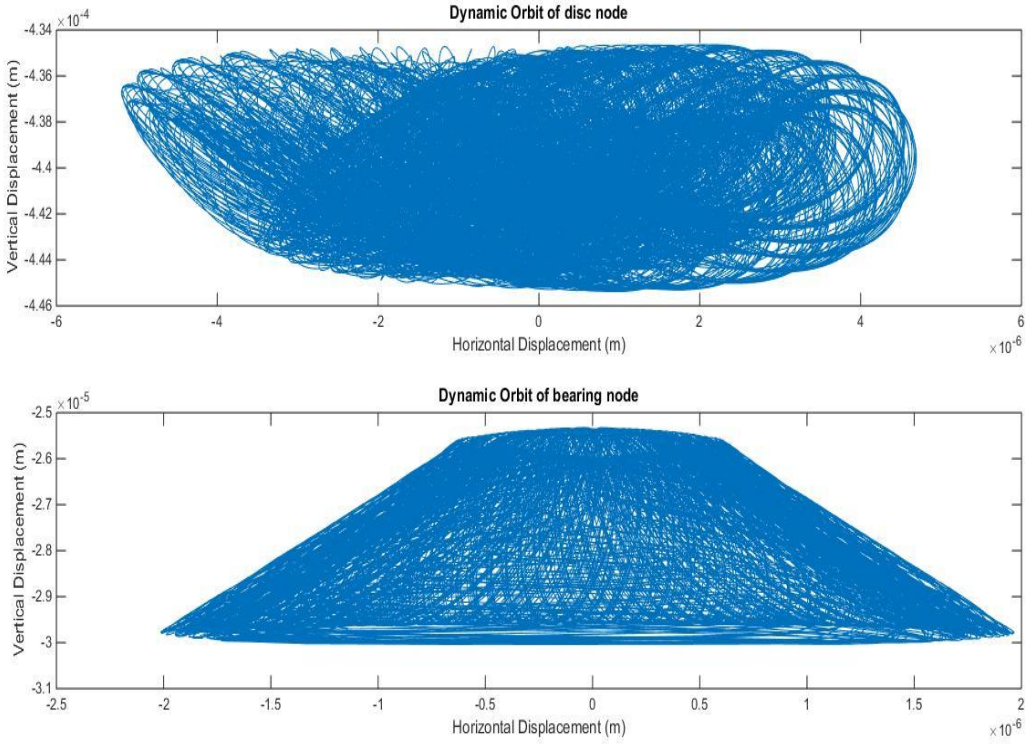

Fig. 4.18: Dynamic orbits of rotor with bearings having inner race surface waviness of order 16

In vertical FFT plot, the frequency $2N_b(f_r - f_c)$ dominates, which is predicted by Yhland for 16 waviness order as given in Table 4.2. This frequency also appears in Horizontal FFT plot, but of very low amplitude. The FFT plot of bearing location's displacement, shown in Fig. 4.20, gives similar trend as of frequency $2N_b(f_r - f_c)$, that appears at disk node FFT plots. Other frequency appears as varying compliance frequency and at its harmonics. The frequency spectra of

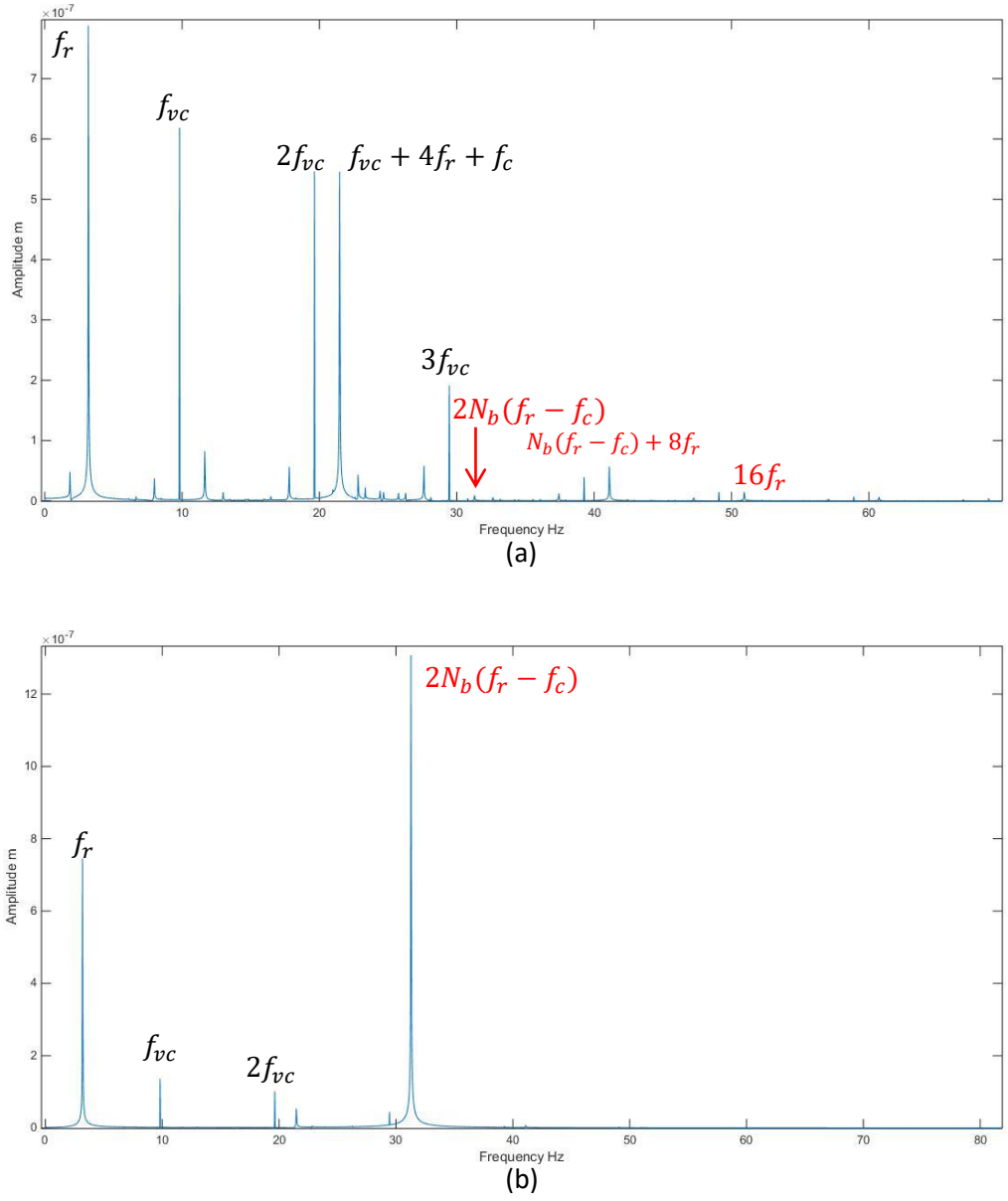

Fig. 4.19: Frequency Spectra of rotor center at disk with inner race waviness of order 16 (a) Horizontal Direction (b) Vertical Direction

Horizontal displacement of both bearing and disk location are denser than vertical displacement's FFT plot. As discussed earlier, the Hertzian contact force dominates the unbalance force at bearing location. Because of that, the variable compliance frequency dominates the rotational frequency at bearing location FFT plots and at disk location FFT plots, rotational frequency dominates the varying compliance frequency.

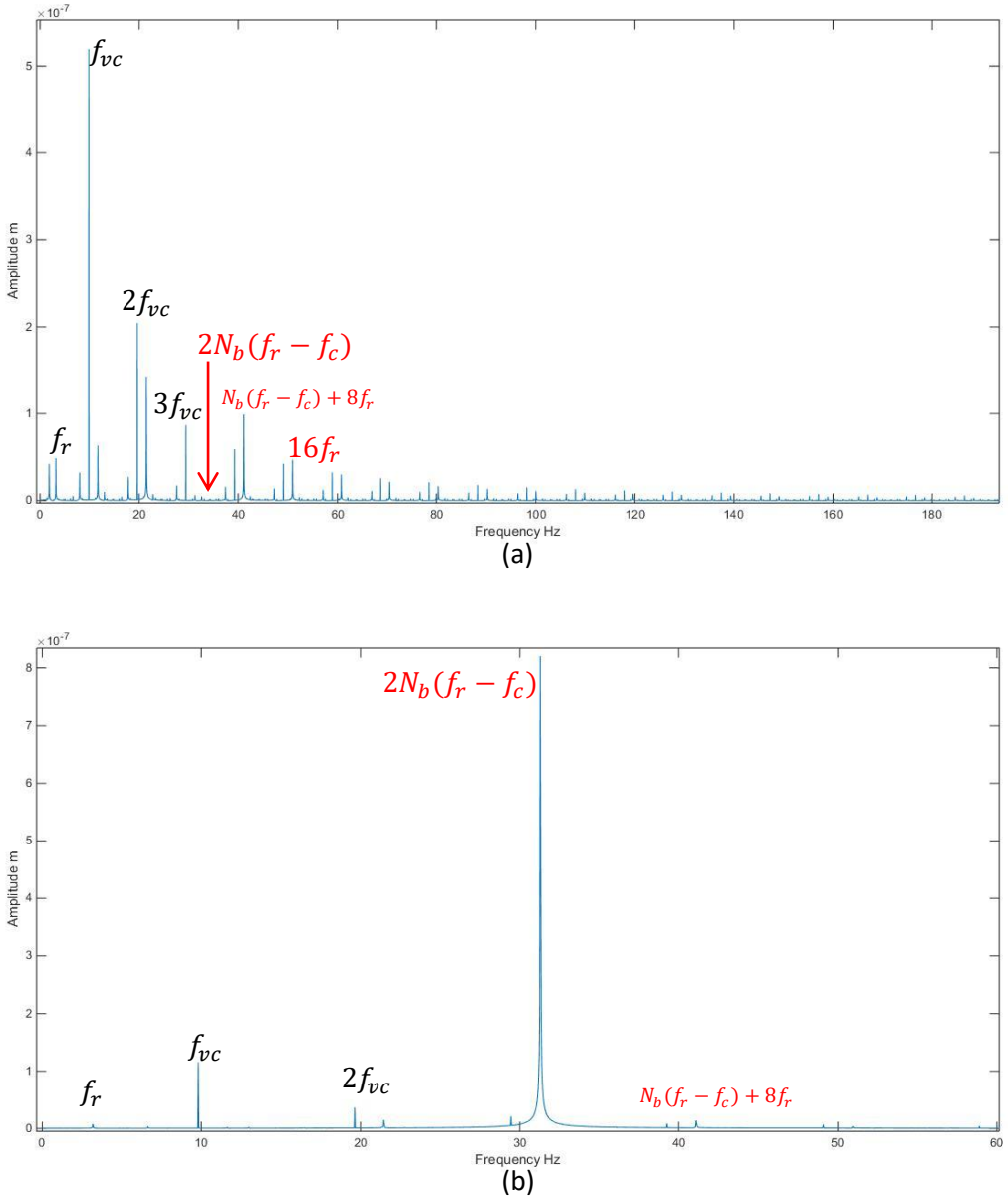

Fig. 4.20: Frequency Spectra of rotor center at bearing with inner race waviness of order 16 (a) Horizontal Direction (b) Vertical Direction

In the vertical FFT plots of both disc and bearing node the highest frequency of vibration appears is $2N_b(f_r - f_c)$.

4.3 Outer Race Waviness effect

The outer race waviness is the sinusoidal wave of maximum amplitude of 2 µm, considered at the inner surface of outer race of the ball bearing as shown in Fig. 3.5. Here also, the waviness order is varied by 5, 8, 13 and 16. The displacement plots, dynamic responses are plotted for disk node horizontal and vertical displacement, and for bearing node horizontal and vertical displacements. With the help of displacement plots, the frequency spectra are created for the system. The frequency spectra with outer race waviness are validated through the same author's work Yhland [24], which was used to validate the frequency spectra with inner race waviness in section 4.1.

Table 4.3 shows the relations between waviness order of outer race and corresponding exciting vibration frequencies, given by Yhland.

Table 4.3: Vibration frequencies excited by outer race waviness [24]

Waviness Order k_o	Vibration Frequency (Hz)
aN_b	$aN_b f_c$
$aN_b \pm n$	$aN_b f_c$

With waviness order 5, which is less than number of balls in bearing, the corresponding vibration frequency comes as $N_b f_c$ which is equal to 9.812 Hz. This is also a varying compliance frequency. Therefore, for outer race waviness of order less than number of balls of bearing, the excited vibration frequency corresponding to that waviness order would be varying compliance frequency. For waviness order 8, which is equal to number of balls, the vibration frequency corresponds to $N_b f_c$. Considering waviness order as 13, the vibration frequency obtained as $2N_b f_c$ which is equal to 19.625 Hz. Similarly for waviness order 16, the vibration frequency comes as $2N_b f_c$. All these frequencies related to outer race waviness order are given in Table 4.4

Table 4.4: Excited vibration frequencies at given outer race waviness

Waviness Order k_o	Vibration Frequency (Hz)
5	9.812
8	9.812
13	19.625
16	19.625

The frequency spectra shown in this section 4.3 are with different waviness order of outer race having good agreement to the frequencies given by Yhland, as shown in Table 4.4. From Fig. 4.3 and Fig. 4.4, it is observed that, with considering outer race waviness, the amplitudes at these mentioned frequencies in FFT plots are higher comparing to FFT plots with ball bearing without outer race surface waviness.

The displacement plots and dynamic orbits for outer race waviness of order 5 are shown in Fig. 4.21 and Fig. 4.22. Fig. 4.23 and Fig. 4.24 shows the FFT plot of disk node and bearing node respectively. In the FFT plot of disk horizontal displacement, the varying compliance frequency dominates. Yhland also predicted this frequency to appear in the FFT plot with waviness order 5. The varying compliance frequency appears in other plots too for waviness order 5 and dominates the frequency spectra, except the FFT plot at disk node in vertical direction, as shown in Fig.4.23 and 4.24. In the frequency spectra of vertical direction, rotational frequency dominates because of higher rotating imbalance force impact to the rotor than Hertzian contact force. In all other FFT plots with waviness order '5', the Hertzian contact force dominates. The frequency spectra also show the presence of frequencies of higher harmonics of varying compliance frequency.

For outer race waviness order 8, the displacement plots, dynamic orbits and frequency spectra at disk node and bearing node are shown in Fig. 4.25 to Fig. 4.26. The dominant frequency appears as f_r in the horizontal FFT plot at disk node as shown in Fig 4.27. In other Frequency spectra at disk node and at bearing node, the dominating frequency appears as varying compliance frequency f_{vc}, as shown in Fig. 4.27 and Fig. 4.28. Yhland has also stated the presence of this

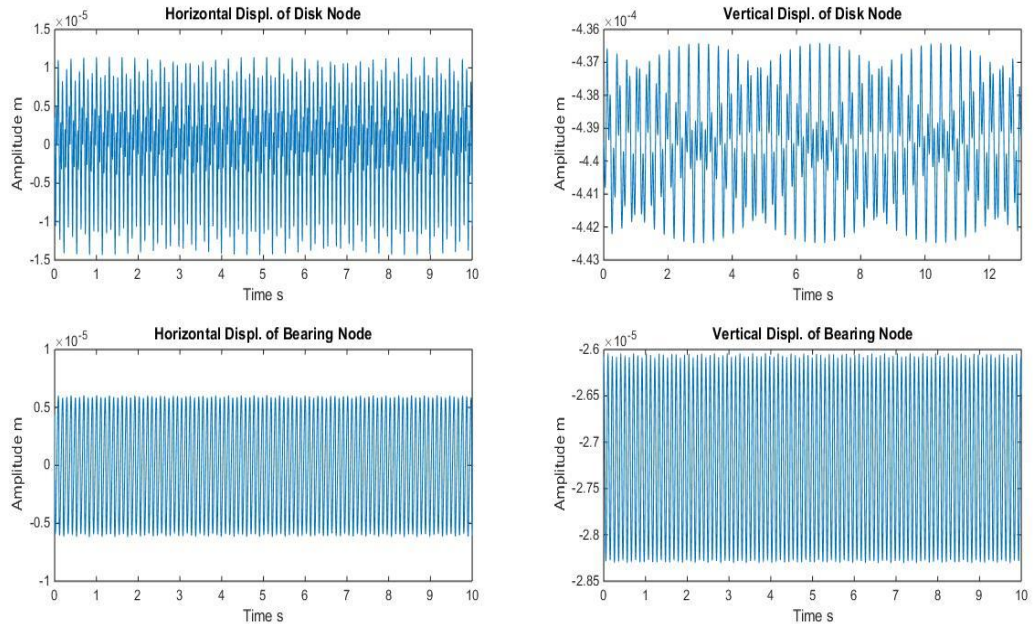

Fig. 4.21: Displacement plots of rotor with bearing having outer race waviness of order 5

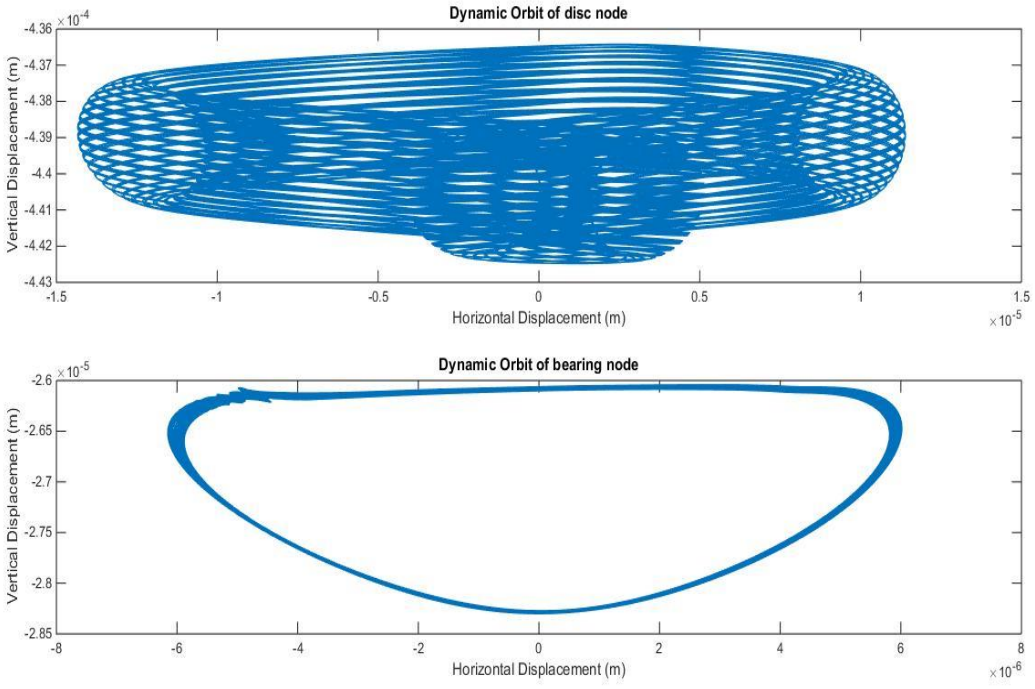

Fig. 4.22: Dynamic orbits of rotor with bearing having outer race waviness of order 5

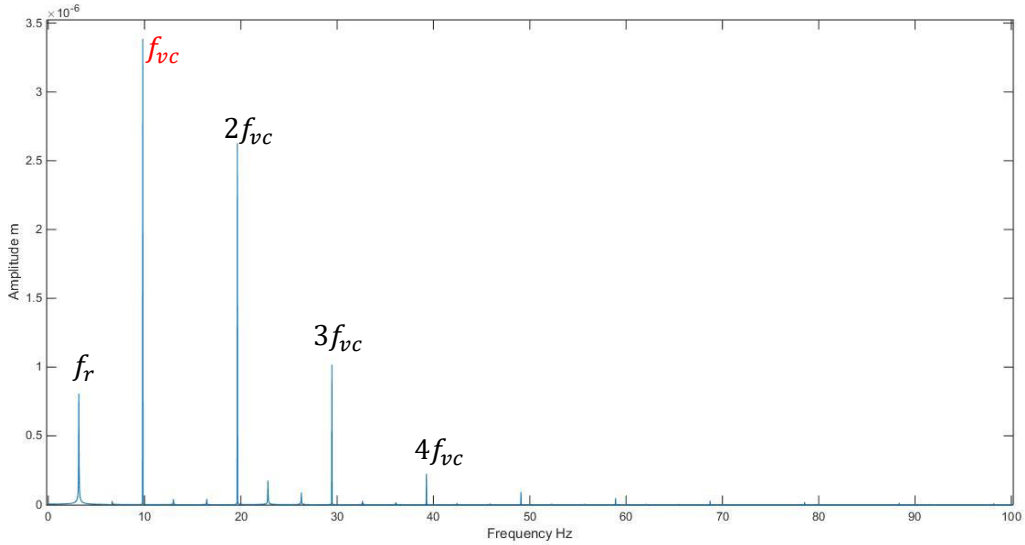

(a)

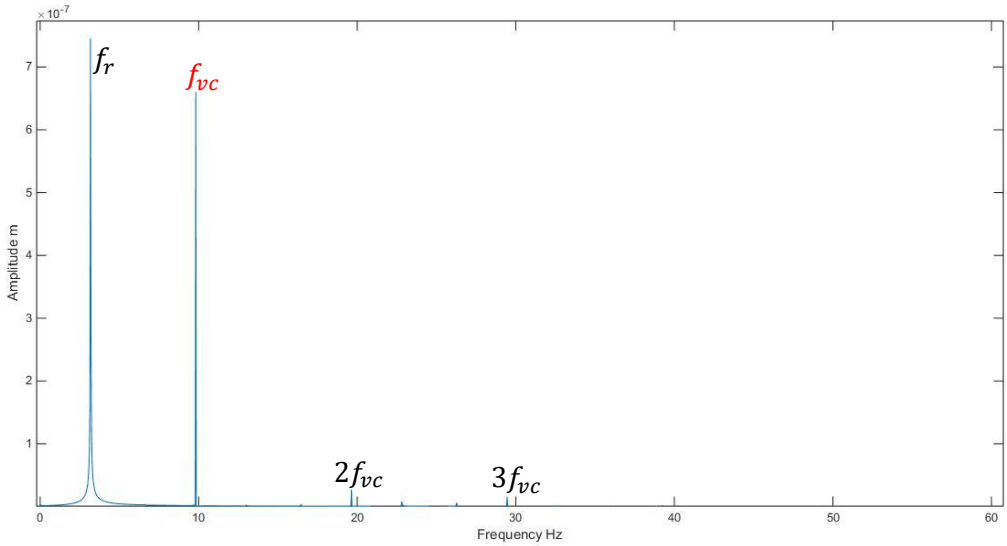

(b)

Fig. 4.23: Frequency Spectra of rotor center at disk with outer race waviness of order 5 (a) Horizontal Direction (b) Vertical Direction

frequency with outer race waviness of order 8, as given in Table 4.4. The amplitude at rotational frequency in horizontal FFT plot and in vertical FFT plot at disk node is coming nearly same, but amplitude at varying compliance frequency in vertical FFT plot increase than the horizontal FFT plot. It is because of the higher Hertzian contact force in vertical direction than horizontal direction at disk node location. At the bearing node, the dominating force is the Hertzian contact

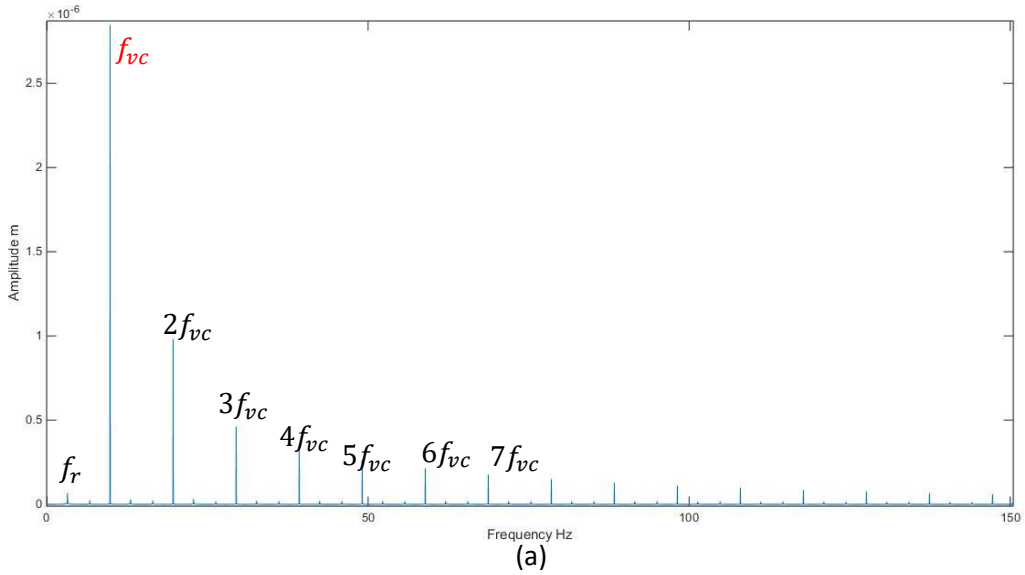

Fig. 4.24: Frequency Spectra of rotor center at bearing with outer race waviness of order 5 (a) Horizontal Direction (b) Vertical Direction

force. This signifies the dominancy of varying compliance frequency at bearing location. In the vertical FFT of bearing location the Hertzian contact force rises significantly and suppresses the effect of rotational imbalance force. Because of that, the rotational frequency component in Vertical FFT plot has negligible amplitude as shown in Fig. 4.28. Other frequencies in the FFT plots with outer race waviness of order 8 are the higher harmonics of varying compliance

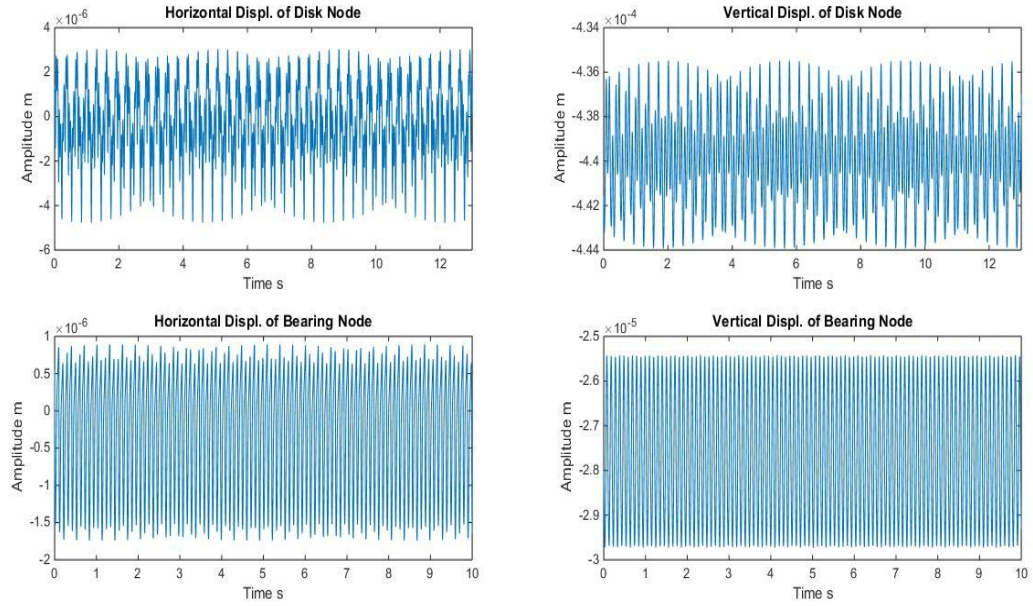

Fig. 4.25: Displacement plots of rotor with bearing having outer race waviness of order 8

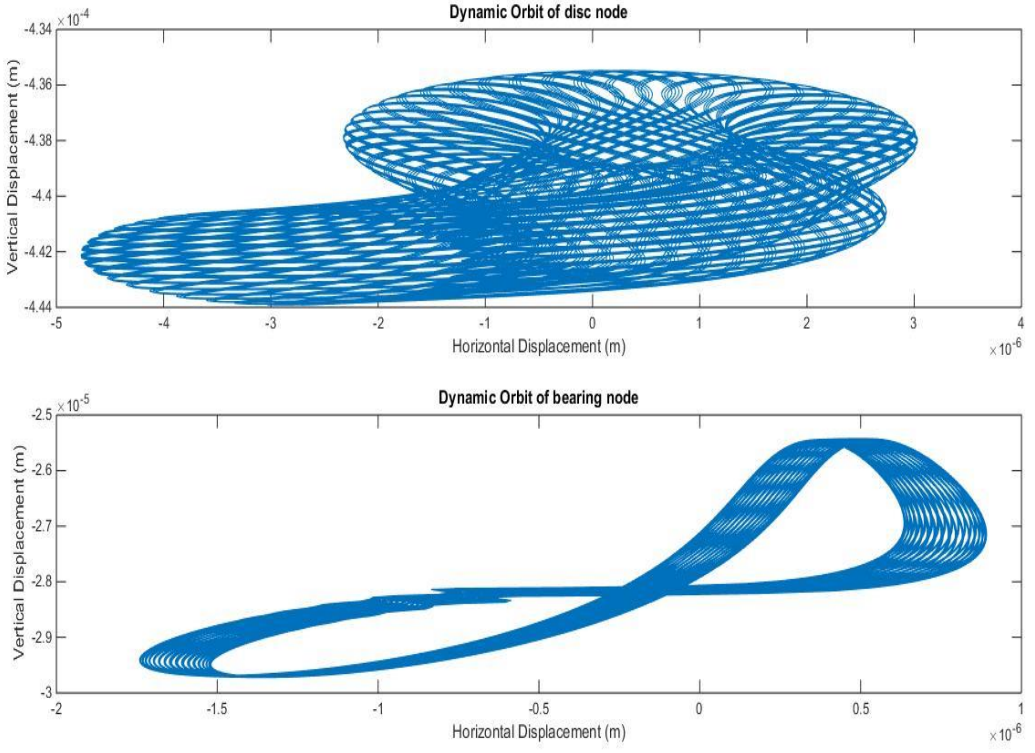

Fig. 4.26: Dynamic orbits of rotor with bearing having outer race waviness of order 8

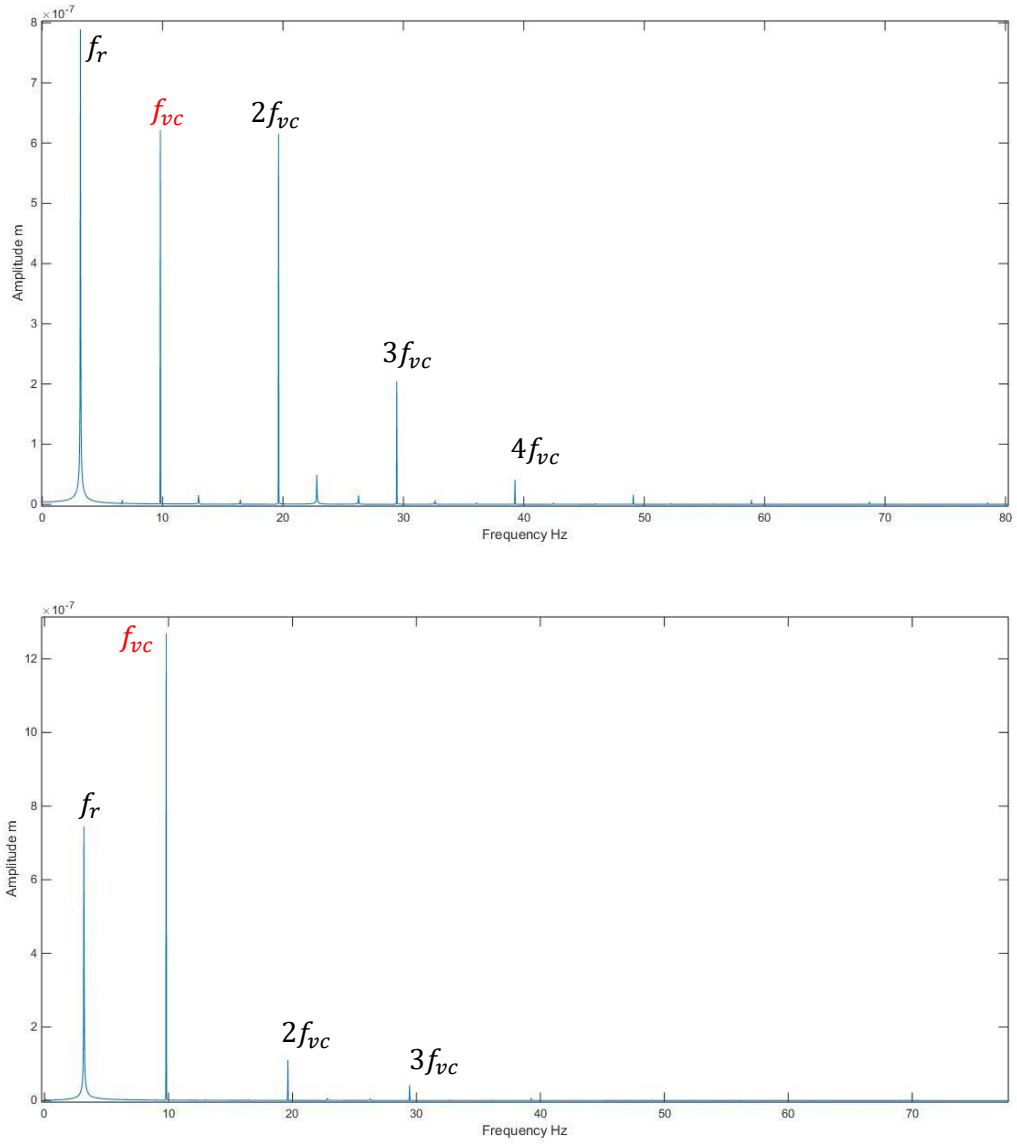

Fig. 4.27: Frequency Spectra of rotor center at disk with outer race waviness of order 8 (a) Horizontal Direction (b) Vertical Direction

frequencies. The Fig. 4.29 to Fig. 4.32 shows displacements plots, dynamic orbits and frequency spectra for outer race surface waviness of order 13 at disk node location and at bearing node location. The dominating frequencies in these FFT plots is second harmonics of varying compliance frequency $2f_{vc}$. The Yhland also mentioned the presence of this frequency with outer race waviness of order 13. In the FFT plot of disk node, the amplitude at f_r are coming same in

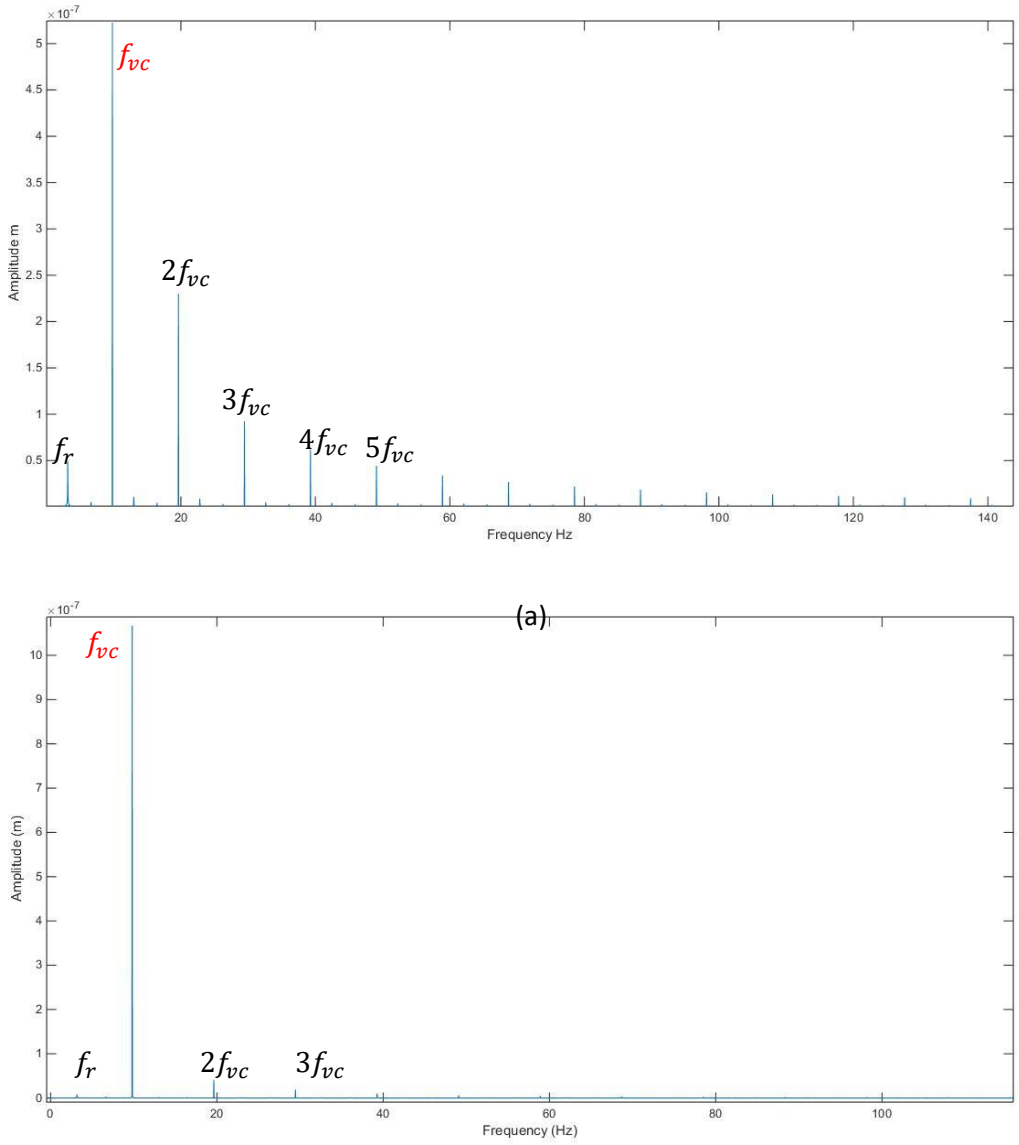

Fig. 4.28: Frequency Spectra of rotor center at bearing with outer race waviness of order 8 (a) Horizontal Direction (b) Vertical Direction

Horizontal and in vertical direction both as shown in Fig. 4.31. This is because; the unbalance force affects the rotor by the same extent in both horizontal and vertical direction. In the Frequency plot of the bearing location in vertical direction as shown in Fig. 4.32, the at rotational frequency is coming negligible with respect to the amplitude at varying compliance frequency

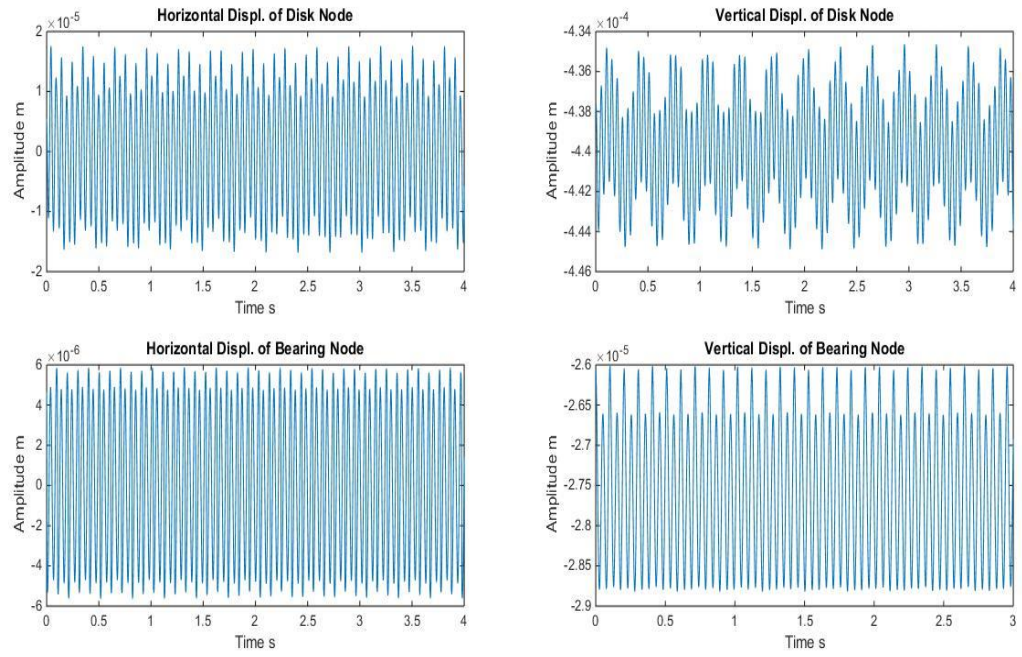

Fig. 4.29: Displacement plots of rotor with bearing having outer race waviness of order 13

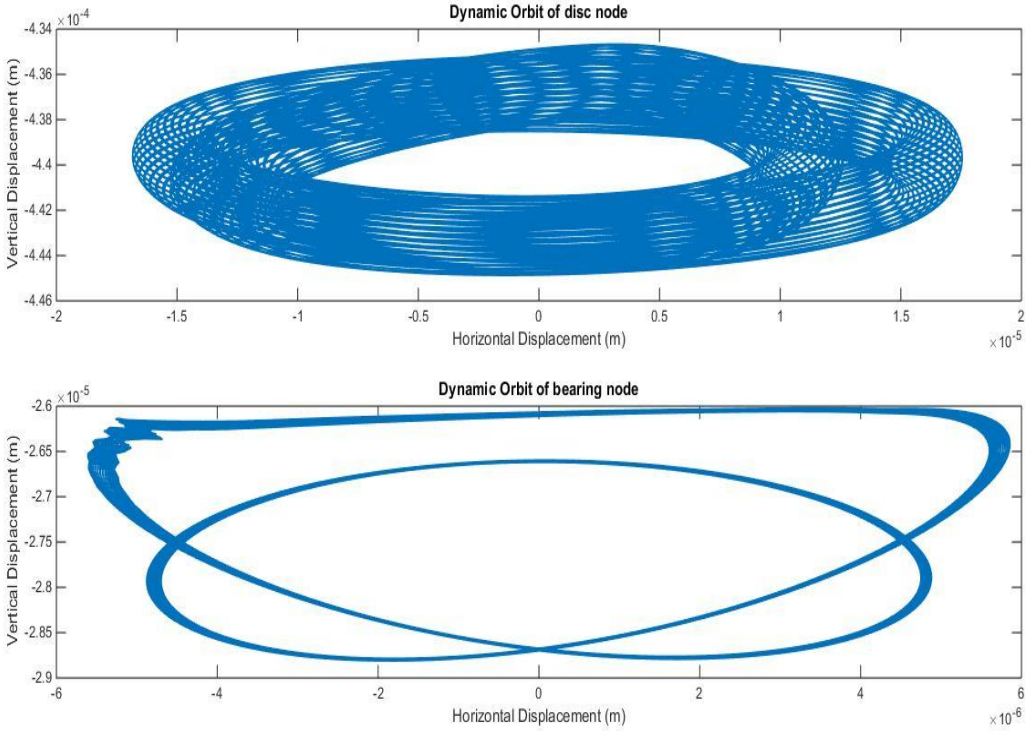

Fig. 4.30: Dynamic orbits of rotor with bearing having outer race waviness of order 13

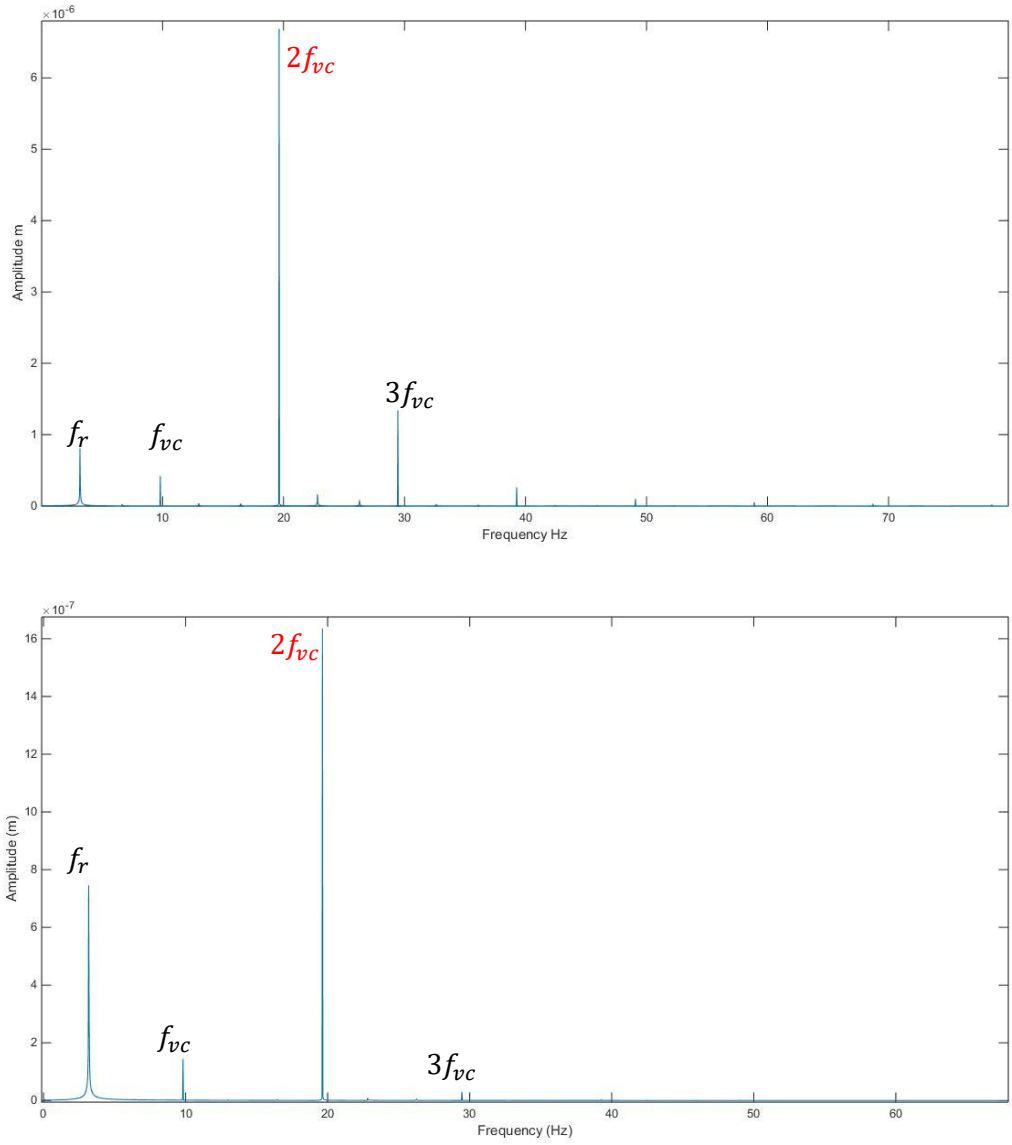

(b)

Fig. 4.31: Frequency Spectra at rotor center at disk with outer race waviness of order 13
(a) Horizontal Direction (b) Vertical Direction

and at its higher harmonics. Other frequencies appear in frequency spectra are the higher harmonics of varying compliance. In the horizontal FFT plot, these higher harmonics showing large in number, where as in vertical FFT plots only few harmonics of varying compliance is coming.

The displacement plots, dynamic orbits and frequency spectra with outer race surface waviness of order 16 are shown in Fig. 4.33 to 4.36. The Fig. 4.35 and Fig. 4.36 shows the vibration

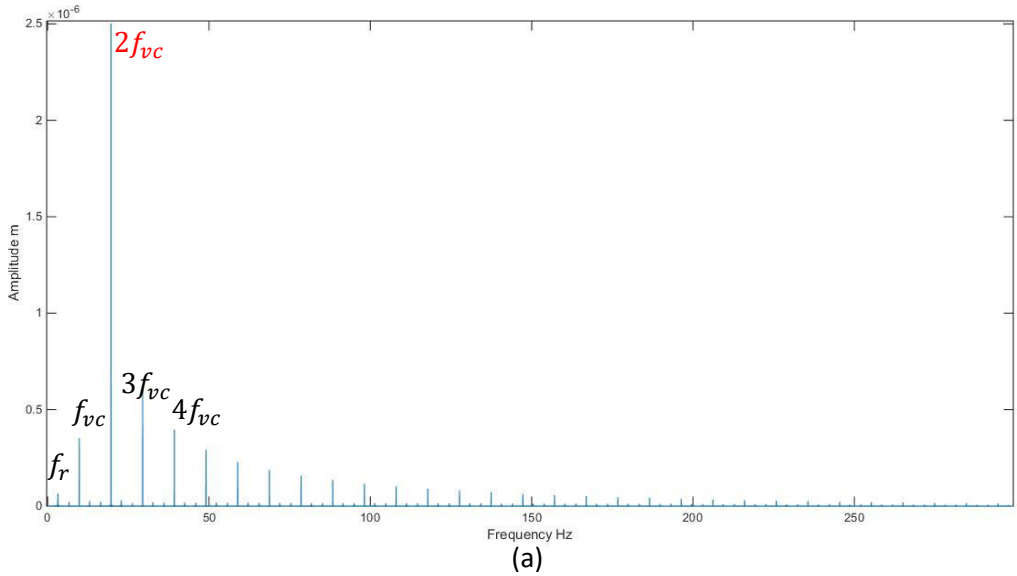

(a)

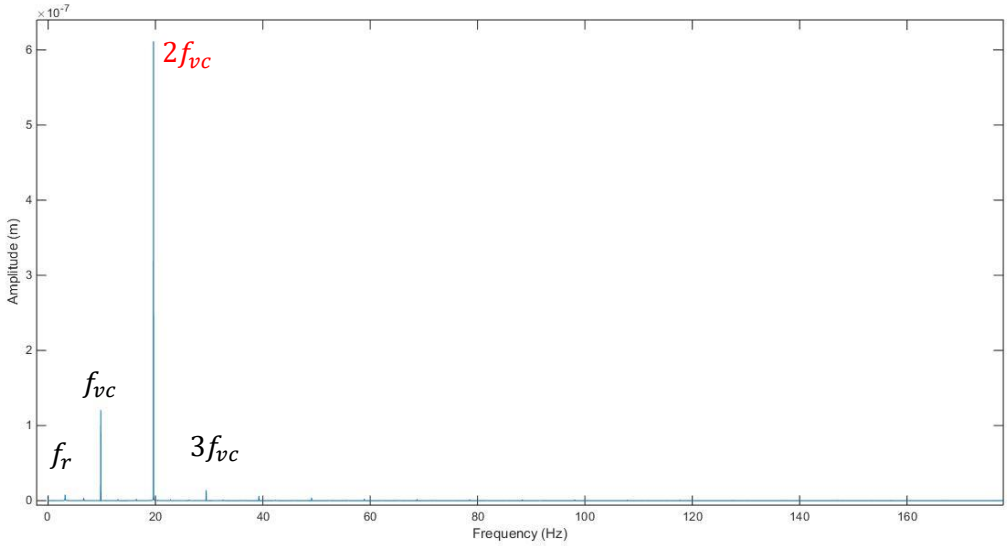

(b)

Fig. 4.32: Frequency Spectra of rotor center at bearing location with outer race waviness of order 13 (a) Horizontal Direction (b) Vertical Direction

spectra with waviness order 16, which is double of the total number of balls in the bearing. Yhland predicted the presence of $2f_{vc}$ in the frequency spectra. This frequency dominates the frequency spectra in vertical direction of both disk node and bearing node location. In the FFT plot of horizontal direction at the disk node, the rotational frequency dominates as shown in Fig. 4.35. At bearing center's horizontal direction the varying compliance frequency dominates, because of higher impact of Hertzian contact force than the rotational imbalance force.

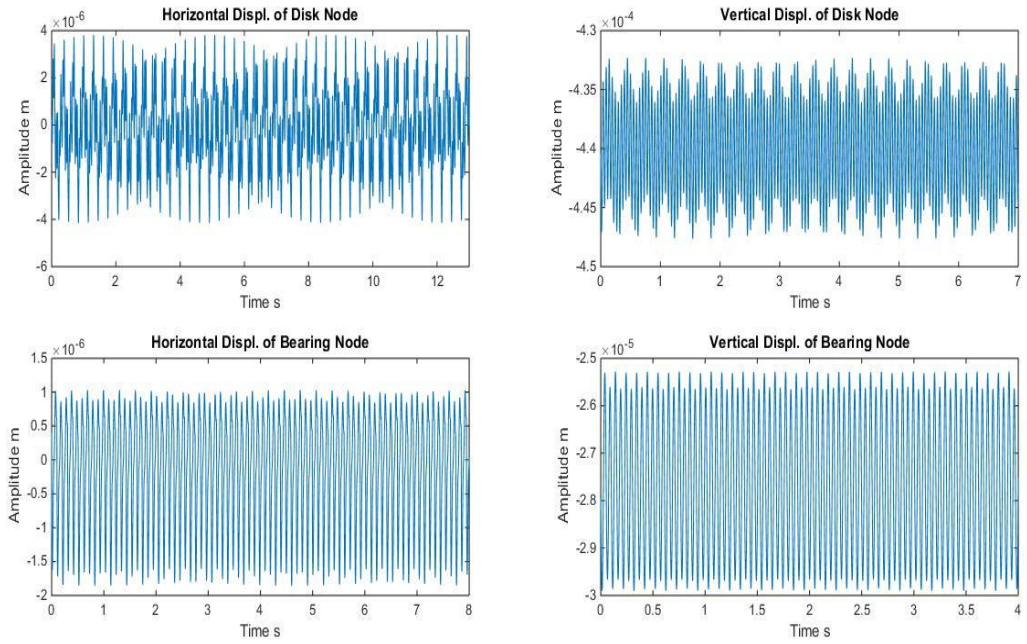

Fig. 4.33: Displacement plots of rotor with bearing having outer race waviness of order 16

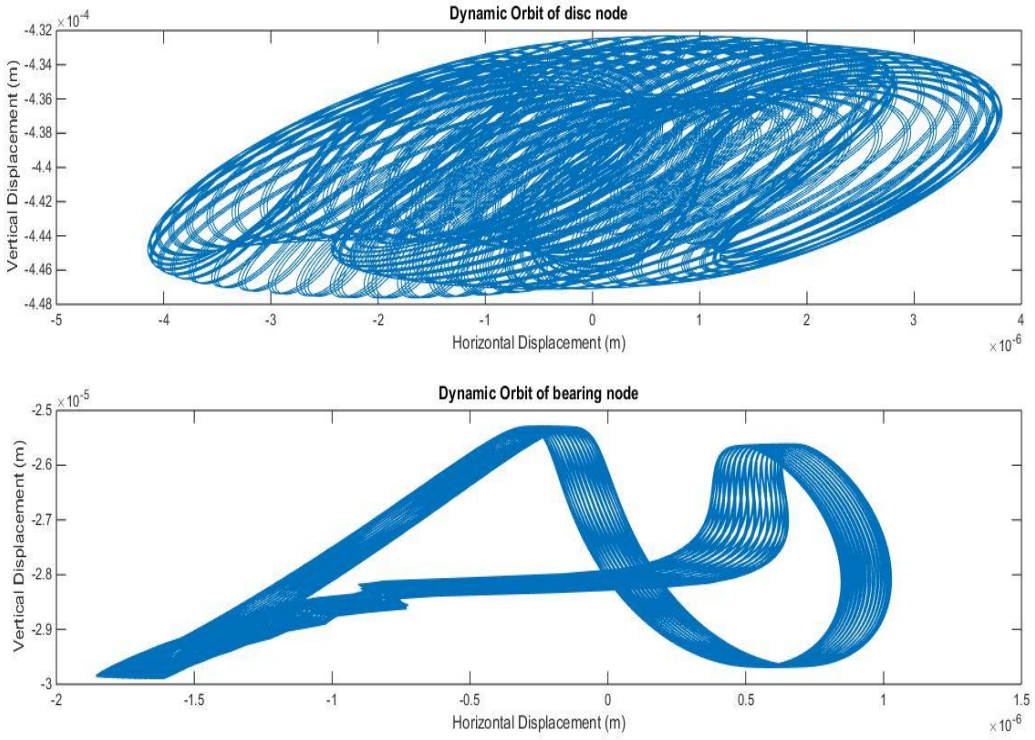

Fig. 4.34: Dynamic orbits of rotor with bearing having outer race waviness of order 16

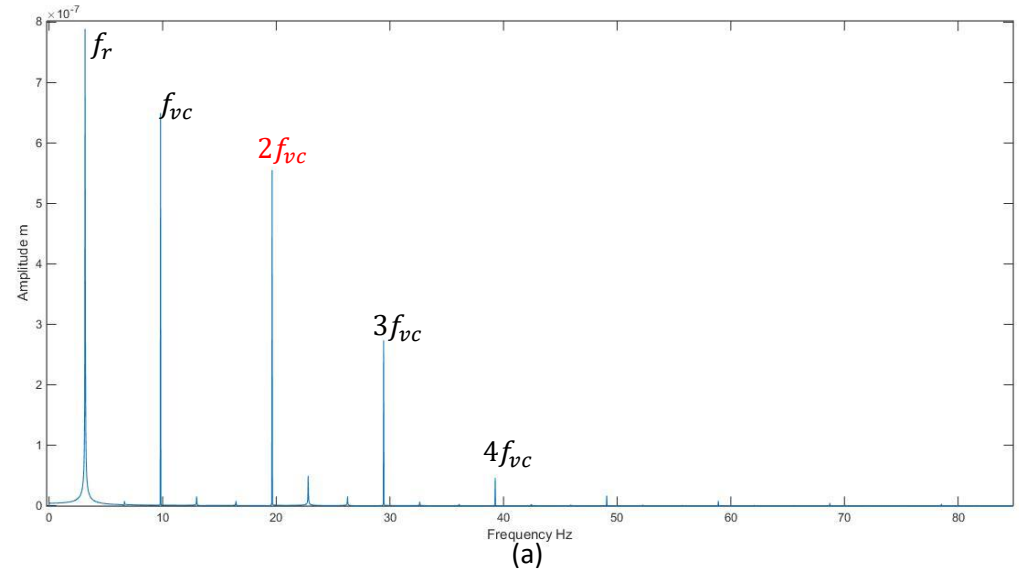

(a)

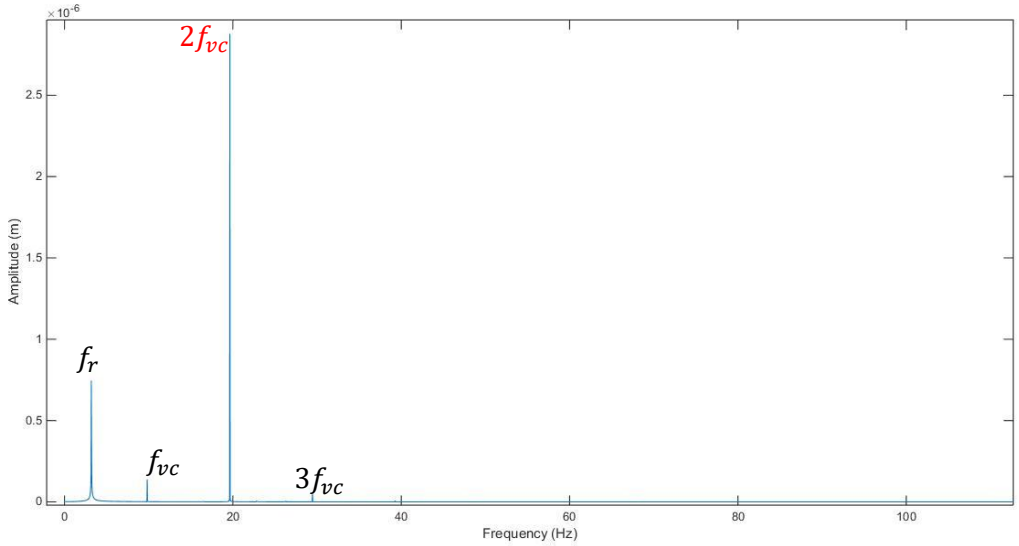

(b)

Fig. 4.35: Frequency Spectra of rotor center at disk with outer race waviness of order 16 (a) Horizontal Direction (b) Vertical Direction

The highest peak found in the entire frequency spectrum with waviness order of outer race as 16, is in the FFT plot of vertical disk node displacement, which is equal to 2.9 µm at frequency $2f_{vc}$ as shown in Fig. 4.35. The other frequencies appear in the frequency spectra are at the higher harmonics of varying compliance. The frequency spectra at bearing node for horizontal

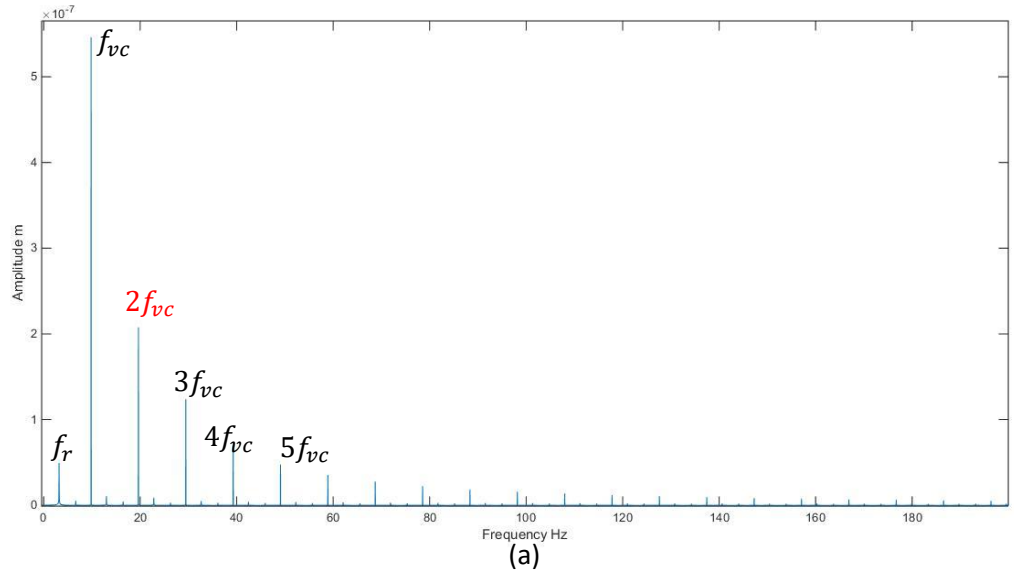

(a)

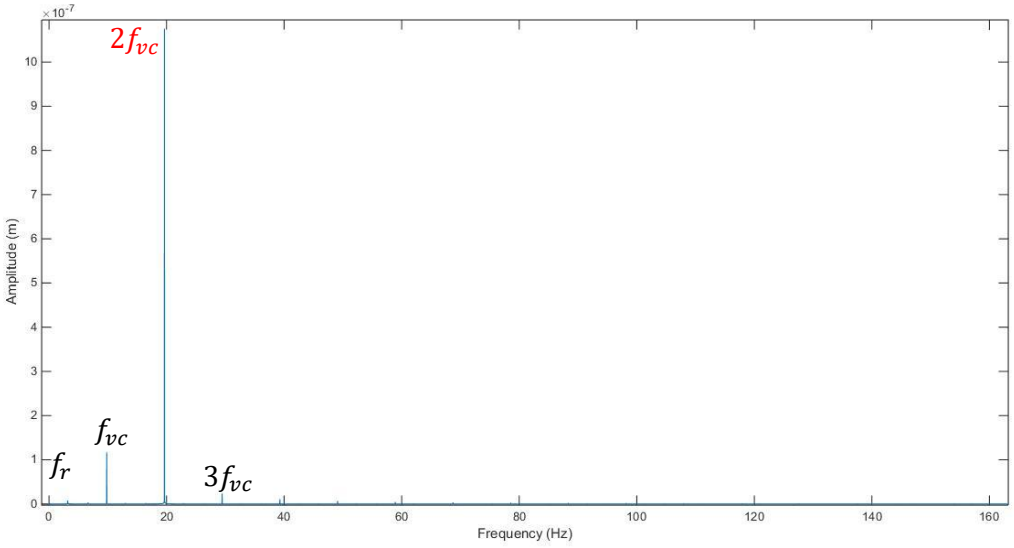

(b)

Fig. 4.36: Frequency Spectra of rotor center at bearing with outer race waviness of order 16
(a) Horizontal Displacement (b) Vertical Displacement

displacement shows large number of higher harmonics of varying compliance, while in the vertical FFT plot, very little number of higher harmonics comes. Highest harmonic appears in this FFT plot is $3f_{vc}$ as shown in Fig. 4.37. The rotational imbalance force has very less influence at bearing node vertical direction, because of which, the amplitude at rotational frequency is negligibly small.

5 Conclusions and Future Works

The Dynamic Model of an Unbalance Flexible Rotor supported on deep groove ball bearing is developed while including surface waviness on the races of ball bearing in the model. Using this dynamic model, a detailed study of frequency spectra is done, to investigate the influence of surface waviness of both inner race and outer race of ball bearing on dynamic response of the system. The major conclusions of results are as follows:

5.1 Mathematical Modeling

The finite element model is prepared of a flexible rotor with rigid disk mounted at the mid span of the rotor shaft, by using Nelson Model [17]. Ball bearing model is developed using Gupta's bearing model [9] and the surface waviness in included in the bearing by using the Waviness model given by Harsha [12]. Derived governing differential equation of complete system (equation 3.52) is solved using time integration technique Newmark β with Newton Raphson iteration method in MATLAB by referring Bathe [4] and Chopra [5]. The surface waviness is demonstrated by number of waves and amplitude. In the present model, the number of waves of the surface waviness of both inner race and outer race are varied separately and independently, which modifies the Hertzian Contact force of the Ball bearing.

5.2 Frequency Spectra of the System Vibration

The frequency spectra are obtained by using Fast Fourier Transformation (FFT) of rotor displacement plots, by transforming it from time domain to frequency domain in MATLAB. The frequency spectrum is derived for both horizontal and vertical displacement at bearing node location and at disk node location.

The frequency spectra are obtained first by considering ball bearing without any surface waviness on its races. Then, the frequency spectra are developed by imposing inner race waviness and outer race waviness separately on the ball bearing's inner race and outer race respectively. Yhland [24] proposed the presence of some specific exciting vibration frequencies in the FFT plots with respect to the waviness order of inner race and outer race (Table 4.1 and 4.3). The rotor-bearing model developed here is showing a good agreement with these

frequencies, given by Yhland in [24]. The surface waviness influenced the displacement of rotor, because of this; the peak amplitude in the frequency spectra is higher when surface waviness is considered on the races than the peak amplitude in frequency spectra without considering surface waviness. The impact of inner race waviness and outer race waviness to the Rotor's vibration is entirely different. These impacts are concluded below:

5.2.1 Bearings without Waviness

In the frequency spectra of disk node location, without including bearing's surface waviness, the peak amplitude is obtained at rotational frequency; and at the bearing node, the peak amplitude appears at varying compliance frequency. This shows that, the Hertzian Contact force of the bearing is comparably larger than Rotational Imbalance Force at bearing location than disk location. Frequencies obtained in the frequency spectra other than rotational frequency and varying compliance frequency are the higher harmonics of varying compliance. The amplitude in these FFT plots decreases as harmonics of varying compliance increases.

5.2.2 Inner Race Waviness effect

To study the impact of inner race waviness on frequency spectra of the system, the waviness order is varied by 5, 8, 13 and 16. On these waviness orders, the frequency proposed by the Yhland is also inspected, and found the presence of these frequencies in the frequency spectra which provide the validation of developed Rotor bearing model.

- For Inner race waviness order 5, in the response:
    - The peak amplitude in FFT plot of disk center horizontal displacement and bearing center horizontal and vertical displacement both appears at $N_b(f_r - f_c) - nf_r$
    - In FFT plot of disk center vertical displacement, the peak amplitude appears at rotational frequency f_r.
    - Other amplitude appears at varying compliance frequency and its higher harmonics, and sum of integer multiple of varying compliance and rotational frequency.

- For Inner race waviness order 8, in the response:

- The peak amplitude in FFT plot of disk node horizontal displacement appears at rotational frequency f_r , and in the FFT plot bearing node vertical displacement, the peak appears at varying compliance frequency f_{vc}.
- The peak amplitude at disk node vertical displacement FFT and bearing center horizontal displacement FFT appears at $N_b(f_r - f_c)$.

- For Inner race waviness of order 13, in the response :
  - The peak amplitude appears at $2N_b(f_r - f_c) - nf_r$ in all frequency spectra.
  - Other amplitude appears at varying compliance and its higher harmonics, rotational frequency and sum of integer multiple of varying compliance and rotational frequency.
- For Inner race waviness of order 16. in the response:
  - The peak amplitude in FFT plot of disk center horizontal displacement appears at rotational frequency f_r , and in the FFT plot bearing center vertical displacement, the peak appears at varying compliance frequency f_{vc}.
  - The peak amplitude for disk center vertical displacement FFT and bearing center horizontal displacement FFT appears at $2N_b(f_r - f_c)$.

5.2.3 Outer Race Waviness effect

The impact of outer race waviness on the vibration of system is studied by varying the waviness order of outer race waviness by 5, 8, 13 and 16, as a result, the frequency spectra changes. With respect to given surface waviness orders, Yhland predicted some specified exciting vibration frequencies to appear in frequency plots. These frequencies are the varying compliance frequency and their higher harmonics. Even without considering surface waviness, the varying compliance frequency and its higher harmonics exist in the frequency spectrum. Although, by including outer race surface waviness, the amplitude in the FFT plots at these frequencies increases (sometimes reaches at peak).

- For Outer Race Waviness of order 5, in the response:
  - The peak amplitude in FFT plot of disk node horizontal displacement and bearing node horizontal and vertical displacement both appears at f_{vc} .

- In FFT plot of disk node vertical displacement, the peak amplitude appears at rotational frequency f_r.
- Other amplitude appears at varying compliance frequency and its higher harmonics.

- For Outer Race Waviness of order 8, in the response:
  - The peak amplitude in FFT plot of disk node horizontal displacement appears at rotational frequency f_r.
  - The peak amplitude for disk node vertical displacement and bearing node horizontal as well as vertical displacement's FFT plot appears at f_{vc}.
- For Outer Race Waviness of order 13, in the response :
  - The peak amplitude appears at $2f_{vc}$ in all frequency spectra.
  - Other amplitude appears at varying compliance and its higher harmonics.
- For Outer Race Waviness of order 16. in the response:
  - The peak amplitude in FFT plot of disk node horizontal displacement appears at rotational frequency f_r , and in the FFT plot for vertical displacements of both disk node and bearing node, the peak appears at $2f_{vc}$.
  - The peak amplitude for bearing node horizontal displacement's FFT plot appears at f_{vc}.

From above discussion, it is concluded that, with considering inner race waviness of ball bearing, the frequency spectra becomes denser, as comparing with frequency spectra of the case with considering outer race waviness and even without considering any waviness on the races of bearing too. As a result, irregular orbits are formed in dynamic orbits plots with inner race waviness. The frequency spectra of system with inner race waviness of bearing show the presence frequencies stated by Yhland. In addition, the varying compliance frequency and its higher harmonics, rotational frequency, and sum of the integer multiple of varying compliance, rotational frequencies and cage rotational frequency also appear. Whereas, for the system with considering only outer race waviness of bearing, the frequency spectra shows Yhland proposed frequencies, with the rotational frequency and varying compliance frequency and its higher harmonics. These frequencies also exist in the frequency spectra when ball bearing model is taken without having any surface waviness, but they come at different amplitudes.

5.3 Future Works

The following work should be helpful for further understanding of Dynamic Behavior of Nonlinear Rotor Bearing system.

- Consider the Waviness on balls of the bearing too with the Waviness on Races. This condition provides the more real time information on the vibration characteristics of Rotor-Bearing System.
- The maximum amplitude of waviness function can be varied. This condition eliminates the assumption of taking surface waviness in the form of sinusoidal wave. In other words, the waviness can be considered as fourier series. Moreover, the axial waviness can also be considered with the radial waviness on balls and races of the bearing
- The Mass, stiffness and Gyroscopic Matrices of finite element of shaft can include the shear deformation effect by considering Timoshenko Beam element.
- The shaft can also have distributed unbalance mass throughout its length. The distribution can be linear or nonlinear, such as the eccentricity of center of mass of any typical internal point in shaft is dependent upon the given eccentricity of center of mass of the either ends of rotor shaft.

References

[1] Babu, C., Tandon, N., and Pandey, R., 2014, "Nonlinear Vibration Analysis of an Elastic Rotor Supported on Angular Contact Ball Bearings Considering Six Degrees of Freedom and Waviness on Balls and Races", J. Vib. Acoust., 136(4), p. 044503.

[2] Babu, C., Tandon, N., and Pandey, R., 2012, "Vibration Modeling of a Rigid Rotor Supported on the Lubricated Angular Contact Ball Bearings Considering Six Degrees of Freedom and Waviness on Balls and Races", J. Vib. Acoust., 134(1), p. 011006.

[3] Bai, C., Zhang, H., and Xu, Q., 2010, "Experimental and Numerical Studies on Nonlinear Dynamic Behavior of Rotor System Supported by Ball Bearings", J. Eng. Gas Turbines Power, 132(8), p. 082502.

[4] Bathe, K., 1996, Finite element procedure, Prentice Hall, Englewood Cliffs, N.J.

[5] Chopra, A., 2012, Dynamics of structures, Prentice Hall, Boston.

[6] Datta, J. and Farhang, K., 1997, "A Nonlinear Model for Structural Vibrations in Rolling Element Bearings: Part I—Derivation of Governing Equations", J. Tribol., 119(1), p. 126.

[7] Datta, J. and Farhang, K., 1997, "A Nonlinear Model for Structural Vibrations in Rolling Element Bearings: Part II—Simulation and Results", J. Tribol., 119(2), p. 323.

[8] El-Sayed, H., 1980, "Stiffness of deep-groove ball bearings", Wear, 63(1), pp. 89-94.

[9] Gupta, T., Gupta, K., and Sehgal, D., 2016, "Nonlinear Vibration Analysis of an Unbalanced Flexible Rotor Supported By Ball Bearings with Radial Internal Clearance", Power for Land, Sea and Air GT2008, Proceedings of ASME Turbo Expo, Berlin.

[10] Harris, T., 1991, Rolling bearing analysis, Wiley, New York,N.Y.

[11] Harsha, S. and Kankar, P., 2004, "Stability analysis of a rotor bearing system due to surface waviness and number of balls", International Journal of Mechanical Sciences, 46(7), pp. 1057-1081.

[12] Harsha, S., Sandeep, K., and Prakash, R., 2004, "Non-linear dynamic behaviors of rolling element bearings due to surface waviness", Journal of Sound and Vibration, 272(3-5), pp. 557-580.

[13] Kankar, P., Sharma, S., and Harsha, S., 2012, "Nonlinear Vibration Signature Analysis of a High Speed Rotor Bearing System Due to Race Imperfection", Journal of Computational and Nonlinear Dynamics, 7(1), p. 011014.

[14] Li, Y., Cao, H., Niu, L., and Jin, X., 2015, "A General Method for the Dynamic Modeling of Ball Bearing–Rotor Systems", Journal of Manufacturing Science and Engineering, 137(2), p. 021016.

[15] Meyer, L., Ahlgren, F., and Weichbrodt, B., 1980, "An Analytic Model for Ball Bearing Vibrations to Predict Vibration Response to Distributed Defects", Journal of Mechanical Design, 102(2), p. 205.

[16] Nelson, H., 1980, "A Finite Rotating Shaft Element Using Timoshenko Beam Theory", Journal of Mechanical Design, 102(4), p. 793.

[17] Nelson, H. and McVaugh, J., 1976, "The Dynamics of Rotor-Bearing Systems Using Finite Elements", Journal of Engineering for Industry, 98(2), p. 593.

[18] Niu, L., Cao, H., He, Z., and Li, Y., 2014, "Dynamic Modeling and Vibration Response Simulation for High Speed Rolling Ball Bearings With Localized Surface Defects in Raceways", Journal of Manufacturing Science and Engineering, 136(4), p. 041015.

[19] N. Aktürk,, 1999, "The Effect of Waviness on Vibrations Associated With Ball Bearings", J. Tribol., 121(4), p. 667.

[20] Patel, V., Tandon, N., and Pandey, R., 2010, "A Dynamic Model for Vibration Studies of Deep Groove Ball Bearings Considering Single and Multiple Defects in Races", J. Tribol., 132(4), p. 041101.

[21] T.A. Harris, 1991, Rolling Bearing Analysis, Wiley, New York.

[22] Wardle, F., 1988, "Vibration Forces Produced by Waviness of the Rolling Surfaces of Thrust Loaded Ball Bearings Part 1: Theory", Proceedings of the Institution of Mechanical Engineers, Part C: Journal of Mechanical Engineering Science, 202(5), pp. 305-312.

[23] Wardle, F., 1988, "Vibration Forces Produced by Waviness of the Rolling Surfaces of Thrust Loaded Ball Bearings Part 2: Experimental Validation", Proceedings of the Institution of Mechanical Engineers, Part C: Journal of Mechanical Engineering Science, 202(5), pp. 313-319.

[24] Yhland, E., 1992, "A Linear Theory of Vibrations Caused by Ball Bearings With Form Errors Operating at Moderate Speed", J. Tribol., 114(2), p. 348.

[25] Armentrount, R. and Gunter, E., 1932, "Transient Modal Analysis of Nonlinear Rotor-Bearing Systems", RODYN Vibration Analysis, Inc.

[26] Friswell, M., 2010, Dynamics of rotating machines, Cambridge University Press, Cambridge.

[27] Singh, R. and Lim, T., 1990, Vibration transmission through rolling element bearings in geared rotor systems, National Aeronautics and Space Administration, Office of Management, Scientific and Technical Information Division, Washington, D.C.

Appendix

A. Matrices

Matrices for finite element of rotor: (as mentioned in section 3.1.1)

$$[\mathrm{M_T^e}] = \frac{\mu l}{420}\begin{bmatrix} 156 & 0 & 0 & 22l & 54 & 0 & 0 & -13l \\ 0 & 156 & -22l & 0 & 0 & 54 & 13l & 0 \\ 0 & -22l & 4l^2 & 0 & 0 & -13l & -3l^2 & 0 \\ 22l & 0 & 0 & 4l^2 & 13l & 0 & 0 & -3l^2 \\ 54 & 0 & 0 & 13l & 156 & 0 & 0 & -22l \\ 0 & 54 & -13l & 0 & 0 & 156 & 22l & 0 \\ 0 & 13l & -3l^2 & 0 & 0 & 22l & 4l^2 & 0 \\ -13l & 0 & 0 & -3l^2 & -22l & 0 & 0 & 4l^2 \end{bmatrix}$$

$$[\mathrm{M_R^e}] = \frac{\mathcal{J}_d}{30l}\begin{bmatrix} 36 & 0 & 0 & 3l & -36 & 0 & 0 & 3l \\ 0 & 36 & -3l & 0 & 0 & -36 & -3l & 0 \\ 0 & -3l & 4l^2 & 0 & 0 & 3l & -l^2 & 0 \\ 3l & 0 & 0 & 4l^2 & -3l & 0 & 0 & -l^2 \\ -36 & 0 & 0 & -3l & 36 & 0 & 0 & -3l \\ 0 & -36 & 3l & 0 & 0 & 36 & 3l & 0 \\ 0 & -3l & -l^2 & 0 & 0 & 3l & 4l^2 & 0 \\ 3l & 0 & 0 & -l^2 & -3l & 0 & 0 & 4l^2 \end{bmatrix}$$

$$[\mathrm{G^e}] = \frac{\mathcal{J}_p}{30l}\begin{bmatrix} 0 & -36 & 3l & 0 & 0 & 36 & 3l & 0 \\ 36 & 0 & 0 & 3l & -36 & 0 & 0 & 3l \\ -3l & 0 & 0 & -4l^2 & 3l & 0 & 0 & l^2 \\ 0 & -3l & 4l^2 & 0 & 0 & 3l & -l^2 & 0 \\ 0 & 36 & -3l & 0 & 0 & 36 & -3l & 0 \\ -36 & 0 & 0 & -3l & 36 & 0 & 0 & -3l \\ -3l & 0 & 0 & l^2 & 3l & 0 & 0 & -4l^2 \\ 0 & -3l & -l^2 & 0 & 0 & 3l & 4l^2 & 0 \end{bmatrix}$$

$$[\mathrm{K^e}] = \frac{\mathrm{E\,I_s}}{\mathrm{l}^3}\begin{bmatrix} 12 & 0 & 0 & 6l & -12 & 0 & 0 & 6l \\ 0 & 12 & -6l & 0 & 0 & -12 & -6l & 0 \\ 0 & -6l & 4l^2 & 0 & 0 & 6l & 2l^2 & 0 \\ 6l & 0 & 0 & 4l^2 & -6l & 0 & 0 & 2l^2 \\ -12 & 0 & 0 & -6l & 0 & 36 & 3l & 0 \\ 0 & -12 & 6l & 0 & 36 & 0 & 0 & 3l \\ 0 & -6l & 2l^2 & 0 & 3l & 0 & 4l^2 & 0 \\ 6l & 0 & 0 & 2l^2 & 0 & 3l & 0 & 4l^2 \end{bmatrix}$$

Matrices for rigid disk (as mentioned in section 3.1.2):

$$[M_T^d] = \begin{bmatrix} m_d & 0 & 0 & 0 \\ 0 & m_d & 0 & 0 \\ 0 & 0 & 0 & 0 \\ 0 & 0 & 0 & 0 \end{bmatrix}$$

$$[M_R^d] = \begin{bmatrix} 0 & 0 & 0 & 0 \\ 0 & 0 & 0 & 0 \\ 0 & 0 & I_d^d & 0 \\ 0 & 0 & 0 & I_d^d \end{bmatrix}$$

$$[G^d] = \begin{bmatrix} 0 & 0 & 0 & 0 \\ 0 & 0 & 0 & 0 \\ 0 & 0 & 0 & -I_p^d \\ 0 & 0 & I_p^d & 0 \end{bmatrix}$$